UC San Diego

UC San Diego Electronic Theses and Dissertations

Title

CK1-mediated TDP-43 Phosphorylation in Amyotrophic Lateral Sclerosis and TDP-43 Proteinopathies

Permalink

https://escholarship.org/uc/item/8hz814b4

Author

Ko, Vivian

Publication Date

2024

Peer reviewed|Thesis/dissertation

eScholarship.org Powered by the California Digital Library
University of California

UNIVERSITY OF CALIFORNIA SAN DIEGO

CK1-mediated TDP-43 Phosphorylation in Amyotrophic Lateral Sclerosis and TDP-43 Proteinopathies

A dissertation submitted in partial satisfaction of the requirements for the degree of

Doctor of Philosophy

in

Neurosciences

by

Vivian Ivy Ko

Committee in charge:

Professor Don W. Cleveland, Chair

Professor John M. Ravits, Co-Chair

Professor Alexandra Newton

Professor Christina Sigurdson

2024

Copyright

Vivian Ivy Ko, 2024

All rights reserved.

The dissertation of Vivian Ivy Ko is approved, and it is acceptable in quality and form for publication on microfilm and electronically.

University of California San Diego

2024

Dedication

This dissertation is dedicated to my loved ones, family, and friends, for their unconditional support. And to my educators and mentors, past and present, whom I would not have pursued this without their inspiration and encouragement.

Epigraph

“To achieve great things, two things are needed: a plan, and not quite enough time.” – Leonard Bernstein

Table of Contents

Dissertation Approval Page iii
Dedication iv
Epigraph v
Table of Contents vi
List of Abbreviations ix
List of Figures x
Acknowledgements xiii
Vita xv
Abstract of Dissertation xvi
Chapter 1 : Overview of ALS 1
Description of ALS 1
Discovery of a unifying pathology for ALS 3
Loss of nuclear TDP-43 function vs. gain of cytoplasmic TDP-43 toxicity 4
Post-translational modifications (PTMs) of TDP-43 8
Kinases in TDP-43 phosphorylation and identification of CSNK1E in ALS 11
Research models of ALS and TDP-43 proteinopathy 14
Challenges and therapeutic developments in ALS 17
Acknowledgements 25
Chapter 2 : Novel cellular models reveal CK1δ/ε kinases regulate TDP-43 phosphorylation and are targets for ALS-related TDP-43 hyperphosphorylation 26
Abstract 26
Introduction 27
Results 31
CK1δ and CK1ε kinases directly phosphorylate TDP-43 and are most favorable to phosphorylate the S409/410 site 31
Expression of TDP-43 in cells displays TDP-43 nuclear mislocalization into cytoplasmic phosphorylated inclusions 36
siRNA-mediated knockdown of either CSNK1D or CSNK1E significantly decreases TDP-43 phosphorylation 41
CK1 inhibitors have selective target engagement of CK1δ and CK1ε 45
CK1 inhibitors are potent compounds that reduce TDP-43 phosphorylation in cellular models 49
The S409/410 sites on TDP-43 is predominantly phosphorylated by CK1δ and CK1ε kinases 53
Discussion 56

Methods 60
Kinase profile studies 60
Stable cell line generation 61
Cell culture 61
siRNA treatments 62
KINOMEscan™ compound selectivity profiles 62
In vitro inhibitor treatment 63
Real-time PCR (qRT-PCR) 64
Immunofluorescence (IF) 65
Protein extraction 66
Immunoblotting 66
Statistical analyses 67
Acknowledgements 68
Chapter 3 : Targeting CK1ε-mediated phosphorylation of TDP-43 through Csnk1e genetic deletion in vivo 69
Abstract 69
Introduction 70
Results 73
Mouse model of inducible TDP-43 proteinopathy has ALS disease-relevant phenotypes 73
Deletion of Csnk1e is gene-specific and does not alter the regulation of Csnk1d .. 78
Deletion of Csnk1e delayed pTDP-43 formation, but was insufficient in reducing TDP-43 proteinopathy 81
Discussion 85
Methods 88
Mouse breeding and maintenance of hTDP-43-ΔNLS mice 88
Generation of Csnk1e knockout mouse line breeding with NEFH-hTDP-43ΔNLS mice 88
Rotarod behavior 89
Grip test behavior 90
Tissue collection for biochemistry assays 90
Tissue collection for histology assays 90
Real-time PCR (qRT-PCR) 91
Protein extraction 92
Immunoprecipitation (IP) 92
Immunoblotting 93
Immunofluorescence (IF) 94
Statistical analyses 95
Acknowledgements 96
Chapter 4 : Manipulation of the S409/410 site on TDP-43 by selective CK1δ/ε inhibition as a candidate therapeutic target 97
Abstract 97

Introduction 98
Results 101
Novel characterization of mouse model reveals supplementary measures of neurodegenerative phenotypes 101
TDP-43 hyperphosphorylation and cytoplasmic accumulation precedes motor behavior deficits in hTDP-43-ΔNLS mice 102
Characterization of CK1 inhibitors as an in vivo tool 104
Selective inhibition of CK1δ/ε reduces TDP-43 phosphorylation and Nf-L levels ..110
Selective inhibition of CK1δ/ε is insufficient to rescue motor deficits for functional benefit 115
Discussion 119
Methods 123
Mouse breeding and maintenance of hTDP-43-ΔNLS mice 123
Rotarod behavior 124
Grip test behavior 124
Compound muscle action potential (CMAP) recordings 124
Neurofilament-Light (Nf-L) measures 126
Pharmacokinetic characterization 126
LC-MS/MS for compound detection 127
Tissue collection for biochemistry assays 128
RNA-sequencing and gene expression analysis 128
Protein extraction 129
Immunoblotting 130
Statistical analyses 131
Acknowledgements 131
Chapter 5 : Conclusion 133
References 139

List of Abbreviations

ALS	Amyotrophic lateral sclerosis
AD	Alzheimer’s disease
CNS	Central nervous system
CSNK1D	Casein kinase 1 delta gene
CSNK1E	Casein kinase 1 epsilon gene
CK1δ	Casein kinase 1 delta protein
CK1ε	Casein kinase 1 epsilon protein
Dox	doxycycline
NLS	Nuclear localization signal
pTDP-43	Phosphorylated TDP-43
PTM	Post-translational modification
S409/410	Serine 409/410 phosphorylation sites on TDP-43
TDP-43	Trans-activation response DNA-binding protein-43

List of Figures

Figure 1.1 Graphical abstract of proposed CK1-mediated phosphorylation of TDP-43 in ALS. 13

Figure 1.2 Images of IHC staining for patient tissue samples. 16

Figure 2.1 TDP-43 is a substrate of CK1δ and CK1ε and multiple serine sites on TDP-43 are bioinformatically predicted to be phosphorylated by CK1δ and CK1ε..... 35

Figure 2.2 Adding N50 small peptide tag to TDP-43 generates cytoplasmic phosphorylated TDP-43 inclusions. 38

Figure 2.3 Cell models expressing TDP43$^{N50\text{-}clover}$ display TDP-43 nuclear clearance and accumulation of cytoplasmic phosphorylated TDP-43 inclusions. 39

Figure 2.4 siRNA-mediated knockdown of either CSNK1D or CSNK1E significantly decreases pTDP-43 expression levels. 43

Figure 2.5 CK1 inhibitors are selective for target engagement of CK1δ and/or CK1ε. .. 48

Figure 2.6 CK1 inhibitors effectively reduce pTDP-43. 51

Figure 2.7 CK1 inhibitors reduce TDP-43 phosphorylation in soluble and insoluble protein fractions. 52

Figure 2.8 Cellular imaging shows reduced cytoplasmic pTDP-43 expression in treated cells. 53

Figure 2.9 CK1δ and CK1ε are the predominant kinases that phosphorylate TDP-43 at ALS-relevant S409/410 sites..... 55

Figure 3.1 Mouse disease model is a tet-off dox inducible system. 75

Figure 3.2 hTDP-43-ΔNLS mice display significant motor deficits and degenerative health. 76

Figure 3.3 hTDP-43-ΔNLS mice display TDP-43 nuclear clearance and cytoplasmic pTDP-43 expression in neurons. 77

Figure 3.4 Characterization and validation of Csnk1e-KO mice. 80

Figure 3.5 TDP-43 phosphorylation was delayed in Csnk1e-KO mice and may be a mechanism that promotes protein solubility. 83

Figure 3.6 Deletion of Csnk1e did not exacerbate motor impairments or overall health of mice..... 84

Figure 3.7 Csnk1e-KO mice developed hallmarks of cellular TDP-43 proteinopathy in the brain and spinal cord. 85

Figure 4.1 Nf-L and CMAP assays demonstrate robust neurodegeneration phenotypes. 102

Figure 4.2 pTDP accumulation precedes motor deficits. 104

Figure 4.3 Pharmacokinetic (PK) profiles of CK1 inhibitors indicate half-lives and exposure levels. 106

Figure 4.4 Characterization of target engagement to TDP-43. 108

Figure 4.5 Treated mice had sufficient compound exposure levels and showed changes in Nf-L levels. 112

Figure 4.6 Treated mice showed reduced pTDP-43 with short-term inhibitor treatment. 113

Figure 4.7 Treated mice did not show a difference in motor behavior assays or health measures. 117

Figure 4.8 Transcriptomic study reveals potential side effects of long-term inhibitor treatment. 118

Figure 5.1 Various roles of TDP-43 phosphorylation in ALS disease..... 138

List of Tables

Table 2.1 Results from The Kinase Library bioinformatic database which identified kinases that phosphorylate serine sites on TDP-43. 34

Table 2.2 %Control for selectivity profiles of CK1 inhibitor compounds. 47

Table 2.3 Selectivity S-scores for CK1 inhibitor compounds 47

Acknowledgements

I would like to acknowledge Professor John Ravits for his tireless support as my mentor and championing our vision and providing the resources to carry out our project. His compassion as a clinical healthcare provider, continuous advocacy for patients, and motivation to understand amyotrophic lateral sclerosis have shaped my own scientific pursuits. The wisdom he shares on science and life is cherished advice. In particular, I'd like to thank Anita Hermann for managing and holding our lab together and ensuring minimal disruptions so I could conduct experiments without worry. To Kailee Ong, my right hand in completing this project, I would be at a loss without your help. I would also like to thank Professor Don Cleveland and his team for their passionate scientific discussions, insights, and collaborations. To the post-doctoral force of mentors between the Ravits and Cleveland labs, I appreciate all your scientific guidance and encouragement over the years. To my mentors before graduate school, I would not have this opportunity without your advocacy and training to prepare me for this endeavor. I thank my committee members for their thoughtful input and constructive feedback for me to research my project comprehensively and critically. I would also like to thank the Neurosciences Graduate Program for providing the environment and resources for me to begin my budding scientific career.

Chapter 1, in part, is a reformatted reprint of the material as it appears in Ko, V. I., Ong, K., Cleveland, D. W., Yu, H., & Ravits, J. M. (2024). CK1δ/ε kinases regulate TDP-43 phosphorylation and are therapeutic targets for ALS-related TDP-43 hyperphosphorylation. *Neurobiology of Disease*, *196*, 106516.

https://doi.org/10.1016/j.nbd.2024.106516. The dissertation author was the primary investigator and author of this paper.

Chapter 2, in full, is a reformatted reprint of the material as it appears in Ko, V. I., Ong, K., Cleveland, D. W., Yu, H., & Ravits, J. M. (2024). CK1δ/ε kinases regulate TDP-43 phosphorylation and are therapeutic targets for ALS-related TDP-43 hyperphosphorylation. *Neurobiology of Disease*, *196*, 106516. https://doi.org/10.1016/j.nbd.2024.106516. The dissertation author was the primary investigator and author of this paper.

Chapters 3 and 4, in full, are being prepared for submission for publication of the material as “Manipulation of the S409/410 site on TDP-43 by selective CK1δ/ε inhibition as a candidate therapeutic target”. Other co-authors will be Kailee Ong, Deborah Y. Kwon, Xueying Li, Alicia Pietrasiewicz, James Harvey, Mukesh Lulla, Guruharsha Bhat, Don W. Cleveland, and senior author John M. Ravits. The dissertation author will be the primary investigator and author of this paper.

Vita

2016 Bachelor of Sciences, Biochemistry and Cell Biology with a Minor in Psychology

University of California San Diego, La Jolla, CA, USA

2024 Doctor of Philosophy, Neurosciences

University of California San Diego, La Jolla, CA, USA

PUBLICATIONS

1. Smith, J.B., Klug, J.K., Ross, D.L., Howard, C.D., Hollon, G.N., **Ko, V.I.**, Hoffman, H., Callaway, E.M., Gerfen, C.R., Jin, X. (2016). Genetic-Based Dissection Unveils the Inputs and Outputs of Striatal Patch and Matrix Compartments. *Neuron, 91*(5): 1069-1084. https://doi.org/10.1016/j.neuron.2016.07.046.

2. Diaz-Garcia, S., **Ko, V.I.**, Vazquez-Sanchez, S., Chia, R., Arogundade, O.A., Rodriguez, M.J., Traynor, B.J., Cleveland, D., Ravits, J. (2021). Nuclear depletion of RNA binding protein ELAVL3 (HuC) in sporadic and familial amyotrophic lateral sclerosis. *Acta Neuropathologica, 142*(6), 985-1001. https://doi.org/10.1007/s00401-021-02374-4.

3. **Ko, V.I.**, Ong, K., Cleveland, D., Yu, H., Ravits, J.M. (2024). CK1δ/ε kinases regulate TDP-43 phosphorylation and are therapeutic targets for ALS-related TDP-43 hyperphosphorylation. *Neurobiology of Disease, 196*, 106516. https://doi.org/10.1016/j.nbd.2024.106516.

ANTICIPATED PUBLICATIONS

1. **Ko, V.I.**, Ong, K., Kwon, D.Y., Li, X., Pietrasiewicz, A., Harvey, J., Lulla, M., Bhat, G., Cleveland, D.W., Ravits, J.M. (2024). Manipulation of the S409/410 site on TDP-43 by selective CK1δ/ε inhibition as a candidate therapeutic target for ALS-related TDP-43 proteinopathy. [Manuscript in preparation].

Abstract of Dissertation

CK1-mediated TDP-43 Phosphorylation in Amyotrophic Lateral Sclerosis

and TDP-43 Proteinopathies

by

Vivian Ivy Ko

Doctor of Philosophy in Neurosciences

University of California San Diego, 2024

Professor Don Cleveland, Chair
Professor John Ravits, Co-Chair

Amyotrophic lateral sclerosis (ALS) is a severely debilitating and fatal adult-onset neurodegenerative disease marked by the progressive loss of nerve cells in the brain and spinal cord leading to loss of voluntary muscle movement. A unifying feature of the majority of familial and sporadic ALS cases is TDP-43 proteinopathy, or the abnormal expression and function of trans-activation response DNA-binding protein (TDP-43 protein encoded by the *TARDBP* gene). The loss-of-function and gain-of-function

associated with TDP-43 nuclear depletion, mislocalization, and cytoplasmic accumulation is being heavily investigated. Further, aberrant post-translational modifications (PTMs) to TDP-43 may contribute to disease mechanisms and toxicity. Most research has focused on the cytoplasmic TDP-43 aggregate formation, which is believed to be a toxic driver of disease progression. Phosphorylation has been implicated alongside cytoplasmic TDP-43 accumulation and aggregation, with contrasting results as to whether serves a protective or toxic role in this context. Further, multiple candidate kinases have been proposed to be the primary facilitator for TDP-43 phosphorylation in ALS disease. This dissertation seeks to provide insight into the role of CK1-dependent TDP-43 phosphorylation in protein solubility, aggregation, and toxicity, and ultimately determine whether targeting this mechanism holds promise for ALS and TDP-43 proteinopathy therapy. Chapter 1 provides an overview of our current understanding on ALS pathophysiology, neuropathology, disease mechanisms, ALS research models, and strategies that are being investigated for therapeutic development. In Chapter 2, we use *in vitro* assays and cellular models to demonstrate that CK1δ and CK1ε are the primary kinases that regulate ALS disease-relevant TDP-43 phosphorylation sites, and that RNAi and pharmacologic strategies that target CK1δ and CK1ε effectively reduce phosphorylated TDP-43 (pTDP-43) levels. Chapter 3 extends the previous findings of Chapter 2 into an *in vivo* inducible ALS mouse model and reveal that *Csnk1e* genetic deletion delays pTDP-43 formation but was insufficient in reducing cellular TDP-43 proteinopathy and motor behavior deficits. Finally, in Chapter 4, we study the efficacy of CK1δ/ε inhibitors *in vivo* and determine that manipulation of the S409/410 site on TDP-43 by selective CK1δ/ε inhibition is not a candidate therapeutic target on its own.

Chapter 1 : Overview of ALS

Description of ALS

Amyotrophic lateral sclerosis (ALS), also known as Lou Gehrig's disease after the notable New York Yankee baseball player who passed away from the disease, is the most common incurable adult-onset motor neuron disease. It is the third most common neurodegenerative disease, after Alzheimer's disease (AD) and Parkinson's disease (PD). ALS was first described by Charles Bell in the 1820s, and then decades later, the symptoms were connected to the neurological problems by neurologist Jean-Martin Charcot in the 1870s who also coined the term *amyotrophic lateral sclerosis* (Rowland, 2001). *A-myo-trophic* is of Greek origin, which means no muscle nourishment, resulting in the observed muscle atrophy during disease. *Lateral* references the affected areas in the spinal cord, specifically the lateral corticospinal tracts, where motor neurons signal to and control the affected muscles. *Sclerosis* is a description of the hardening and scarring of the affected areas that results from this degenerative process.

ALS affects the upper motor neurons in the motor cortex and lower motor neurons in the brain stem and spinal cord (Ragagnin et al., 2019). The age of onset is typically between late 40s to early 70s (average age of 55 years), with a slightly higher occurrence in men over women if the onset is before age 70. The incidence is roughly 2-5 new ALS cases for each 100,000 people every year and the prevalence of the number of people living with ALS is 5-7 cases for each 100,000 persons (Jankovska & Matej, 2021; Oskarsson et al., 2018; Talbott et al., 2016).

Clinical symptoms of ALS are heterogeneous, with varying locations of focal onset, three-dimensional spreading within the upper and lower motor systems, and rates of

progression amongst patients (Ravits & La Spada, 2009). Symptoms include progressive loss of muscle control, muscle weakness, spasms, atrophy, stiffness, trouble swallowing or breathing, slurred or nasal speech, and eventual paralysis. Some 30-50% of ALS patients develop cognitive impairments and behavioral dysfunction, such as dementia and difficulty with executive functions and language (Zarei et al., 2015). Although pain is not directly caused by the neurodegeneration in ALS, pain is a commonly described symptom as a result of the reduced mobility that patients experience. The average life expectancy for most patients is 3-5 years from diagnosis, with progressive neuromuscular respiratory failure as the primary cause of death (R. H. Brown & Al-Chalabi, 2017).

ALS cases fall under either familial or sporadic classifications, where familial cases constitute approximately 15-20% and have a family history with autosomal dominance of an ALS-associated genetic mutation. Over 40 genes with mutations have been identified in ALS cases, but only four of them comprise over 50% of familial ALS. The four most common ALS-associated genetic mutations include *C9orf72* (40%), *SOD1* (12%), *FUS* (4%), and *TARDBP* (4%) (Gendron et al., 2012; Lattante et al., 2015). The remaining 80-85% of all ALS cases are considered sporadic, where there is no family history present, and multiple genes and environmental risk factors may contribute (Fang et al., 2015; S.-C. Ling et al., 2013; Polymenidou et al., 2012; Swinnen & Robberecht, 2014; Turner et al., 2013). Generally, what causes sporadic ALS remains largely unknown and is thus often considered an idiopathic disease.

Discovery of a unifying pathology for ALS

Across all familial and sporadic ALS cases is the primary histopathological hallmark of inclusion bodies and protein aggregates in the cytoplasm of motor neurons in the central nervous system (CNS) (Neumann, 2009; Nolan et al., 2020). Despite heterogeneity in ALS, nearly 97% of all familial and sporadic patients exhibit TDP-43 proteinopathy, which is characterized by altered trans-activation response DNA-binding protein (TDP-43 protein encoded by the *TARDBP* gene) expression and function (Brettschneider et al., 2013; S.-C. Ling et al., 2013). Features of TDP-43 proteinopathy include the loss of nuclear TDP-43, mislocalized TDP-43 to the cytoplasm where the protein is accumulated, and presence of TDP-43 inclusions which are also referred to as aggregates. Interestingly, ALS cases with *SOD1* or *FUS* mutations do not exhibit TDP-43 proteinopathy, and instead, have either SOD1 or FUS protein aggregated into inclusion bodies (Da Cruz et al., 2017; Lagier-Tourenne & Cleveland, 2009; Mackenzie et al., 2007).

TDP-43, encoded by the *TARDBP* gene, is an RNA binding protein that is ubiquitously expressed in the nucleus of cells, and its proper functioning is vital to cell development, health, and survival. Some of TDP-43's functions include regulating gene expression, transcriptional repression, RNA biogenesis and processing, RNA alternative splicing, translational regulation, non-homologous end joining, and maintaining mitochondrial homeostasis. TDP-43 is 43 kDa in weight and is composed of 414 amino acids which includes regions that contain a nuclear localization signal (NLS), nuclear export signal (NES), RNA binding domains (RRM1, RRM2), and a low complexity glycine-rich domain on the 3' C-terminal end. This glycine-rich domain enables self-self-

interaction of TDP-43 into aggregates and bestows prion-like properties. This region also contains nearly all of the TDP-43 mutations associated with familial ALS, as well as multiple serine, threonine, and tyrosine phosphorylation sites (Prasad et al., 2019). In ALS disease, there is complete nuclear clearance of TDP-43 to the cytoplasm where it accumulates, and TDP-43 inclusions have been observed to be hyperphosphorylated and modified. These TDP-43 inclusions have numerous abnormalities and modifications such as acetylation, liquid–liquid phase separation (LLPS), mislocalization, phosphorylation, solubilization, proteolytic cleavage, truncation, and ubiquitination (Arai et al., 2006; Neumann et al., 2006; Polymenidou et al., 2012; Prasad et al., 2019). The significance of TDP-43 proteinopathy is increasing in other neurodegenerative diseases as its mechanistic role is also being studied in frontotemporal lobar degeneration/ frontotemporal dementia (FTLD/FTD), Alzheimer's disease (AD), limbic-predominant age-related TDP-43 encephalopathy (LATE), and Lewy body disease (LBD) (Kwong et al., 2007; Montalbano et al., 2020; Neumann, 2009; Prasad et al., 2019; Tomé et al., 2020).

Loss of nuclear TDP-43 function vs. gain of cytoplasmic TDP-43 toxicity

The altered nuclear trafficking and localization of TDP-43 accompanied by aberrant phase separation and accumulation of cytoplasmic aggregates has generally been considered to be a toxic disease-driving mechanism (L. Guo et al., 2019; Klim et al., 2021; Prasad et al., 2019; Scotter et al., 2015; Suk & Rousseaux, 2020; J. P. Taylor et al., 2016; Tziortzouda et al., 2021). A study that examined TDP-43 nucleo-cytoplasmic shuttling by expressing TDP-43 mutants that possessed either a defective nuclear

localization signal (NLS) or defective nuclear export signal (NES) resulted in TDP-43 aggregate formation either solely in the cytoplasm or solely in the nucleus, respectively (Winton et al., 2008). In addition, it was found that the C-terminal region was also essential for regulating TDP-43 solubility and localization (Ayala et al., 2008). These data indicated that alterations to the balance and homeostatic function of TDP-43 nucleo-cytoplasmic shuttling had a significant role in aggregate formation and TDP-43 solubility. However, a remaining key debate centers on the respective contributions of TDP-43 loss of nuclear function versus cytoplasmic gain of toxicity to ALS disease pathogenesis.

Research of ALS disease mechanisms has largely centered on toxic gain-of-function roles for cytoplasmic TDP-43. The functions of TDP-43 in the cytoplasm includes mRNA stability and transport, regulating translation, miRNA processing, stress response, regulating autophagy and synaptic function (Birsa et al., 2020; Hergesheimer et al., 2019). TDP-43 binds the 3' untranslated region (UTR) of mRNAs to facilitate mRNA stability and transport, and has been found to interact with ribosomal subunits to regulate translation both as a repressor and enhancer depending on the target (Tollervey et al., 2011). TDP-43 has been shown to bind immature miRNAs and affect the maturation of particular miRNAs (Kawahara & Mieda-Sato, 2012; Sambandan et al., 2017). The formation of stress granules and P-bodies have been observed *in vitro* when cells were stressed and TDP-43 was mislocalized to the cytoplasm, however this phenotype has not been detected in neuropathological studies and it is unknown if stress granules and P-bodies are relevant to human disease (Colombrita et al., 2009; Markmiller et al., 2018). Studies have demonstrated that altered TDP-43 expression (either through knockdown or overexpression methods) affected the regulation of particular transcript levels related to

autophagic activity, mostly indicating autophagy as a protective mechanism in cellular studies (Bose et al., 2011; Torres et al., 2018; X. Wang et al., 2015; Xia et al., 2016). TDP-43 expression levels have also been found to be associated with neurite morphology, where overexpression of TDP-43 resulted in impaired spine formation and axon outgrowth and neurite length (Fallini et al., 2012; Han et al., 2013; Herzog et al., 2017; Majumder et al., 2012). The N-terminal region of TDP-43 holds important stable biological roles for protein folding, functional homodimerization, and RNA splicing, but has also been found to be a critical component in mediating cytoplasmic TDP-43 aggregation with contrasting effects depending on whether the study was done in cells or in mice (Sasaguri et al., 2016; Zhang et al., 2013). Generally, TDP-43 serves many important functions in the cytoplasm normally and its dysregulation impacts these processes, likely leading to neuron death.

The presence of accumulated insoluble cytoplasmic TDP-43 truncated C-terminal fragments in brain tissue has been observed in neuropathological studies (Arai et al., 2010; Hasegawa et al., 2008; Igaz et al., 2008, 2009; Inukai et al., 2008; Kametani et al., 2016; Neumann et al., 2006). However, the contrasting results of *in vitro* studies has not definitively substantiated these TDP-43 C-terminal fragments as a toxic disease-driving component in ALS disease (Berning & Walker, 2019; Chhangani et al., 2021). It has been shown that expression of the TDP-43 C-terminal fragment in HEK293 cells led to insoluble cytoplasmic inclusion formation contained TDP-43 with phosphorylation and ubiquitination modifications (Zhang et al., 2009). But then in mouse models, the expression of TDP-43 C-terminal fragments did not cause neurodegeneration or cell

death, indicating the fragments as a by-product of disease mechanisms (Berning & Walker, 2019).

Some critics argue that TDP-43 aggregates are an artifact of neuronal degeneration and not essential components to drive disease mechanisms or cell toxicity (E. S. Arnold et al., 2013; Barmada et al., 2010; Hergesheimer et al., 2019; Igaz et al., 2011; Liu et al., 2013; Sasaguri et al., 2016; Walker et al., 2015). For example, expressing mutant TDP-43 was toxic to neurons in primary cortical cell models, but the presence of cytoplasmic aggregates was not necessary for cell toxicity, suggesting that TDP-43 mislocalization to the cytoplasm was the main toxic driver of disease mechanisms and cell death (Barmada et al., 2010).

There is a growing literature on the role of TDP-43 nuclear loss-of-function in ALS disease. Depletion of nuclear TDP-43 in motor neurons in mice generated ALS phenotypes of kyphosis, motor dysfunctions, muscle weakness, motor neuron loss, and astrocytosis in the spinal cord (Iguchi et al., 2013; L.-S. Wu et al., 2012). When comparing the effect of TDP-43 mislocalization on neuronal viability between two mouse models, one with full length wild-type TDP-43 and the other with TDP-43 containing a defective NLS, cytoplasmic TDP-43 inclusions were not necessary for cell toxicity and death (Igaz et al., 2011). Further, studies in cellular and mouse models of TDP-43 nuclear depletion showed defective axon growth and mitochondrial functions along with reduced protein synthesis, and significant changes in hundreds of mRNAs levels and altered splice events, primarily affecting genes that either encoded synaptic activity or genes with long introns (Briese et al., 2020; Cao et al., 2023; Polymenidou et al., 2011). TDP-43 nuclear depletion has been shown to result in altered RNA splicing and processing events

including alternative cryptic exon splicing and cryptic polyadenylation of genes such as *STMN2* and *UNC13A* (Baughn et al., 2023; A.-L. Brown et al., 2022; Buratti & Baralle, 2010; Jeong et al., 2017; Klim et al., 2019; J. P. Ling et al., 2015; Ma et al., 2022; Melamed et al., 2019; Polymenidou et al., 2011; Rot et al., 2017; Tollervey et al., 2011; L.-S. Wu et al., 2019). More recently, a set of studies demonstrated how TDP-43 nuclear loss induced cryptic polyadenylation at the 3' end of last exons in ALS, revealing a novel mechanism resulting from TDP-43 proteinopathy (F. J. Arnold et al., 2024; Bryce-Smith et al., 2024; Zeng et al., 2024). When TDP-43 was depleted from the nucleus of cells, cryptic exons were found to splice into mRNAs and alter translation and promote nonsense-mediated decay (NMD), which could be a central disease-driving mechanism underlying ALS and TDP-43 proteinopathies (J. P. Ling et al., 2015). Overall, the important regulatory roles of TDP-43, when normally in the nucleus, become severely impacted when mislocalized to the cytoplasm in ALS, and it is likely that the nuclear depletion is a critical component of disease-driving toxicity resulting in neurodegeneration.

Post-translational modifications (PTMs) of TDP-43

Post-translational modifications (PTMs) are important for the normal function of many proteins, TDP-43 included (Buratti, 2018; T. J. Cohen et al., 2012, 2015; Ikeda & Tsuchiya, 2004; McGurk et al., 2018). However, in disease, the role of aberrant PTMs is poorly understood. As mentioned previously, some of the TDP-43 abnormalities and modifications observed in ALS disease include acetylation, liquid–liquid phase separation (LLPS), mislocalization, phosphorylation, solubilization, proteolytic cleavage, truncation, and ubiquitination (Buratti, 2018; Prasad et al., 2019; Sternburg et al., 2022). The roles

of each modification may influence each other and contribute to a mixture of dynamic interactions or be completely independent of each other, and it is also unknown whether the modifications occur in a particular sequence or as a hodgepodge of events with indiscriminate occurrence.

Acetylation of lysine residues on TDP-43 normally regulates RNA binding, protein interactions, and localization (Choudhary et al., 2014). In neuropathological studies of ALS spinal cord tissue, acetylated TDP-43 was found to colocalize with full-length pTDP-43, suggesting acetylation as a pathological feature (T. J. Cohen et al., 2015; P. Wang et al., 2017). When TDP-43 was acetylated through transient stress or mutagenesis strategies in cell models, it resulted in impaired RNA binding and regulatory splicing abilities, altered TDP-43 phase separation, and increased the presence of insoluble aggregates that were also hyperphosphorylated (T. J. Cohen et al., 2015; Garcia Morato et al., 2022; Yu et al., 2021). Further, studies have demonstrated that lysine acetylation triggered an increase in TDP-43 phosphorylation and ubiquitination, suggesting phosphorylation and ubiquitination as mechanisms that counteracted TDP-43 acetylation and aggregation (Garcia Morato et al., 2022; P. Wang et al., 2017).

Ubiquitination has been identified as a PTM that regulates neuronal development and differentiation, as well as two degradation pathways: the ubiquitin-proteasome system and the autophagy-lysosomal pathway (Schmidt et al., 2021; Segref & Hoppe, 2009). Studies have shown that inhibiting the ubiquitin-proteasome or autophagy-lysosomal pathways resulted in increased TDP-43 aggregation (Urushitani et al., 2010; Van Eersel et al., 2011), suggesting ubiquitination as a mechanism in opposition of TDP-43 aggregation. In ALS neuropathological studies, cytoplasmic TDP-43 aggregates have

been found to be ubiquitinated and studies have revealed a genetic link between the mutations of genes within the degradation pathways (i.e. *UBQLN2, VCP, OPTN,* and *SQSTM1*) and TDP-43 binding (Budini et al., 2017; Cassel & Reitz, 2013; Deng et al., 2011; Ikeda & Tsuchiya, 2004; Neumann et al., 2006). Interestingly, overexpression of the Ubiquilin2 gene (*UBQLN2*) was found to promote the accumulation of cytoplasmic TDP-43 aggregates (Osaka et al., 2016; Picher-Martel et al., 2015). The results of these contrasting studies suggest ubiquitination as either an adaptive response to counteract protein misfolding and toxicity or a driver of TDP-43 dysregulation and aggregate formation.

The role that phosphorylation of TDP-43 may have in ALS progression is also highly debated—either participating in and possibly driving toxicity or protecting and possibly defending the affected neuron (Eck et al., 2021). In addition, the contributions of TDP-43 protein solubility and insolubility, phase changes, and aggregation add complexity to the overall disease mechanism. The phosphorylation sites of TDP-43 have been characterized using bioinformatic and biochemical methods, although definitive studies are lacking. Of the 64 predicted potential phosphorylation sites, there are 41 serine (S), 15 threonine (T), and 8 tyrosine (Y) residues. The common serine sites observed to be hyperphosphorylated in postmortem ALS cases are S369, S379, S403/404, and S409/410 (Hasegawa et al., 2008a; Inukai et al., 2008; Kametani et al., 2016; Neumann et al., 2009, 2020, 2021). The most implicated and studied phosphorylation site in ALS pathogenesis is S409/410.

Phosphorylation may regulate the phase separation of TDP-43 and alter its solubility and polymerization, affecting TDP-43's resistance to proteasomal degradation

or localization and resulting in converting TDP-43 into irreversible aggregates (Eck et al., 2021; Gasset-Rosa et al., 2019; Guenther et al., 2018; Newell et al., 2019; Nonaka et al., 2013; A. Wang et al., 2018; Yamashita et al., 2016). Some studies demonstrate phosphorylation of TDP-43 as a toxic mechanism where oligomers attenuated aggregates in cells, fruit flies, and nematode models (Chiang et al., 2022; Choksi et al., 2014; Hicks et al., 2020; Kim et al., 2015; Liachko et al., 2010; Nonaka et al., 2016; Zhang et al., 2010). Other studies suggest phosphorylation as a compensatory mechanism resulting from TDP-43 aggregation and may play a protective role (Brady et al., 2011; Gruijs Da Silva et al., 2022; H.-Y. Li et al., 2011). The temporal dynamics of TDP-43 phosphorylation remain unknown, such as how far upstream in pathogenesis or whether it precedes or follows TDP-43 aggregation. Overall, little is known about the mechanism responsible for TDP-43 phosphorylation and its influence on the formation of cytoplasmic, aggregated, and pathological TDP-43.

Kinases in TDP-43 phosphorylation and identification of *CSNK1E* in ALS

Many kinases have been proposed to phosphorylate TDP-43 and promote aggregate formation and cell toxicity, the main kinases being CK1δ, CK1ε, CK2α, CDC7, TTBK1/2 and others (Alquezar et al., 2016; Carlomagno et al., 2014; Liachko et al., 2013, 2014; Nozal et al., 2022; Rojas-Prats et al., 2021; Salado et al., 2014; L. M. Taylor et al., 2018; Tian et al., 2021). Our previously published study used laser capture microdissection technique to isolate motor neurons in lumbar spinal cords of sporadic ALS patients for RNA-sequencing and eCLIP analysis. The eCLIP dataset revealed that TDP-43 directly bound the 3' untranslated region (3' UTR) of *CSNK1E*, and TDP-43

knockdown via shRNA *in vitro* led to reduced *CSNK1E* mRNA levels. By comparison of the list of genes significantly altered in the RNA-sequencing dataset and genes that directly bound TDP-43 in the eCLIP dataset, we identified the upregulation of casein kinase 1 epsilon gene (*CSNK1E*, encoding CK1ε protein) as being tightly correlated with phosphorylated TDP-43 (pTDP-43) pathology (Krach et al., 2018). This evidence suggested that CK1ε was a regulator of TDP-43 phosphorylation and may have a toxic gain of function role in ALS (Figure 1.1A).

CSNK1E is a member of the casein kinase 1 family which consists of monomeric, constitutively active, serine/threonine-selective enzymes that regulate various signal transduction pathways in most eukaryotic cell types. CK1 isoforms are involved in Wnt signaling, circadian rhythms, nucleocytoplasmic shuttling of transcription factors, DNA repair, and DNA transcription. There are seven family members in the CK1 family, alpha, beta 1, gamma 1, gamma 2, gamma 3, delta, and epsilon, and each isoform is encoded by a distinct gene. A closely related family member, *CSNK1D* (encoding CK1δ protein), shares 84% homology with *CSNK1E*, largely in their kinase domain and autoregulatory C-terminus end (Cheong & Virshup, 2011; Fish et al., 1995; Fulcher & Sapkota, 2020). CK1δ and CK1ε have been primarily studied for their roles in circadian rhythms. Selective inhibition of CK1ε either genetically or pharmacologically had little effect on circadian timing whereas altering CK1δ activity significantly lengthened the regulation of circadian phase-shifting in mice (Badura et al., 2007; Eide et al., 2005; Eide & Virshup, 2001; Etchegaray et al., 2009, 2010; Lee et al., 2001; Meng et al., 2010; Walton et al., 2009).

Given the significant sequence overlap between CK1δ and CK1ε, it would be imperative to dissect whether they possess redundant roles in particular signaling

pathways or if they may serve independent functions in regulating these biological processes. Further, either or both CK1δ and CK1ε may contribute to the aberrant TDP-43 protein phosphorylation observed in ALS, as mentioned above. Multiple phosphorylation sites have been identified to be phosphorylated by CK1, including ALS-disease relevant S403/404 and S409/410 on the C-terminus end of TDP-43, although it was unclear which isoform(s) of CK1 were capable of doing so (Kametani et al., 2009). Various studies in *in vitro* and *in vivo* models using either genetic or pharmacologic methods have implicated either only CK1δ or CK1ε in phosphorylating TDP-43 and demonstrating increased cytoplasmic TDP-43 aggregates and contribution to cell toxicity (Choksi et al., 2014; Hicks et al., 2020; Liachko et al., 2010; Martínez-González et al., 2020). No study has thoroughly completed a side-by-side comparison of the effects resulting from CK1δ- and CK1ε-mediated TDP-43 phosphorylation within the same research model.

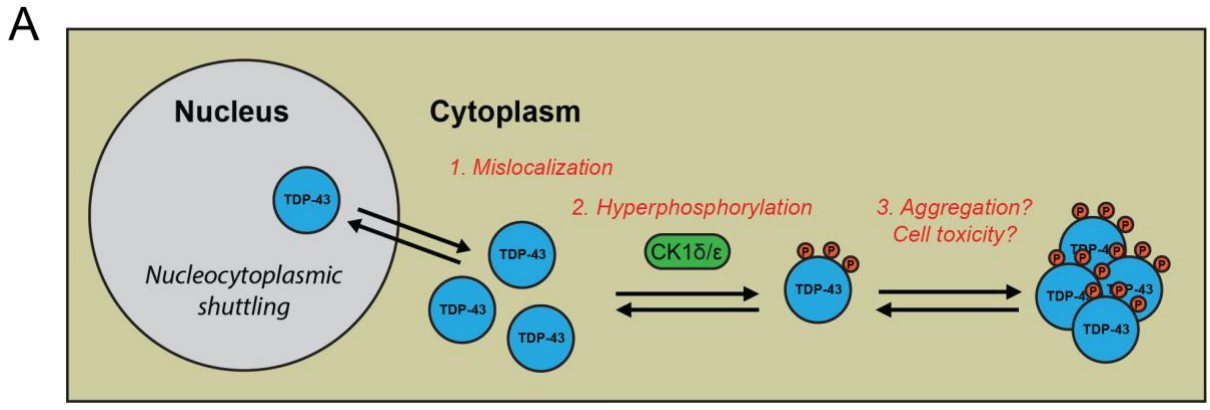


Figure 1.1 Graphical abstract of proposed CK1-mediated phosphorylation of TDP-43 in ALS.

(A) Dysregulated CK1δ and CK1ε protein kinases hyperphosphorylate TDP-43 which then contribute to neurotoxicity in ALS.

Research models of ALS and TDP-43 proteinopathy

As mentioned previously, TDP-43 nuclear clearance and cytoplasmic accumulation into inclusions in motor neurons are primary histopathological hallmarks of familial and sporadic ALS cases (Neumann, 2009; Nolan et al., 2020). Striking observations in patient histological neuropathology studies revealed different types of TDP-43 inclusions, which includes skein-like, diffuse, dot-like, and dense-round inclusions. Of these varietals, dot-like inclusions seem to be the most frequently observed type of inclusion in surviving motor neurons from patient spinal cord tissues (Saberi et al., 2015). When developing cellular and animal models for ALS research, it is important for the model to generate relevant symptom phenotypes observed in patient disease progression and molecular and cellular signatures of neuropathological studies. Advances in ALS disease modeling have been able to recapitulate some features of TDP-43 proteinopathy, but not all, and most of the cellular and animal models possess significant limitations and remain discordant with human disease.

There are a variety of cell models used in ALS-related research, each with their own set of limitations. Commonly used cell lines include HEK293, U2OS, SH-SY5Y, and NSC-34 cells, most of which require an external stressor or genetic manipulation to induce features of TDP-43 proteinopathy. A growing number of studies utilize iPSC models, which require significant resources and time to generate. However, studies utilizing patient iPSC-derived motor neurons or differentiated neural stem cells develop heterogeneous cultures with phenotypic variations and typically require a stressor to induce phenotypes, almost all of which lack resemblance to essential neuropathological observations such as TDP-43 mislocalization and phosphorylation (Giacomelli et al.,

2022; W. Guo et al., 2017; Richard & Maragakis, 2015; Volpato & Webber, 2020). Many of the commonly used cell models do not exhibit progressive cell toxicity or death, so most conclusions are limited in interpretation and the disease mechanisms need to be explored through *in vivo* mammalian studies.

Advancements in genetic engineering have facilitated the development of over 100 mouse strains available for ALS-related research, which are offered through The Jackson Laboratory (JAX) repository. Some of the most popularly used mutation-associated ALS mouse models include expressions of *SOD1-G38A, C9orf72, FUS, ATXN2, TDP-43-M337V, TDP-43-Q331K, TDP-43-A315T,* and *STMN2*. Each mouse model displays variable disease phenotypes, none of which completely capture all the observations in ALS human patients (Lutz, 2018; Philips & Rothstein, 2015). Most notably, mouse models do not generate TDP-43 inclusions that reflect the skein-like, dot-like, or dense-round inclusions, but may demonstrate diffuse cytoplasmic TDP-43 accumulation. Further, only a subset of cellular and animal models generates PTMs, like phosphorylation, ubiquitination, or acetylation on the mislocalized TDP-43, which is suitable for studying and testing specific research questions, but it is imperative to interpret results sparingly and acknowledge the limitations of the experimental system.

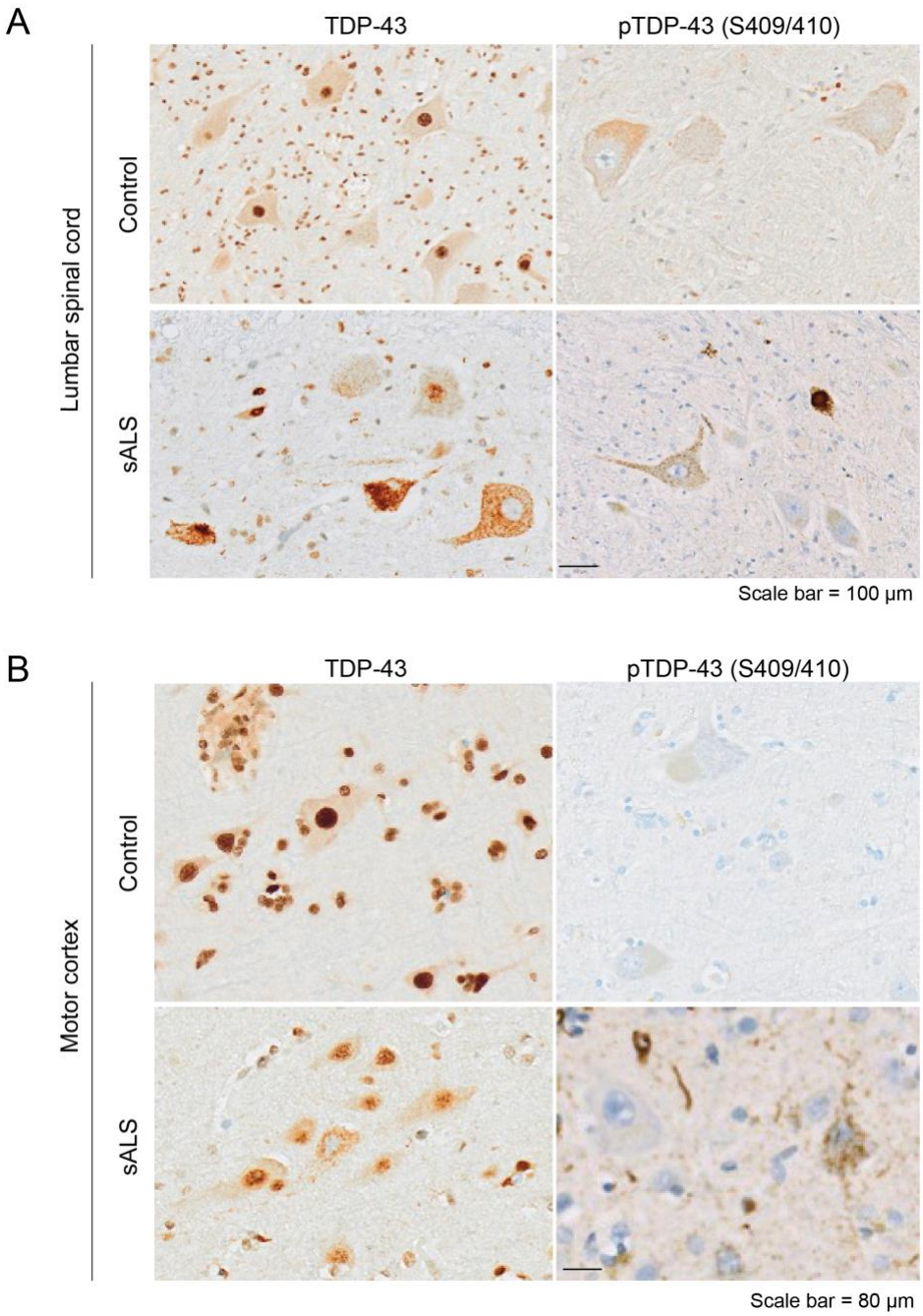


Figure 1.2 Images of IHC staining for patient tissue samples.

(A-B) Representative IHC images of control and sALS patient lumbar spinal cord (A) and brain motor cortex tissue (B) with staining for TDP-43 and pTDP-43. Control patients have normal nuclear TDP-43 and no pTDP-43 signal (one cell in pTDP-43-stained control image displays lipofuscin, a consistent feature of aging). sALS samples have diseased motor neurons with nuclear-depleted and mislocalized cytoplasmic TDP-43 inclusions that are dot-like, dense-round, diffuse, and skein-like. Few surviving motor neurons in sALS cases appear to have normal TDP-43 expression at end-stage.

Challenges and therapeutic developments in ALS

Clinical trial designs require the use of biomarkers and other clinical outcome measures to determine if a treatment has a meaningful effect in patients. What is lesser known, is that biomarker approval by the FDA and Clinical and Laboratory Standards Institute (CLSI) takes an average of 5 to 8 years, costing over $10 million. These challenges to biomarker discovery, assay development, and validation can be daunting for some commercial entities with limited motivation and resources. Nevertheless, biomarker identification for clinical and research application has been and continues to be an important research area for neurodegenerative diseases. A good biomarker is imperative for demonstrating a biological response to a therapeutic intervention and can also help categorize or stage patients by the levels of biomarker presence or absence. Biomarkers that are currently being studied for therapy development for ALS include blood neurofilament light chain (Nf-L), phosphorylated neurofilament heavy chain (pNFH), SOD1 in CSF, urinary p45 neurotrophin receptor extracellular domain, magnetic resonance imaging (MRI), electrophysiological measures, and motor strength assessments (Benatar et al., 2016).

TDP-43 and pTDP-43 expression are defining hallmarks of TDP-43 proteinopathy in ALS cases and are being studied for their biomarker potential in CSF and plasma patient samples. These studies have generated contrasting results where measuring TDP-43 in plasma displayed increased TDP-43 levels in ALS disease, but variable changes amongst patients in a longitudinal study were detected (Ren et al., 2021; Verstraete et al., 2012). Generally, more longitudinal studies are necessary to determine

whether TDP-43 or pTDP-43 could be used as a marker of disease progression or prognosis (Feneberg et al., 2018; Goossens et al., 2015; Verber et al., 2019).

There are currently six approved drugs by the U.S. Food and Drug Administration (FDA) for ALS treatment. Drugs are either considered symptomatic therapies or disease-modifying therapies. The approved disease-modifying drugs include Rilutek (riluzole), Tiglutik (thickened riluzole), Exservan (riluzole oral film), Radicava (edaravone), and Qalsody (tofersen). Nuedexta, approved in 2011, is the only drug for symptomatic ALS therapy and treats pseudobulbar affect (PBA), which is the frequent involuntary behavior of exaggerated crying and laughing that is not reflective of actual feelings in patients (Brooks et al., 2004). Various strategies are actively under investigation for therapeutic development as treatments for ALS and related TDP-43 proteinopathies. These strategies include small molecule inhibitor compounds, antisense oligonucleotides (ASOs), viral-mediated gene therapy, and antibody-based immunotherapy.

Rilutek (riluzole), a small molecule compound, was approved in 1995, making it the first approved drug to treat ALS. Rilutek is formulated as an oral pill, but other forms of riluzole have been developed and approved, such as Tiglutik which is a thickened liquid form of riluzole to prevent tablet crushing, and Exservan which is an oral film formulation of riluzole for patients that have difficulty swallowing and can be dissolved on the tongue. The continued prescribed use of riluzole in patients has been hotly debated since it has been shown to only prolong patient lifespan by a few months on average (R. Miller et al., 2002). The mechanism of action for riluzole was thought to be glutamate inhibition, but the molecular target(s) have been contested (Bensimon et al., 1994). Since its approval, it has been proposed that Riluzole could be an ATP-competitive inhibitor that targeted

CK1δ based upon computational modeling analysis (Bissaro et al., 2018). Radicava (edaravone), also a small molecule, was approved in 2017 as an oral pill and then had an oral formulation approved in 2022. It is a free radical scavenger and its mechanism of action is likely reduction of oxidative stress in ALS patients (Luo et al., 2019; Rothstein, 2017; Yoshino & Kimura, 2006).

ASOs are synthetic oligonucleotides, usually 16-20 nucleotides in length, that selectively bind to, cleave, and degrade target RNAs (Bennett, 2019). ASO technology has advanced and matured rapidly, and the first ASO therapy, Nusinersen (Spinraza), was FDA approved in 2016 for the treatment of spinal muscular atrophy (SMA) (Chiriboga, 2017; Finkel et al., 2017). SMA is caused by *SMN1* gene loss-of-function mutations and Nusinersen modifies the alternative splicing of the *SMN2* gene to produce functional *SMN1* gene and increase the level of SMN protein for cell survival (Ramos et al., 2019; Rigo et al., 2012; Zanetta et al., 2014). ASO therapy holds potential as a viable strategy for gene mutation-associated neurodegenerative diseases and is currently being studied in preclinical and clinical trial stages for ALS, Huntington's disease (HD), Parkinson's disease (PD), and Alzheimer's disease (AD) (Alarcón-Arís et al., 2020; Bennett, 2019; Cole et al., 2021; Grabowska-Pyrzewicz et al., 2021; McCampbell et al., 2018; Mummery et al., 2023; Suvarna et al., 2022; Tabrizi et al., 2019).

For *FUS* mutation-associated ALS, silencing *FUS* expression in mouse models and preclinical human studies using an ASO approach effectively reduced mutant FUS protein aggregates and delayed motor neuron degeneration (Korobeynikov et al., 2022). Studies in cells, mice, and human, have shown proof-of-concept for ASO therapy in the treatment of *C9orf72* mutation-associated ALS by targeting the dipeptide repeat

expansions (DPRs) of the *C9orf72* gene, which have been presumed to have a toxic gain-of-function role in disease (Donnelly et al., 2013; Tran et al., 2022). Clinical trials testing ASO treatment for *C9orf72* mutation-associated ALS were recently discontinued due to poorer trends compared to the placebo group despite demonstrating successful target engagement of reduced DPRs (Sattler et al., 2023). ASOs targeting *ATXN2* mutation-associated ALS have demonstrated efficacy in preclinical studies to extend survival and improve motor function in mouse models (Becker et al., 2017; Scoles et al., 2017) and is now being tested in human clinical trials. This work is particularly interesting since *ATXN2* interacts with TDP-43, thereby *ATXN2* holds promise as a genetic target to modulate TDP-43 as a possible therapy for sporadic ALS patients. Very recently, Qalsody (tofersen) was approved in 2023 to treat *SOD1* mutation-associated ALS, and the drug effectively targeted the mutant *SOD1* mRNA and reduced the production of mutant SOD1 protein (T. Miller et al., 2020; T. M. Miller et al., 2013; Mullard, 2021). Like many other therapeutic development initiatives, the inherent differences between animal models and humans presents additional challenges on top of reducing toxicities and improving delivery methods for ASO therapy to be effective. However, new drug delivery systems are emerging, one being a cholesterol functionalized DNA/RNA heteroduplex capable of crossing the CNS blood-brain barrier which may improve ASO delivery into the target tissues (Nagata et al., 2021).

Lentivirus (LV)- and adeno-associated virus (AAV)-mediated gene therapy using gene supplementation, gene silencing, or genome editing approaches have advanced in recent years, where a single injection may have a long-lasting therapeutic effect (Abulimiti et al., 2021; Amado & Davidson, 2021; Q. Ling et al., 2023). Gene supplementation

provides a healthy copy of the affected gene to compensate for the loss-of-function resulting from the mutated gene. Gene silencing leverages mechanisms of RNA interference (RNAi), which reduces gene expression and translation of a specific mRNA and is used for diseases caused by gene mutations with a toxic gain-of-function role. Short interfering RNAs (siRNAs), short hairpin RNAs (shRNAs), and micro RNAs (miRNAs) are common methods of RNAi (Castanotto & Rossi, 2009). Genome editing uses CRISPR-Cas9 methods to execute precise nucleotide base modifications and correct for either loss-of-function or gain-of-function genetic mutations.

Currently, there are three FDA-approved gene replacement therapy treatments for CNS and neuromuscular disorders, which are Zolgensma for spinal muscular atrophy (SMA), Skysona for cerebral adrenoleukodystrophy (CALD), and Elevidys for Duchenne muscular dystrophy (DMD) (Day et al., 2020; Hoy, 2019; Keam, 2021; Larkin, 2022; Mendell et al., 2020, 2024; Muntoni et al., 2023; Rodriguez-Calienes et al., 2021; Stevens et al., 2020; Zaidman et al., 2023). There are no FDA-approved drugs for gene silencing or genome editing gene therapies, but proof-of-concept preclinical studies are heavily underway for neurodegenerative diseases like spinocerebellar ataxia (SCA), Huntington's disease (HD), Parkinson's disease (PD), and Alzheimer's disease (AD) (Curtis et al., 2017; Franich et al., 2008; Kang et al., 2023; Kiyota et al., 2015; Martier & Konstantinova, 2020; Miniarikova et al., 2017; Mittermeyer et al., 2012; Niethammer et al., 2017; Zhao et al., 2016).

For ALS in particular, studies in *SOD1* mutation-associated ALS mouse models and non-human primates, even a couple human cases, have demonstrated safety and efficacy with AAV-mediated shRNA or miRNA gene therapy strategies targeting mutant

SOD1 in ameliorating motor deficits and neurodegeneration phenotypes (Biferi et al., 2017; Borel et al., 2016, 2018; Bravo-Hernandez et al., 2020; Foust et al., 2013; Iannitti et al., 2018; Mueller et al., 2020; Stoica et al., 2016; H. Wang et al., 2014). Emerging studies have also utilized AAV-miRNA methods to reduce accumulation of toxic DPRs in cellular models of *C9orf72* mutation-associated ALS (Martier, Liefhebber, García-Osta, et al., 2019; Martier, Liefhebber, Miniarikova, et al., 2019). It has been shown that intrathecal injection of AAV1 expressing a shRNA targeting CK1δ mitigated neurodegeneration of peripheral nerves in a TDP-43 mutant mouse model (Gonzalez-Gonzalez et al., 2021). RNAi strategies have shown preclinical efficacy and next steps are to advance into human studies.

CRISPR-Cas9 is a gene editing technique that leverages the nuclease activity of the Cas9 protein to cut at specific target sites directed by a guide RNA (gRNA) and cause DNA double stranded breaks (DSB) and subsequent DNA damage spontaneous repair to achieve genetic edits. CRISPR-Cas9 techniques have been explored for proof-of-concept as a therapeutic strategy in cellular and mouse models of neurodegenerative disease for AD, PD, and HD (Kantor et al., 2018; Konstantinidis et al., 2022; Ortiz-Virumbrales et al., 2017; Shin et al., 2016; S. Yang et al., 2017). For ALS disease, studies have use CRISPR-Cas9 methods to reduce DPR levels, RNA foci, haploinsufficiency, and other hallmarks of *C9orf72* mutation-associated ALS *in vitro* and *in vivo* (Ababneh et al., 2020; Deng et al., 2021; Krishnan et al., 2020; Meijboom et al., 2022; Piao et al., 2022). Similarly, improved motor function, decreased muscle atrophy, and prolonged survival was observed when CRISPR-Cas9 was used to reduce mutant *SOD1* levels in a

SOD1 mutation-associated ALS mouse model (Duan et al., 2020; Gaj et al., 2017; Lim et al., 2020).

Despite these proof-of-concept results, the gene therapy field still lacks knowledge of target specificity, potential off-target effects, and host immune responses from virus-mediated and CRISPR-Cas9 techniques. There are limitations on the vector construct and gene insert sizes, so only relatively small genes associated with disease can currently be targeted. More studies are needed to optimize the timing and critical period for treatment delivery and improve dosing routes (i.e. intrathecal, intravenous, intracerebroventricular, and spinal subpial delivery) to deliver past the blood brain barrier into the CNS. CRISPR-Cas9 in particular faces ethical concerns for its use in human therapeutics. Generally, a better understanding and additional studies to improve safety and efficacy of gene therapy techniques are imperative to advance these strategies and apply them to the treatment of CNS disorders and neurodegenerative diseases (Lubroth et al., 2021).

Monoclonal antibody (mAb) immunotherapy research has largely focused on creating mAbs that can bind specifically to extracellular targets and block their function, thus preventing disease mechanisms from advancing (Poulin-Brière et al., 2021). Recently, the FDA has approved the drug Lecanemab, a monoclonal antibody that binds to Aβ fibrils as a treatment for AD patients (Van Dyck et al., 2023). Strategies using mAbs for ALS treatment are being studied, with some having demonstrated pre-clinical efficacy for binding to misfolded SOD1 in a *SOD1* mutation-associated ALS mouse model (Boulis & Donsante, 2023; Gros-Louis et al., 2010; Maier et al., 2018) and binding to polyGA proteins in a *C9orf72* mutation-associated ALS mouse model (Nguyen et al., 2020) to

improve survival, behavior, and neurodegenerative phenotypes. In addition, studies have shown that mAb-mediated targeting of the C-terminal domain of TDP-43 helped reduce signs of neurodegeneration and TDP-43 aggregation *in vitro* and *in vivo* (Afroz et al., 2023; Riemenschneider et al., 2023). However, mAb immunotherapy is severely limited by the large size of antibodies, making it challenging to cross the blood brain barrier and resulting in poor CNS penetrance and ineffective uptake into target tissues for therapeutic availability.

The development of small molecules for ALS therapy has advanced in recent years to target various mechanisms thought to contribute to disease progression. These compounds were developed to target TPD-43 phase separation, RNA-protein interactions, TDP-43 phosphorylation, autophagy pathways, and more (D. G. Brown et al., 2020). Many studies have suggested kinase dysregulation as a disease mechanism in ALS and various kinase inhibitors are being tested in human clinical trials in North America and Europe. These include Masitinib (c-KIT receptor inhibitor), Fasudil (ROCK1/2 inhibitor), Rapamycin (mTOR inhibitor), Bosutinib (Src/c-Abl inhibitor), Lithium (GSK-3 inhibitor), GDC-0134 (DLK inhibitor), and DNL747 (RIPK1 inhibitor). Protein kinase inhibitors that are in pre-clinical development for ALS include compounds that target CK1, CDC7, MAP3K/ASK1, p38/MAPK, PTK2, PKC, EpHA4, TrKB, TTBK1/2, MAPK4K, HIPK2, CDK5, MEK5, JNK, PKR, and S6K1 (Palomo et al., 2021).

Kinases that affect TDP-43 phosphorylation have been tested *in vitro* and *in vivo* to varying degrees of success (W. Guo et al., 2020). CK1 kinases, are of particular interest for development, due to studies revealing its involvement in many disorders like ALS, AD, familial advanced sleep phase syndrome, and cancer (Cozza & Pinna, 2016; S.-S. Li et

al., 2021; Perez et al., 2011). Given the pleiotropic roles kinases have in regulating biological pathways, kinase cocktail approaches have been proposed, where a combined treatment strategy may help achieve optimal clinical benefit for patients. However, the use of kinase inhibitors in ALS still requires a better understanding of potential off-target effects, host immune response, identification of phosphorylation sites that are affected during treatment, and clarity on whether the inhibition is mediating TDP-43 toxicity directly or a pathway downstream of TDP-43 (D. G. Brown et al., 2020). Generally, kinases are a favorable druggable target and high throughput screens can be used to efficiently evaluate the therapeutic potential for novel synthesized or commercially established inhibitor compounds.

Acknowledgements

Chapter 1, in part, is a reformatted reprint of the material as it appears in Ko, V. I., Ong, K., Cleveland, D. W., Yu, H., & Ravits, J. M. (2024). CK1δ/ε kinases regulate TDP-43 phosphorylation and are therapeutic targets for ALS-related TDP-43 hyperphosphorylation. *Neurobiology of Disease*, *196*, 106516. https://doi.org/10.1016/j.nbd.2024.106516. The dissertation author was the primary investigator and author of this paper.

Chapter 2 : Novel cellular models reveal CK1δ/ε kinases regulate TDP-43 phosphorylation and are targets for ALS-related TDP-43 hyperphosphorylation

Abstract

Hyperphosphorylated TAR DNA-binding protein 43 (TDP-43) aggregates in the cytoplasm of neurons is the neuropathological hallmark of amyotrophic lateral sclerosis (ALS) and a group of neurodegenerative diseases collectively referred to as TDP-43 proteinopathies that includes frontotemporal lobar degeneration/ frontotemporal dementia (FTLD/FTD), Alzheimer's disease (AD), limbic-predominant age-related TDP-43 encephalopathy (LATE), and Lewy body disease (LBD). The mechanism of TDP-43 phosphorylation is poorly understood. Previously we reported casein kinase 1 epsilon gene (*CSNK1E* gene encoding CK1ε protein) as being tightly correlated with phosphorylated TDP-43 (pTDP-43) pathology. We pursued studies to investigate in cellular models and *in vitro* how CK1ε and CK1δ (a closely related family sub-member) mediate TDP-43 phosphorylation in disease. Kinase activity assays and predictive bioinformatic database were used to determine whether either CK1δ and/or CK1ε directly bound to TDP-43. In our novel inducible cellular models, which generated translocated phosphorylated TDP-43 (pTDP-43) and cytoplasmic aggregation, we used siRNA and small molecule inhibitors to reduce kinase activity and examine the effect on TDP-43 phosphorylation. Immunoblotting and immunofluorescence staining were used to measure pTDP-43 levels and expressions. We validated the direct binding interaction

between TDP-43 and either CK1δ and CK1ε using kinase activity assays and predictive bioinformatic database. Reducing CK1 kinase activity with siRNA or small molecule chemical inhibitors resulted in significant reduction of pTDP-43, in both soluble and insoluble protein fractions. We also established CK1δ and CK1ε are the primary kinases that phosphorylate TDP-43 compared to CK2α, CDC7, ERK1/2, p38α/MAPK14, and TTBK1, other identified kinases that have been implicated in TDP-43 phosphorylation. Throughout our studies, we were careful to examine both the soluble and insoluble TDP-43 protein fractions, the critical protein fractions related to protein aggregation diseases. These results identify CK1s as critical kinases involved in TDP-43 hyperphosphorylation and aggregation in cellular models and *in vitro* and in turn are potential therapeutic targets by way of CK1δ/ε inhibitors.

Introduction

ALS is a fatal adult-onset neurodegenerative disease hallmarked by TDP-43 proteinopathy phenotypes which includes TDP-43 nuclear clearance and the presence of cytoplasmic TDP-43 inclusions where a portion has been observed to contain hyperphosphorylated aggregates. TDP-proteinopathy is observed in 97% of all sporadic and familial ALS cases, making it a significant unifying disease-related mechanism despite varying causes of disease (R. H. Brown & Al-Chalabi, 2017; S.-C. Ling et al., 2013; Polymenidou et al., 2012; Swinnen & Robberecht, 2014).

The role phosphorylation of TDP-43 in ALS pathogenesis and progression is poorly understood, with some studies claiming it drives toxicity and aggregate formation and others suggesting it protects and defends the affected neuron. The primary

phosphorylation sites on TDP-43 that have been observed in neuropathological studies include S369, S379, S403/404, S409/410 (Hasegawa et al., 2008, 2011; Inukai et al., 2008; Kametani et al., 2016; Neumann et al., 2009, 2020, 2021). Phosphorylation has been proposed to regulate the solubility, phase separation, and polymerization properties of TDP-43 which affects its susceptibility for degradation (Gasset-Rosa et al., 2019; Newell et al., 2019; Nonaka et al., 2013; A. Wang et al., 2018; Yamashita et al., 2016). Some studies have demonstrated increased toxicity and aggregate formation with TDP-43 phosphorylation in varying models such as cells, fruit flies, and nematode models (Choksi et al., 2014; Hicks et al., 2020; Kim et al., 2015; Liachko et al., 2010; Nonaka et al., 2016; Zhang et al., 2010). However, there has also been an emergence of literature that suggests phosphorylation as a protective compensatory mechanism as a result of aggregate formation (Brady et al., 2011; Gruijs Da Silva et al., 2022; H.-Y. Li et al., 2011). Interestingly, in a study on the FUS subtype of ALS (where FUS ALS patients do not develop TDP-43 proteinopathy), CK1δ/ε-mediated phosphorylation of FUS increased the solubility of FUS *in vitro* and overexpression of CK1δ significantly rescued degeneration in a transgenic fly model (Kishino et al., 2022). Given the lack of consensus within the field on the role of TDP-43 phosphorylation in disease mechanisms, we sought to identify the primary kinase responsible for phosphorylating TDP-43 in ALS and study its influence on the formation of cytoplasmic, aggregated, and pathological TDP-43.

We previously studied motor neurons in lumbar spinal cords of sporadic ALS patients by leveraging laser capture microdissection technique to isolate motor neurons for RNA-sequencing and eCLIP analysis. Through this work, we identified the upregulation of casein kinase 1 epsilon gene (*CSNK1E*, encoding CK1ε protein) as being

strongly correlated with phosphorylated TDP-43 (pTDP-43) pathology (Krach et al., 2018). The relationship between *CSNK1E* and TDP-43 was further explored in iPSC-derived motor neuron models, where overexpression of *CSNK1E* resulted in increased pTDP-43 formation in the cytoplasm of cells (Krach et al., 2018). This evidence suggested that CK1ε was a regulator of TDP-43 phosphorylation and may have a toxic gain of function role in ALS.

CSNK1E is a member of the casein kinase 1 (CK1) family which consists of monomeric, constitutively active, serine/threonine-selective enzymes that are encoded by distinct genes for alpha, beta 1, gamma 1, gamma 2, gamma 3, delta, and epsilon isoforms. CK1 kinases regulate various signal transduction pathways in most eukaryotic cell types. *CSNK1E* shares 84% homology with *CSNK1D* (which encodes CK1δ protein), with 98% sequence similarity in their kinase domain and 53% in their C-terminal regulatory domain (Cheong & Virshup, 2011; Fish et al., 1995; Fulcher & Sapkota, 2020). CK1δ and CK1ε are essential in regulating the genetic transcription-translation feedback loops of circadian rhythm biology in mammals. Selective inhibition of CK1ε either genetically or pharmacologically had little effect on circadian timing whereas altering CK1δ activity significantly affected the regulation of circadian phase-shifting in mice (Badura et al., 2007; Etchegaray et al., 2009, 2010; Meng et al., 2010; Walton et al., 2009). With the differential effects of CK1δ and CK1ε in circadian biology despite their sequence identity, it would be critical to study both CK1δ- and CK1ε- mediated phosphorylation of TDP-43 in ALS disease. Various studies in *in vitro* and *in vivo* models using either genetic or pharmacologic methods have implicated either only CK1δ or CK1ε in phosphorylating TDP-43 and contributing to cell toxicity and the formation of oligomeric

TDP-43 species (Choksi et al., 2014; Hicks et al., 2020; Liachko et al., 2010; Martínez-González et al., 2020). No study has thoroughly completed a side-by-side comparison of the effects resulting from CK1δ- and CK1ε-mediated TDP-43 phosphorylation.

In this study, we demonstrate that both CK1δ and CK1ε are upstream regulators that phosphorylate TDP-43 and we leverage multiple intervention strategies to examine the emerging complex dynamics between CK1δ and CK1ε in soluble and insoluble protein fractions of TDP-43 in ALS-related disease. First, our cell-free kinase assay shows that TDP-43 is a substrate of both CK1δ and CK1ε, and CK1 kinases are most favorable for phosphorylating the S409/410 sites. Using novel doxycycline (dox) inducible U2OS and SH-SY5Y cell models, we generated cytoplasmic pTDP-43 inclusions to study CK1-dependent phosphorylation. We show that siRNA-mediated knockdown of CK1δ and CK1ε results in significantly decreased pTDP-43 at the S409/410 sites. Furthermore, testing highly selective small molecule CK1 inhibitors also yields significant dose-dependent reduction of cytoplasmic pTDP-43 in our cell models. In comparison to compounds selective for inhibiting other kinases identified to bind TDP-43, our studies demonstrate CK1δ and CK1ε kinases as the predominant kinases responsible for phosphorylating TDP-43 at disease-relevant S409/410 sites. Finally, we provide proof-of-principle for utilizing CK1 inhibitors *in vivo* to reduce pTDP-43 levels in soluble and insoluble TDP-43 protein fractions and underscore the importance of examining both soluble and insoluble TDP-43 levels in future studies related to ALS and other TDP-43 proteinopathies.

Results

CK1δ and CK1ε kinases directly phosphorylate TDP-43 and are most favorable to phosphorylate the S409/410 site

We designed a cell-free kinase assay to test whether TDP-43 protein was a substrate that could be phosphorylated by either CK1δ or CK1ε protein kinase. In this assay, the recombinant human full-length CK1δ or CK1ε enzyme (which was titrated with 5-fold serial dilutions) was incubated with 1 µM recombinant human full-length TDP-43 substrate and 1 µM radiolabeled [γ-^{33}P] ATP. In this reaction mixture, [γ-^{33}P]-labeled phosphate group transferred from ATP to TDP-43 and then the remaining radiolabeled ATP was separated from radiolabeled TDP-43 by spotting the reaction mixture on a filter membrane (Figure 2.1A). Samples were analyzed after 1 hour and 2 hours of incubation and the activity was calculated as a percentage of ATP to ADP conversion. We included control conditions of reaction mixtures that contained only CK1 enzyme with [γ-^{33}P] ATP in buffer without TDP-43 substrate because CK1δ and CK1ε undergo autophosphorylation (Cullati et al., 2022), so this measured value was subtracted as background.

Our results demonstrate comparable dose-dependent phosphorylation of TDP-43 by CK1δ and CK1ε, where enzyme concentrations of 10 nM for CK1δ and 15 nM for CK1ε resulted in approximately 10% ATP to ADP conversion at 2 hours (Figure 2.1B-C). The phosphate transfer onto TDP-43 by CK1, for example, was 553 nM phosphate with 200 nM of CK1δ and 540 nM phosphate with 200 nM of CK1ε with 1 hour incubation, resulting in a stoichiometry of roughly 3 phosphates for each CK1δ and CK1ε kinase molecule. The kinetics differed slightly between CK1δ and CK1ε where CK1ε did not plateau as much

as CK1δ. This data supports TDP-43 as a substrate that can be phosphorylated by CK1δ and CK1ε kinases.

To determine serine/threonine (Ser/Thr) sites on TDP-43 that could be phosphorylated by CK1 kinases, we utilized a publicly available bioinformatic database, The Kinase Library (Johnson et al., 2023). Previous work using postmortem patient tissues and other models indicated that CK1 kinases generally phosphorylate TDP-43 (Hasegawa et al., 2008; Kametani et al., 2009). The Kinase Library resource contained data from positional scanning peptide arrays which determined optimal substrate sequence specificities of 303 human Ser/Thr kinases. It could then use the data to computationally identify kinases that were strongly predicted to phosphorylate a particular residue on any given substrate. The recognition motif profiles cover every branch of the human Ser/Thr kinase family tree, of which CK1 kinases are considered to be a part of the acidophilic group.

The Kinase Library provides unbiased identification of candidate kinases most likely to phosphorylate TDP-43 at particular serine residues of interest. The percentile score rankings for the given kinase-substrate pair indicates the favorability for a kinase to score higher than all other profiled kinases in the atlas for the substrate of interest. Most notably, we identified 11 out of the 22 serine residues within the C-terminus glycine-rich domain of TDP-43 to have 99-100% favorability to be phosphorylated by CK1δ or CK1ε (Figure 2.1D, Table 2.1). These 11 sites included S379, S409, and S410 that have been strongly implicated in ALS disease.

Kinases are involved in complex and intricate pathways, sometimes requiring an initiation event to carry out its own activity. CK1 kinase phosphorylation cascades have

been studied and found to depend on phospho-priming at the n-3 or n-4 serine sites (Bustos et al., 2005; Flotow et al., 1990; Xu et al., 1995). One consensus phosphorylation motif for CK1 is pS/T-X-X-S*/T*, where pS/T is a phosphorylated serine or threonine residue, X is any amino acid, and S*/T* is the CK1 target site. Another motif for CK1 that does not require phospho-priming is an N-terminal cluster of acidic amino acids to the target S/T site with an acidic residue (such as aspartic or glutamic acid) at n-3 and a C-terminal cluster of hydrophobic residues (Flotow & Roach, 1991; Pulgar et al., 1999; Y. Yang et al., 2017). A phospho-priming event may be relevant along the C-terminus end where many serine residues are in close proximity with each other. Both motifs are compatible with multiple serine sites on TDP-43's C-terminus end, where the cascade may be initiated through phospho-priming at S403/404 and subsequent phosphorylation occurs on S407, S409, and S410 by CK1δ and CK1ε. This unbiased search using a bioinformatic approach supports CK1δ and CK1ε as top candidate kinases that phosphorylate TDP-43 at key ALS disease-relevant serine sites, such as S409/410. These bioinformatic results support CK1δ and CK1ε as strongly favorable candidate kinases to phosphorylate disease-relevant serine sites on TDP-43, such as S409/410.

Attempts to support these bioinformatic results *in vitro* using mass spectrometry-based phosphoproteomic profiling of TDP-43 were ineffective due to the challenging nature of achieving peptides of appropriate resolution for the C-terminal glycine-rich domain of TDP-43 which was resistant to enzymatic digestions. Thus, we were not able to further test *in vitro* the bioinformatic data predicting CK1δ- and CK1ε-mediated TDP-43 phosphorylation sites via mass spectrometry approaches.

Table 2.1 Results from The Kinase Library bioinformatic database which identified kinases that phosphorylate serine sites on TDP-43.

Candidate kinases predicted to phosphorylate specific serine sites on TDP-43 were identified using The Kinase Library. Scores for CK1δ and/or CK1ε to phosphorylate individual serine sites are shown above. Sites not phosphorylated by CK1δ or CK1ε have the corresponding top scoring kinase under "Others" column along with its site score.

Region	AA ser site	CK1δ score	CK1ε score	Others	
N-term	20	99.43%			
N-term	29			TTBK1	97.62%
N-term	48			TTBK2	98.60%
NLS	91			NEK6	99.58%
NLS	92	99.28%	98.20%		
n/a	104			CDC7	88.68%
RRM1	125	95.78%	94.29%		
RRM1	144			PDHK1	98.75%
RRM1	162			WNK3	99.89%
n/a	180			CHAK1	99.62%
n/a	183	100.00%	99.96%		
n/a	190			NEK8	99.45%
RRM2	212			CK1A	98.29%
RRM2	242			CK1A	97.44%
RRM2	254			TTBK1	98.86%
RRM2	258	99.90%			
n/a	273			NEK5	99.97%
Glycine C-term	292			NEK9	99.97%
Glycine C-term	305			TLK2	99.41%
Glycine C-term	317			PDHK4	99.01%
Glycine C-term	332			ULK2	99.16%
Glycine C-term	333			HUNK	97.00%
Glycine C-term	342			CAMKK1	99.85%
Glycine C-term	347			GAK	97.94%
Glycine C-term	350	100.00%	100.00%		
Glycine C-term	369			MASTL	99.06%
Glycine C-term	373	99.98%	99.63%		
Glycine C-term	375	99.81%	98.80%		
Glycine C-term	377	100.00%			
Glycine C-term	379*	100.00%	99.98%		
Glycine C-term	387			MARK4	98.62%
Glycine C-term	389	100.00%	99.99%		
Glycine C-term	393	100.00%	99.98%		
Glycine C-term	395	100.00%	99.90%		
Glycine C-term	403*			NIM1	99.60%
Glycine C-term	404*			PDHK4	99.75%
Glycine C-term	407	100.00%	100.00%		
Glycine C-term	409*	100.00%	99.98%		
Glycine C-term	410*	100.00%	100.00%		
* Denotes serine sites identified in human post-mortem ALS tissue samples.					

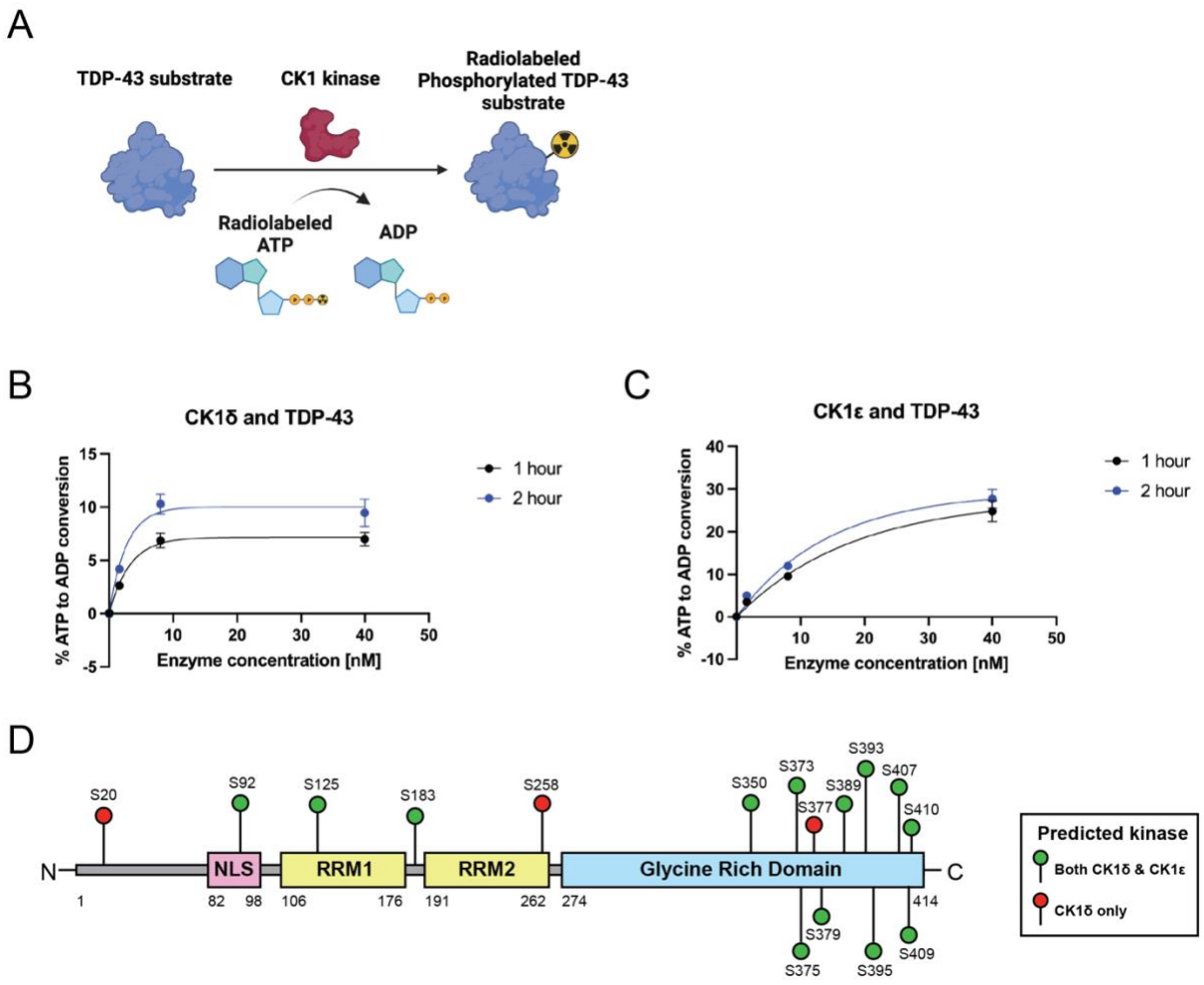


Figure 2.1 TDP-43 is a substrate of CK1δ and CK1ε and multiple serine sites on TDP-43 are bioinformatically predicted to be phosphorylated by CK1δ and CK1ε.

(A) Design of the cell-free protein kinase assay to test the phosphorylation reaction between TDP-43 and CK1δ and CK1ε when incubated with ATP. (B, C) Graphical representation of the data resulting from the kinase assay for either CK1δ or CK1ε binding to TDP-43 after 1-hour and 2-hour incubation. (D) Schematic of results from an unbiased search for candidate kinases predicted to phosphorylate TDP-43 serine sites using The Kinase Library. The green dots represent serine residues where both CK1δ and CK1ε were predicted to phosphorylate TDP-43. The red dots represent serine residues where only CK1δ was predicted to bind and phosphorylate TDP-43. Individual site scores are listed in Table 1.

Expression of TDP-43 in cells displays TDP-43 nuclear mislocalization into cytoplasmic phosphorylated inclusions

We used a novel cell model of TDP-43 proteinopathy to study TDP-43 phosphorylation mechanisms. The addition of doxycycline (dox) to the media would induce overexpression of full-length human TDP-43 which was tagged with a N50 aggregation sequence and a clover sequence on the C-terminus end. (Figure 2.2A-B). The N50 sequence coded for a small peptide that promoted oligomeric proteins, such as TDP-43, to form inclusions whereas monomeric proteins like FKBP did not form inclusions (Figure 2.2C). The TDP-43 inclusions formed were also found to be phosphorylated (Figure 2.2D). Stable cells lines for U2OS and SH-SY5Y cells were generated containing this dox-inducible TDP43$^{N50\text{-}clover}$ sequence.

In both U2OS-TDP43$^{N50\text{-}clover}$ and SH-SY5Y-TDP43$^{N50\text{-}clover}$ cells, dox induction over 36-48 hours resulted in *TARDBP* RNA expression levels 10-15-fold higher than those of uninduced control cells (Figure 2.3A). In addition, there was significant upregulated gene expression for *CSNK1D* and *CSNK1E* (Figure 2.3B-C), which was similarly observed in our patient spinal cord laser capture RNA-sequencing dataset with *CSNK1E* upregulation (Krach et al., 2018).

Post-mortem ALS patient neuropathology analysis has revealed pathological cytoplasmic TDP-43 to exist in soluble diffuse and insoluble aggregated protein states. There is no consensus as to appropriate biochemical protein extraction methods to isolate these two protein states. Despite this challenge, we developed a reliable protocol to fractionate the protein lysate into a soluble fraction using RIPA buffer and an insoluble protein fraction using urea-SDS buffer. To then detect phosphorylated TDP-43 (pTDP-

43) within soluble and insoluble protein fractions, we turned to immunoblots. The ability to detect different phosphorylated TDP-43 species using antibodies has been challenging due to limited antibodies and variable efficiencies depending on the application for use. With this in mind, we tested all commercially available phosphorylated TDP-43 antibodies that detected the S403, S404, S409, S410 sites for immunoblot and immunofluorescence applications. Through this rigorous validation process, our primary readout for our assays used antibodies that detected the S409/410 sites on TDP-43, which has been considered a reliable and consistent hallmark found in postmortem ALS patient tissue. All other antibodies tested were determined to be either poor quality or inconsistent for analysis.

With our tools and methods established for detecting pTDP-43, more specifically by probing the S409/410 sites of TDP-43, in immunoblot and immunofluorescence readouts, we characterized both U2OS-TDP43$^{N50\text{-clover}}$ and SH-SY5Y-TDP43$^{N50\text{-clover}}$ cell models. We found both cell types contained highly detectable pTDP-43 protein levels in soluble and insoluble protein fractions after 48 hours of dox incubation (Figure 2.3D-E). Additionally, the TDP-43 protein accumulated into phosphorylated cytoplasmic inclusions, as observed using immunofluorescence staining (Fig. 2.3F). These dox-induced cells also displayed complete TDP-43 nuclear clearance, recapitulating neuropathic observations of ALS postmortem tissue. Quantification of our cell models revealed 20-30% of dox-induced TDP-43 positive cells to also contain pTDP-43, which was comparable between U2OS and SH-SY5Y cell models. The phenotypes generated in these cell models will allow us to study CK1-dependent phosphorylation of TDP-43.

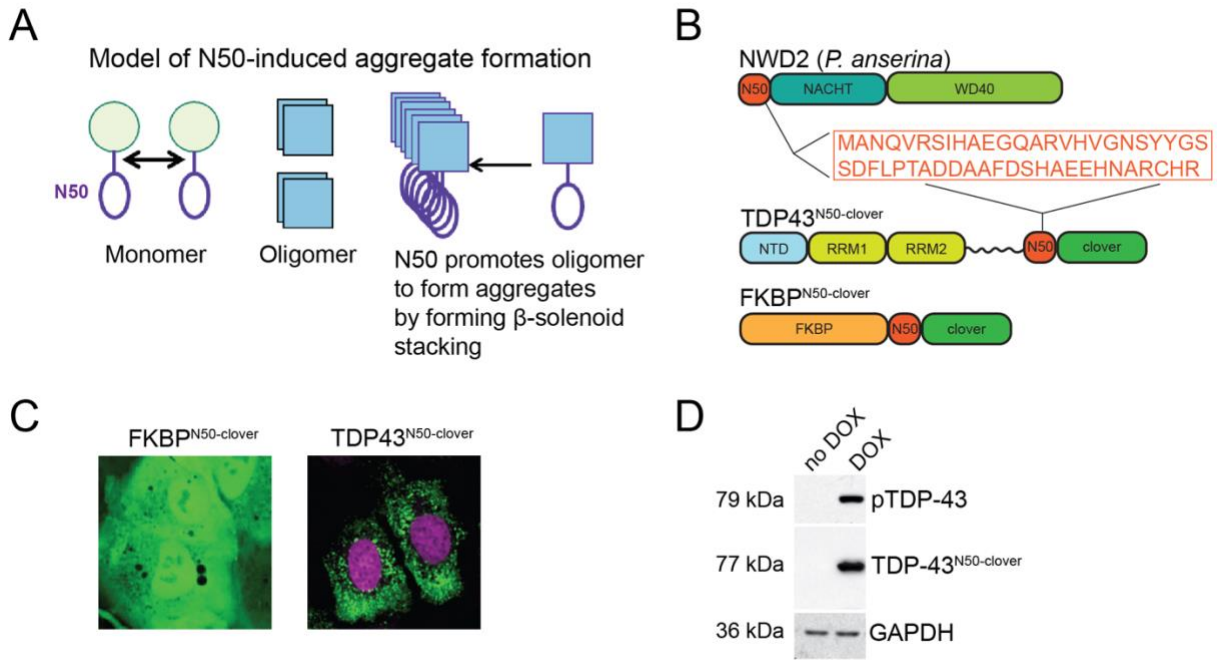
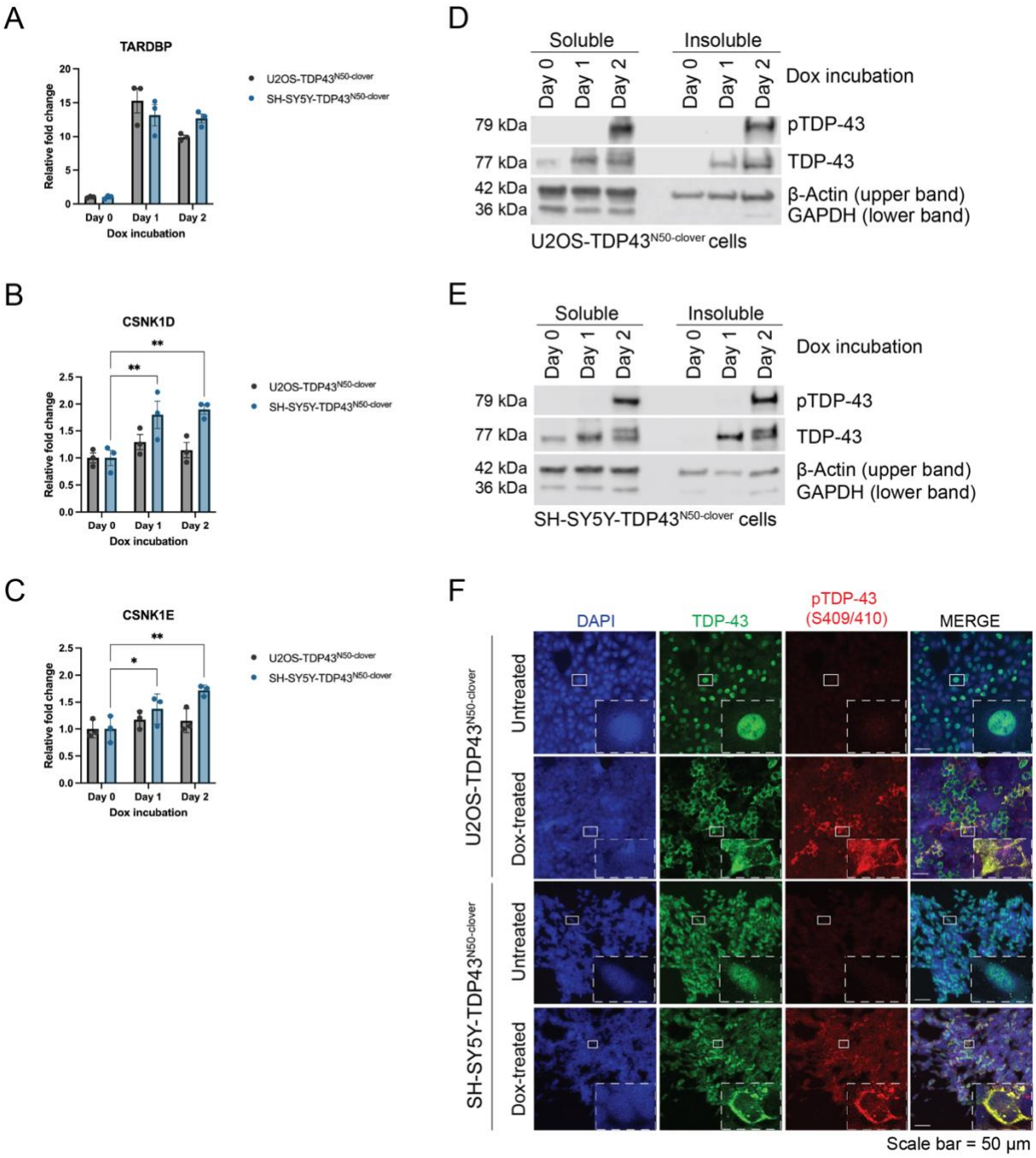


Figure 2.2 Adding N50 small peptide tag to TDP-43 generates cytoplasmic phosphorylated TDP-43 inclusions.

(A) The small peptide N50 tag will only promote oligomeric proteins like TDP-43 to form aggregates. This is accomplished through the formation of a stable β-solenoid stacked structure. When N50 is tagged to a monomeric protein, the N50 peptides are spatially separated and unable to promote aggregation. (B) Sequence design of TDP-43$^{N50\text{-}clover}$ that was transfected into U2OS and SH-SY5Y cells to generate stable cells lines. The N50 sequence is 50 amino acids long from the N-terminal polypeptide of NWD2 protein from filamentous fungus *Podospora anserina*. The N50 sequence was tagged to the C-terminus end of TDP-43 to promote TDP-43 aggregation and the clover tag (a bright GFP variant) allowed for tracing of the TDP-43 expression. (C) Fluorescent imaging showed the monomeric protein FKBP$^{N50\text{-}clover}$ did not form spontaneous aggregates while oligomeric protein TDP-43$^{N50\text{-}clover}$ did form aggregates. (D) The TDP-43$^{N50\text{-}clover}$ protein demonstrates phosphorylation at S409/410 sites in immunoblots, reflecting pathological phosphorylation observations.

Figure 2.3 Cell models expressing TDP43$^{N50\text{-}clover}$ display TDP-43 nuclear clearance and accumulation of cytoplasmic phosphorylated TDP-43 inclusions.

(A-C) Quantitative real-time PCR (qRT-PCR) data of gene expression for *TARDBP*, *CSNK1D*, and *CSNK1E* mRNA levels in U2OS-TDP43$^{N50\text{-}clover}$ (gray bars) and SH-SY5Y-TDP43$^{N50\text{-}clover}$ cells (blue bars). *GAPDH* mRNA was used as endogenous control. (A) Dox induction for 48 hours resulted in significant increased *TARDBP* gene expression. (B, C) Upregulation of *CSNK1D* and *CSNK1E* were observed when dox was added. One-way ANOVA, *$p < 0.03$, ** $p < 0.002$, $n = 3$. Error bars represent SEM. (D, E) Representative immunoblots from cell lysates showed pTDP-43 protein levels being highly detectable in soluble and insoluble protein fractions after 48 hours of dox incubation. GAPDH signal was used to indicate the quality of fractionation between insoluble and soluble protein fractions. (F) Representative immunofluorescence images of un-induced and dox-induced U2OS-TDP43$^{N50\text{-}clover}$ and SH-SY5Y-TDP43$^{N50\text{-}clover}$ cells with staining for TDP-43 (green), pTDP-43 (red), and DAPI (blue). Cells incubated with dox displayed TDP-43 nuclear clearance and accumulation of cytoplasmic phosphorylated TDP-43 inclusions. Three fields of view were captured by confocal imaging for each condition, with approximately 50-60 dox-induced TDP-43 positive cells in each field of view. Quantitively, findings were comparable between U2OS and SH-SY5Y cell lines with 20-30% of dox-induced TDP-43 positive cells also expressing pTDP-43. Scale bars represent 50 μm. The results shown represent three independent experiments.


A
TARDBP
Relative fold change
Day 0
Day 1
Day 2
Dox incubation
U2OS-TDP43N50-clover
SH-SY5Y-TDP43N50-clover
B
CSNK1D
**
**
C
CSNK1E
**
*
D
Soluble
Insoluble
Dox incubation
79 kDa
77 kDa
42 kDa
36 kDa
pTDP-43
TDP-43
β-Actin (upper band)
GAPDH (lower band)
U2OS-TDP43N50-clover cells
E
SH-SY5Y-TDP43N50-clover cells
F
DAPI
TDP-43
pTDP-43 (S409/410)
MERGE
Untreated
Dox-treated
Scale bar = 50 µm

siRNA-mediated knockdown of either CSNK1D or CSNK1E significantly decreases TDP-43 phosphorylation

Having identified CSNK1D and CSNK1E as kinases that interacted with and phosphorylated TDP-43, we tested how knockdown of either the CSNK1D or CSNK1E gene using RNA interference would affect pTDP-43 expression in our cell models. Cells were plated and grown to 60-70% confluency and cell-cycle arrested, and then siRNA was transfected into them. After overnight incubation, doxycycline was added to the cell media to induce pTDP-43 inclusion formation. Samples for RNA and protein were collected the following day for either qRT-PCR or immunoblotting and analysis (Fig. 2.4A).

Multiple siRNAs were tested for their knockdown efficiency and target specificity, and we continued experiments with 2-3 validated constructs for each gene of interest. Knockdown of gene target for each construct tested was effective, with over 80% gene expression significantly reduced for either *CSNK1D* or *CSNK1E* in U2OS-TDP43$^{N50\text{-clover}}$ cells (Figure 2.4B). These siRNAs also had minimal nonsignificant effect on the gene and protein expression for the other untargeted CK1 gene, indicating strong target specificity (Figure 2.4B). In addition, the reduced expression of either the *CSNK1D* or *CSNK1E* gene did not significantly alter the *TARDBP* gene expression (Figure 2.4C), thus, changes observed in TDP-43 phosphorylation expression could reasonably be an effect resulting from CK1-dependent phosphorylation and not altered *TARDBP* gene expression. The negative control scramble siRNA also confirmed our results were not a consequence of the transfection reagent and protocol (Figure 2.4B-C).

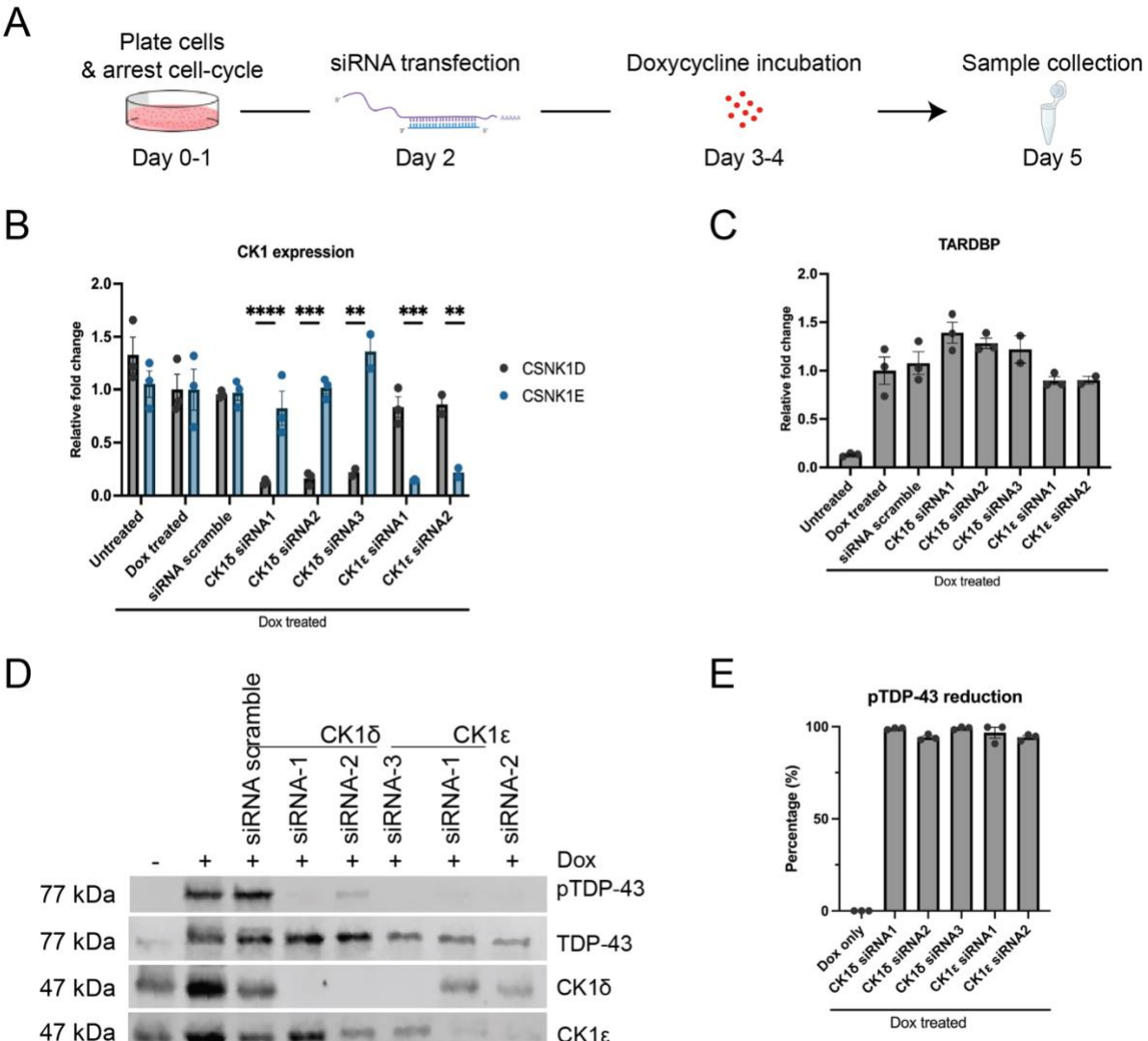
Under siRNA-treated conditions in U2OS-TDP43$^{N50\text{-clover}}$ cells, there was a nearly 100% complete reduction in pTDP-43 levels (Figure 2.4D-E). Quantification of pTDP-43

reduction was calculated as a percentage based upon immunoblot densitometry values (Figure 2.4E). The pTDP-43 band signal was first normalized to β-Actin, as was the total TDP-43 band signal. These two normalized values were then computed as a ratio with pTDP-43 relative to total TDP-43, and then compared to untreated dox-induced samples. This analysis, and future analysis used throughout the rest of this research work, incorporated normalization not only to an internal gene control within each sample using the housekeeping gene β-Actin, but also took into account the expression of the total TDP-43 (TDP43$^{N50\text{-clover}}$ transgene) since there may have been inherent genetic regulatory variability between samples. The results from siRNA-mediated knockdown of *CSNK1D* and *CSNK1E* strongly support CK1δ and CK1ε as integral upstream regulators of TDP-43 phosphorylation, particularly when analyzing the S409/410 sites.

We conducted parallel studies in SH-SY5Y-TDP43$^{N50\text{-clover}}$ cells with multiple genetic knockdown strategies including siRNA transfection and lentiviral shRNA transduction, but these methods were either extremely toxic to the cells or lacked significant efficacy. Thus, we were unable to further our studies of genetic reduction of *CSNK1D* or *CSNK1E* in an *in vitro* neuronal cell model.

Figure 2.4 siRNA-mediated knockdown of either CSNK1D or CSNK1E significantly decreases pTDP-43 expression levels.

(A) Diagram of the experimental timeline for siRNA transfection and sample collection. (B) qRT-PCR analysis of RNA expression established the target specificity and efficiency of siRNA-mediated knockdown for either *CSNK1D* or *CSNK1E* genes in U2OS-TDP43$^{N50\text{-}clover}$ cells. *GAPDH* was used as endogenous control. The reduced gene expression of the targeted CK1 gene had little effect on the expression of the other untargeted CK1 gene. One-way ANOVA, *p < 0.03, ** p < 0.002, ***p < 0.0002, ****p < 0.0001, n = 3. Error bars represent SEM. (C) siRNA-mediated knockdown of either *CSNK1D* or *CSNK1E* had no significant effect on *TARDBP* gene expression. (D) Representative immunoblot images of cell lysates demonstrate significantly reduced pTDP-43 levels in siRNA treated conditions when *CSNK1D* and *CSNK1E* is reduced. siRNAs used were specific for the target CK1 gene as validated by the protein knockdown as well. (E) pTDP-43 reduction was quantified as a percentage based on immunoblot signal intensity data. The signal intensity for each pTDP-43 band was first normalized to β-Actin, then calculated as a ratio relative to total TDP-43 (which was also normalized to β-Actin) levels and then compared to untreated dox-induced condition. The results shown represent three independent experiments.


A
Plate cells
& arrest cell-cycle
siRNA transfection
Doxycycline incubation
Sample collection
Day 0-1
Day 2
Day 3-4
Day 5
B
CK1 expression
Relative fold change
CSNK1D
CSNK1E
****
***
**
***
**
Untreated
Dox treated
siRNA scramble
CK1δ siRNA1
CK1δ siRNA2
CK1δ siRNA3
CK1ε siRNA1
CK1ε siRNA2
Dox treated
C
TARDBP
Relative fold change
Dox treated
D
siRNA scramble
CK1δ
CK1ε
siRNA-1
siRNA-2
siRNA-3
siRNA-1
siRNA-2
Dox
77 kDa
pTDP-43
77 kDa
TDP-43
47 kDa
CK1δ
47 kDa
CK1ε
42 kDa
β-Actin
U2OS-TDP43N50-clover cells
E
pTDP-43 reduction
Percentage (%)
Dox only
CK1δ siRNA1
CK1δ siRNA2
CK1δ siRNA3
CK1ε siRNA1
CK1ε siRNA2
Dox treated

CK1 inhibitors have selective target engagement of CK1δ and CK1ε

To advance our genetic knockdown studies towards pharmacological inhibition for translational application, we studied whether CK1 small molecule chemical inhibitors could effectively reduce pTDP-43 in cells. CK1 kinase inhibitors with varying levels of selectivity for binding CK1δ and CK1ε have been synthesized by various companies in recent years. These compounds are mature-developed, potent with low IC_{50} values, ATP-competitive, and cross the blood-brain barrier (BBB) well. We tested CK1δ/ε-selective PF-05236216 inhibitor (Figure 2.5A) and CK1ε-selective PF-4800567 inhibitor (Figure 2.5B), which were developed by Pfizer Global Research and Development and are commercially available (Badura et al., 2007; Cozza & Pinna, 2016; Etchegaray et al., 2010; S.-S. Li et al., 2021; Long et al., 2012; Meng et al., 2010; Wager et al., 2017).

We sought to characterize the selectivity profiles for our two compounds of interest before further testing in our cell models. KINOME*scan*™ is an active site-directed competition binding assay which measures the interactions between the inhibitor and 468 human kinases (Fabian et al., 2005) (Figure 2.5C). The data gathered from this panel assay was used to generate TREE*spot*™ interaction maps which is a visualization of the inhibitor's selectivity at a specified concentration in reference to the human kinome phylogenetic tree. Larger circles on the map represent higher-affinity binding, which both CK1δ/ε-selective PF-05236216 inhibitor and CK1ε-selective PF-4800567 inhibitor was strongly selective to bind CK1δ and/or CK1ε (Figure 2.5D-G). Closer examination of the TREE*spot*™ interaction maps reveals both inhibitors having some selectivity to bind to other kinases at 10,000 nM (10 μM) concentration. This off-target effect is not of concern for our cell experiments since this observation is only observed at higher concentrations,

typically accompanied with cell toxicity, and this 10 μM dose was not necessary for efficacy in our *in vitro* cell experiments discussed below.

To evaluate each compound's selectivity and differentiate the interaction patterns, we calculated the S-score (selectivity score), which was found by dividing the number of kinases below a specified potency threshold by the total number of distinct kinases tested (which was 468 human kinases) (Karaman et al., 2008). The %Control measurements were used as the potency threshold and was calculated as the percentage conversion of test compound signal divided by the DMSO negative control signal, with lower values indicating stronger binding. Both compounds demonstrated strong target engagement selectivity for CK1ε, and PF-05236216 showed additional selectivity for CK1δ in contrast to that of PF-4800567 (Table 2). Using these %Control measurements as the potency threshold, the S-scores for compounds PF-05236216 and PF-4800567 at 1000 nM and 10,000 nM with %Control<35 or <10 or <1 were calculated (Table 3). The S-scores were low at the three levels calculated, with less than 1% of the 468 kinases found to bind either of the CK1 compounds at a 1000 nM concentration. This assay indicated that both compounds PF-05236216 and PF-4800567 bound a small number of kinases with high affinity, demonstrating selective target engagement.

Table 2.2 %Control for selectivity profiles of CK1 inhibitor compounds.

The %Control was calculated for each binding interaction, which was the percentage conversion of the test compound signal divided by the DMSO negative control signal. Lower numbers indicated stronger target hits out of the 468 kinases tested. Both compounds demonstrated strong selectivity for CK1ε, and PF-05236216 showed additional selectivity for CK1δ in contrast to that of PF-4800567. The %Control measure was then used as the potency threshold to calculate S-scores, shown below in **Table 2.3**.

%Control	PF-05236216		PF-4800567	
	1000 nM	10,000 nM	1000 nM	10,000 nM
CK1δ	3.4	2.4	18	3.5
CK1ε	0.4	0.1	0.6	0.3

Table 2.3 Selectivity S-scores for CK1 inhibitor compounds

The S-score measures of compound selectivity for each inhibitor, CK1δ/ε-selective PF-05236216 and CK1ε-selective PF-4800567, with %Control <35, 10, or 1 are shown at the two concentrations tested (1000 nM and 10,000 nM). Both CK1δ/ε-selective PF-05236216 and CK1ε-selective PF-4800567 were selective for their respective kinase target engagement. The S-score shown was calculated by dividing the number of kinases that the compound bound to by the total number of distinct kinases tested (468 kinases).

S-Score	PF-05236216		PF-4800567	
	1000 nM	10,000 nM	1000 nM	10,000 nM
S(35)	2.564%	7.906%	1.709%	13.675%
S(10)	1.068%	2.564%	0.214%	5.128%
S(1)	0.214%	0.641%	0.214%	0.641%

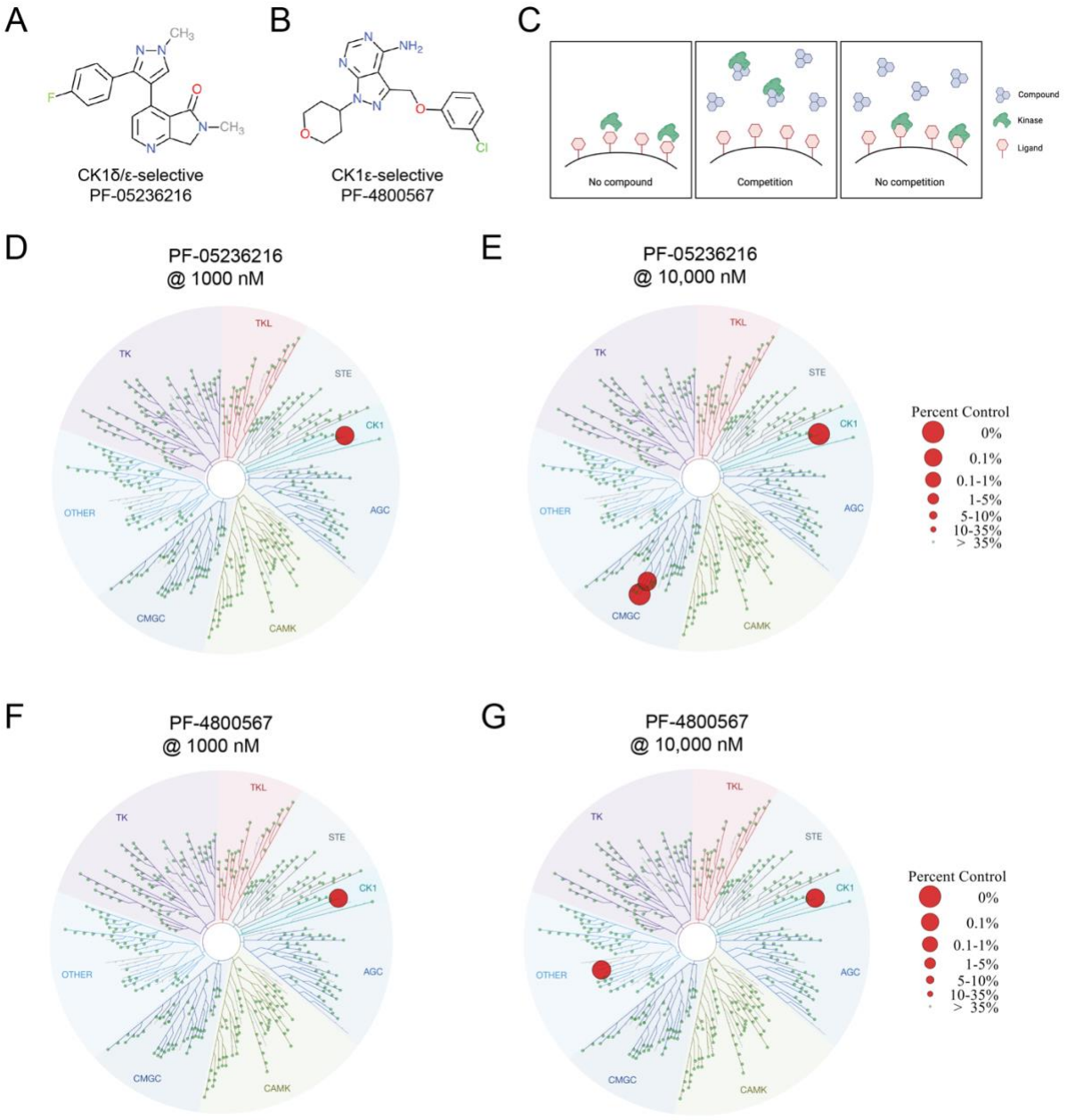


Figure 2.5 CK1 inhibitors are selective for target engagement of CK1δ and/or CK1ε.

(A, B) Chemical structures for CK1δ/ε-selective PF-05236216 and CK1ε-selective PF-4800567 inhibitors are shown. Chemical structures were made using ChemDoodle Web. (C) Schematic of the KINOMEscan™ assay design to test inhibitor selectivity against different kinase targets. (D-G) TREEspot™ interaction maps of kinase selectivity profiles for CK1 inhibitors PF05236216 (D, E) and PF-4800567 (F, G) were generated to show selectivity for intended kinase targets. Two different concentrations were tested, 1000 nM (1 μM) and 10,000 nM (10 μM), in this assay. Larger red circles indicated higher-affinity binding of inhibitor compound to target.

CK1 inhibitors are potent compounds that reduce TDP-43 phosphorylation in cellular models

Having demonstrated selective target engagement of the CK1 inhibitors, we tested whether they were efficacious in reducing pTDP-43 in U2OS-TDP43$^{N50\text{-clover}}$ and SH-SY5Y-TDP43$^{N50\text{-clover}}$ cells. For these sets of experiments, the cells were plated, and cell-cycle arrested at G1/S phase with palbociclib. After recovery, dox was added to the media to induce TDP43$^{N50\text{-clover}}$ expression with pTDP-43 formation, and then inhibitor (either CK1δ/ε-specific PF-05236216 or CK1ε-specific PF-4800567) was added for overnight incubation until the next day when samples were collected. was added for overnight incubation before collecting samples for analysis the following day (Figure 2.6A).

Adding either of the CK1 inhibitors to cells resulted in striking dose-dependent response of reduced pTDP-43 levels as evidence in immunoblots of U2OS and SH-SY5Y cell lysates (Figure 2.6B-C, Figure 2.7A-B). A dose range of 0.01 μM to 90 μM was tested for each CK1 inhibitor in both cell types to determine their respective half maximal inhibitory concentrations (IC_{50}) as a measure of compound potency. The IC_{50} value indicated the inhibitor concentration sufficient to reduce TDP-43 phosphorylation response by 50%. The IC_{50} for CK1δ/ε-specific inhibitor PF-05236216 was approximately 0.7 μM (700 nM) in both U2OS and SH-SY5Y cell models (Figure 2.6D, Figure 2.7C). The IC_{50} for CK1ε-specific PF-4800567 was approximately 3 μM (3000 nM) in both U2OS and SH-SY5Y cell models (Figure 2.6E, Figure 2.7D). These IC_{50} values showed that the CK1δ/ε-specific PF-05236216 inhibitor was more potent than the CK1ε-specific PF-4800567 inhibitor at reducing TDP-43 phosphorylation in both U2OS and SH-SY5Y cell models, and that the IC_{50} is similar across different cell types. It is worth noting that at

higher doses of CK1ε-selective PF-4800567 inhibitor where significant pTDP-43 reduction was observed, there may have been some off-target inhibition of CK1δ in addition to CK1ε.

The soluble and insoluble fractions were analyzed for pTDP-43 expression after cells were treated with CK1 inhibitor (Figure 2.7A-B). The dose-dependent reduction for both CK1 inhibitors was more efficacious with the soluble protein than the insoluble protein (Figure 2.7E-F), suggesting that the inhibitor is more effective at targeting the phosphorylation sites of TDP-43 in the soluble state over the insoluble state. Additionally, when we added CK1 inhibitors to our cell models and performed immunofluorescence staining, we observed reduced cytoplasmic pTDP-43 signal even when there was strong overexpression of TDP-43 (Figure 2.8A-B). This may suggest that phosphorylation occurs after inclusion formation and generally has a limited, if any, contribution towards cytoplasmic TDP-43 inclusion formation. However, our inducible cell model utilized an artificial strategy to generate this phosphorylation phenotype, so results must be interpreted sparingly. The results from these pharmacological inhibition experiments establish that these CK1 inhibitors reduce the phosphorylation of TDP-43 proteinopathy in our cell models. Taken together, inhibiting CK1δ and CK1ε functional activity, not just gene expression, is sufficient to effectively reduce pTDP-43 levels in cells and establishes CK1δ and CK1ε inhibitors for further testing *in vivo*.

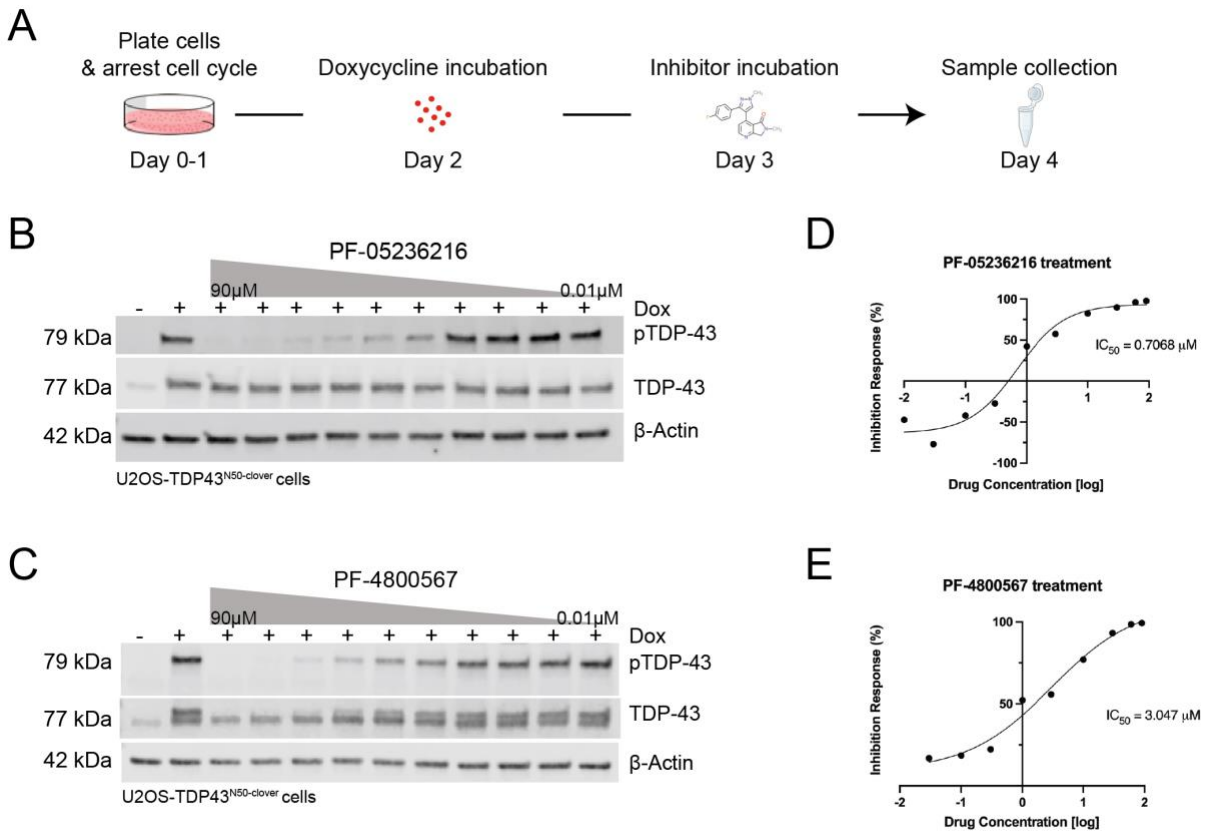


Figure 2.6 CK1 inhibitors effectively reduce pTDP-43.

(A) Schematic of the experimental timeline for testing CK1 inhibitors in cell models. (B, C) Representative blot images for U2OS-TDP43$^{N50\text{-clover}}$ protein lysates show that the addition of either inhibitor resulted in a dose-dependent response for pTDP-43 reduction. (D, E), Based on the IC_{50} curves, a lower dose was needed to reduce TDP-43 phosphorylation when using CK1δ/ε-selective PF-05236216 inhibitor.

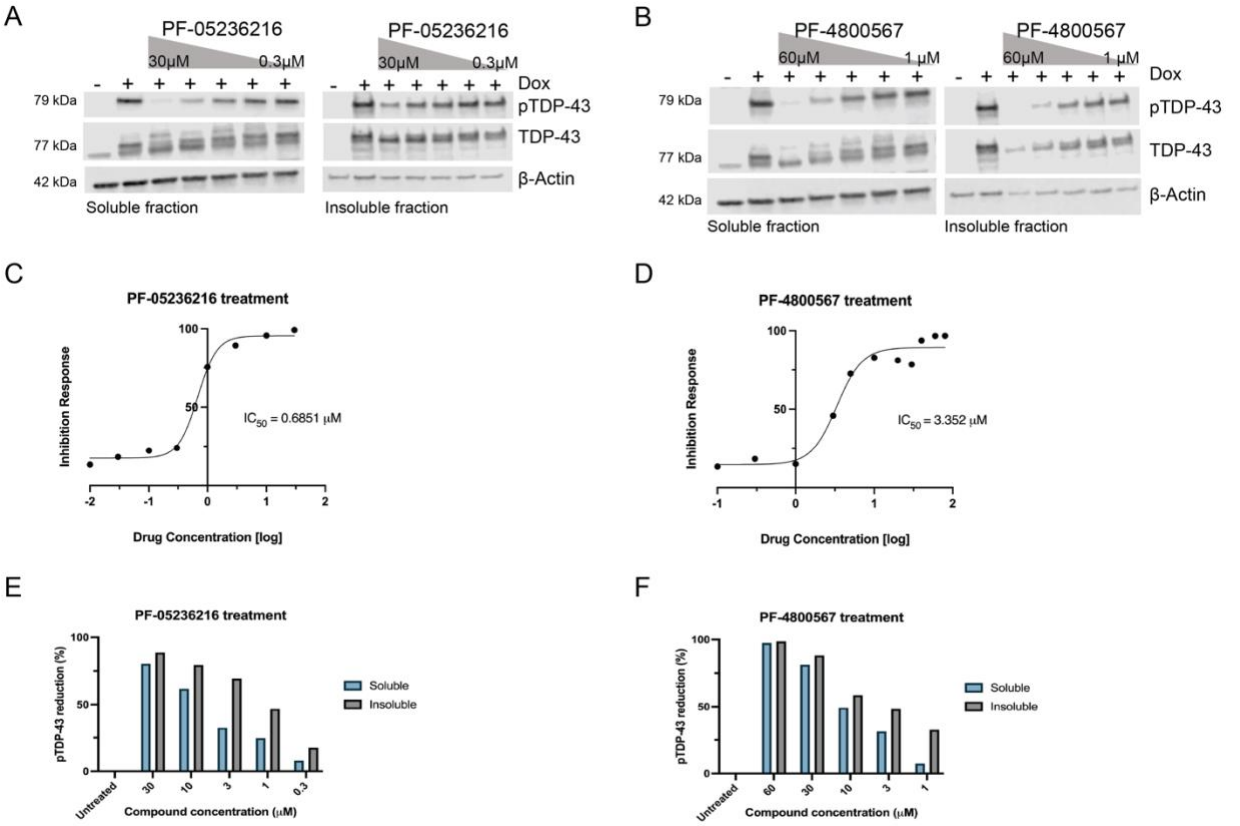


Figure 2.7 CK1 inhibitors reduce TDP-43 phosphorylation in soluble and insoluble protein fractions.

(A, B) Representative blot images for SH-SY5Y-TDP43$^{N50\text{-clover}}$ soluble and insoluble protein lysates. Adding CK1 compounds resulted in a dose-dependent reduction of pTDP-43. (C, D) Similar to U2OS cells, the IC_{50} curves suggested that a lower dose was needed to reduce TDP-43 phosphorylation when using CK1δ/ε-selective PF-05236216 inhibitor. (E, F) Quantification of pTDP-43 reduction in soluble and insoluble protein fractions as a percentage based on immunoblot data. The signal intensity for each pTDP-43 band was first normalized to β-Actin, then calculated as a ratio relative to total TDP-43 levels (which was also normalized to β-Actin) and then compared against untreated dox-induced condition.

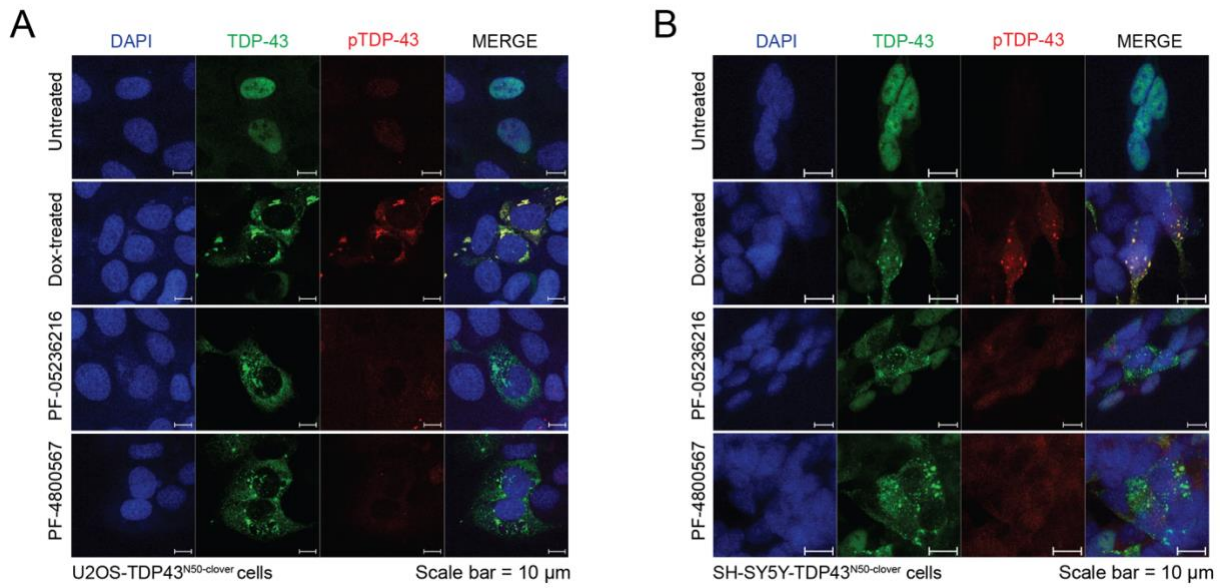


Figure 2.8 Cellular imaging shows reduced cytoplasmic pTDP-43 expression in treated cells.

(A, B) Representative immunofluorescence images with TDP-43 (green), pTDP-43 (red), and DAPI (blue). When CK1 inhibitors were added to U2OS or SH-SY5Y cells, cytoplasmic pTDP-43 expression was markedly reduced. Scale bars represent 10 μm. The results shown represent three independent experiments.

The S409/410 sites on TDP-43 is predominantly phosphorylated by CK1δ and CK1ε kinases

To evaluate the exclusivity of CK1δ and CK1ε kinases in TDP-43 phosphorylation, particularly with regard to the S409/410 site, we tested commercially available kinase inhibitors of other potential kinase targets that have been implicated in this ALS-related mechanism (Aikio et al., 2021; Carlomagno et al., 2014; Dewil et al., 2007; Gibbs et al., 2018; Liachko et al., 2013, 2014; Romano et al., 2020; Sahu et al., 2021; L. M. Taylor et al., 2018; Tian et al., 2021). We selected inhibitor compounds using the criteria of low IC_{50} values, indicating high selectivity for their respective target. From this search, we identified the following kinases and their respective inhibitors that had potent selectivity

profiles to test: ERK1/2 (Ravoxertinib inhibitor, GDC-0994), p38α/MAPK14 (Neflamapimod inhibitor, VX-745), TTBK1 (TTBK 1-IN-1 inhibitor), CDC7 (simurosertib inhibitor, TAK-931) and CK2α (silmitasertib inhibitor, CX-4945).

For these inhibitors, we tested doses ranging from 0.1 μM to 30 μM in our SH-SY5Y-TDP43$^{N50\text{-clover}}$ cells. Inhibitors targeting ERK1/2, p38α/MAPK14, and TTBK1 did not affect pTDP-43 levels even when used at very high doses of 10 μM or more (Figure 2.9A), which were accompanied by signs of cell toxicity (Figure 2.9B). When inhibiting either CDC7 or CK2α using doses 3 μM or higher, we observed a reduction in pTDP-43 (Figure 2.9A), but cells exhibited altered cell morphology and increased cell death, which was also reflected by the decreased β-actin levels in the immunoblots (Figure 2.9B). The toxicity observed when these other kinases inhibitors were added was much less apparent when either of the CK1 inhibitors, CK1δ/ε-selective PF-05236216 or CK1ε-selective PF-4800567, was added to SH-SY5Y-TDP43$^{N50\text{-clover}}$ cells (Figure 2.9B) indicating better tolerability. Our results support CK1δ and CK1ε as the primary kinases that mediate the phosphorylation of TDP-43 at S409/410. This work also validates the bioinformatic results from The Kinase Library as mentioned earlier. Overall, the two CK1 inhibitors we profiled and studied *in vitro* are viable compounds to further test their efficacy *in vivo*.

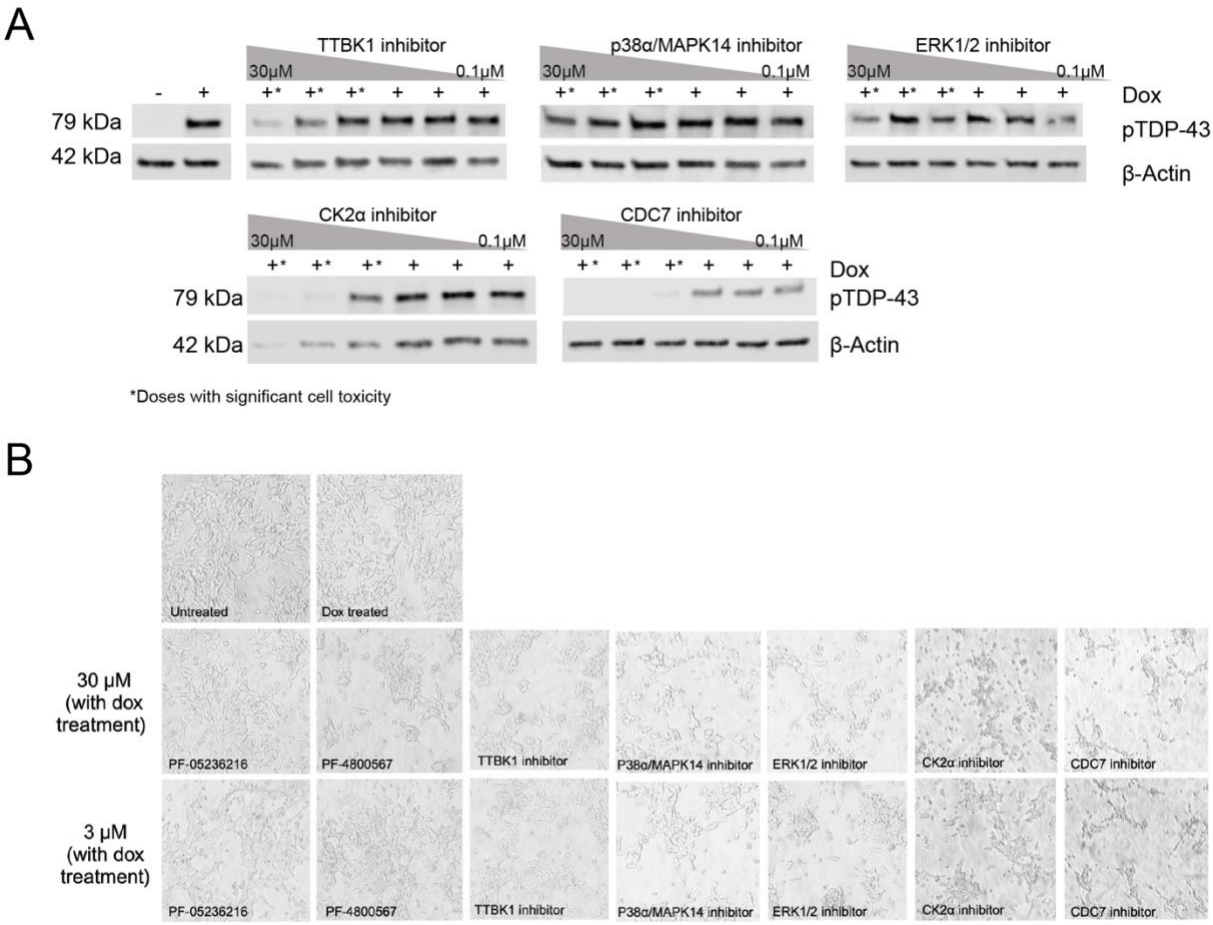


Figure 2.9 CK1δ and CK1ε are the predominant kinases that phosphorylate TDP-43 at ALS-relevant S409/410 sites.

(A) Representative blot images of SH-SY5Y-TDP43$^{N50\text{-clover}}$ cell lysates when other kinase inhibitors were added. The inhibitors tested targeted CK2α, CDC7, ERK1/2, p38α/MAPK14, and TTBK1. Generally, these inhibitors did not reduce TDP-43 phosphorylation at the S409/410 sites unless used at highly toxic doses. (B) Adding inhibitors at concentrations of 3 μM or more resulted in altered cell morphology and increased cell toxicity. These adverse observations were not detected when either CK1 inhibitors (CK1δ/ε-selective PF-05236216 and CK1ε-selective PF-4800567) were used. The results shown represent three independent experiments.

Discussion

Despite the significant neuropathological presence of phosphorylated TDP-43 in aggregates of diseased motor neurons of ALS patients, the relevance and contribution of TDP-43 phosphorylation to disease pathogenesis and progression remain unclear. In the present study, we demonstrated that both CK1δ and CK1ε kinases regulate TDP-43 phosphorylation by testing genetic and pharmacological intervention strategies in novel *in vitro* models of TDP-43 proteinopathy and determined CK1δ and CK1ε as viable targets for reducing disease-relevant TDP-43 hyperphosphorylation related to ALS disease and other TDP-43 proteinopathies.

We established that TDP-43 is a substrate for both CK1δ and CK1ε kinases using a cell-free kinase assay and by leveraging bioinformatic tools, we identified CK1δ and CK1ε as the most favorable kinases to phosphorylate TDP-43 at key ALS-relevant pathological serine residues, including S409/410. We attempted to validate the results of our bioinformatic search using phosphoproteomic mass spectrometry methods but were limited by the ability of enzyme digestions to cut TDP-43 within the C-terminal glycine-rich domain into peptides for analysis. CK1 kinases are known to depend on phospho-priming at nearby sites; thus, TDP-43 phosphorylation at S409/410 and other sites may have complex events further upstream where a cascade is initiated. For example, it is possible that a phospho-priming event(s) at S403/404 spurs phosphorylation at S407 and subsequent phosphorylation at S409/410 by CK1δ and CK1ε. Several kinases, such as NIM1, MASTL, PDHK4, DSTYK, and NEK5/6/7, which are involved in ATP binding, microtubules, mitochondria function, mitosis, and cell death, are predicted to favor the S403/404 site, indicating that this could be a multipurpose regulatory event.

Our novel inducible cell models recapitulated ALS disease hallmarks of cytoplasmic pTDP-43 inclusion formation and nuclear TDP-43 depletion. There are a variety of cell models used in ALS-related research, each with their own set of limitations. Studies utilizing patient iPSC-derived motor neurons or differentiated neural stem cells develop heterogeneous cultures with phenotypic variations and typically require a stressor to induce phenotypes, almost all of which lack resemblance to essential neuropathological observations such as TDP-43 mislocalization and phosphorylation and thus would not enable testing of our hypothesis (Giacomelli et al., 2022; W. Guo et al., 2017; Richard & Maragakis, 2015; Volpato & Webber, 2020). Our models, by contrast, allowed for the detailed study of CK1-dependent phosphorylation of TDP-43 using genetic knockdown and pharmacological inhibition strategies with reproducibility and bypassed the clonal selection and lack of TDP-43 mislocalization, phosphorylation, and aggregation that underlies iPSC models, while acknowledging that they are not motor neurons, the primary vulnerable cell type in ALS.

We were able to demonstrate in two different cell types, U2OS mammalian cells and neuroblastoma-derived SH-SY5Y neuron-like cells, that reduced CK1δ and CK1ε expression and activity was able to significantly decrease pTDP-43 by probing the S409/410 sites. Overall, these consistent results suggest that similar findings may be observed in other cell types, such as motor neurons. Note that other serine sites along TDP-43 could not be probed due to the lack of pTDP-43 antibody tools. Importantly, our models (and many of the commonly used cell models) do not exhibit progressive cell toxicity or death, so our conclusions are limited to only the phosphorylation status of TDP-43, and we are unable to determine how this mechanism relates to cell health and

survival, which ultimately needs to be explored with *in vivo* studies. Through an alternative strategy via highly selective small molecule CK1 inhibitors, CK1δ/ε-selective PF-05236216 and CK1ε-selective PF-4800567 inhibitors, we were able to achieve robust dose-dependent reduction of pTDP-43 in both soluble and insoluble protein fractions for both U2OS and SH-SY5Y cell models. Throughout our studies, we critically examined the soluble and insoluble protein fractions, underscoring the importance of distinguishing these protein fractions with rigorous methods in studying diseases characterized by protein aggregates such as ALS.

Therapeutic development for ALS and other related TDP-43 proteinopathies has largely focused on downstream cell pathways, excitability, and protein aggregation but not directly on phosphorylation. CK1δ upregulation was found to be strongly associated with tau pathology in Alzheimer's disease (AD) brains, and the degree of upregulation correlated with regional disease pathology, where the brain region with most significantly increased CK1δ expression was observed in AD hippocampus (Yasojima et al., 2000). Further, AD disease-associated phosphorylation sites on tau were identified to be mediated by CK1δ (Roth et al., 2022) and targeting CK1δ/ε using an inhibitor rescued working memory deficits in an AD mouse model (Adler et al., 2019). As a potentially independent mechanism from CK1δ-mediated tau phosphorylation, CK1δ- and CK1ε-mediated phosphorylation of TDP-43 and resulting cytoplasmic aggregation affected tau mRNA stability and exon 10 inclusion, which was rescued when pTDP-43 was dephosphorylated (Chen et al., 2017; Gu et al., 2020; R. Wu et al., 2021; M. Yang et al., 2023). Another study in AD lymphoblasts found that a CK1δ/ε inhibitor restored TDP-43 homeostasis and prevented cell-to-cell propagation of TDP-43 pathology (Martinez-

Gonzalez et al., 2023). A similar disease mechanism may take place with CK1δ- and CK1ε-mediated TDP-43 phosphorylation in ALS, where dephosphorylation of pTDP-43 via chemical inhibitors may rescue downstream phenotypes (Cuevas et al., 2024; Martínez-González et al., 2020).

Kinase inhibition has been effective in cancer therapeutics, and recent advances in kinase inhibitor development have addressed previous concerns about specificity/off-target effects, tolerability, potency, and CNS penetration (P. Cohen et al., 2021; Ferguson & Gray, 2018). The high target specificity and BBB-penetrant profile of CK1δ/ε-selective PF-05236216 and CK1ε-selective PF-4800567 inhibitors combined with our *in vitro* results on mechanism potency support our proof-of-concept for utilizing CK1 inhibitors *in vivo* to reduce pTDP-43 levels in both soluble and insoluble TDP-43 protein fractions and thus hold the potential for future studies testing their efficacy and possible application for preclinical therapeutic development. This work highlights CK1δ and CK1ε as viable targets for reducing disease-relevant TDP-43 hyperphosphorylation related to ALS disease and other TDP-43 proteinopathies.

Methods

Kinase profile studies

The cell-free radiometric kinase RBC HotSpot Assays were carried out by the commercial vendor Reaction Biology using their proprietary protocol. The substrate, which was recombinant human full-length TARDBP/TDP-43 (NKMAX Bio #ATGP3502), was prepared in the assay buffer at constant concentration of 1 μM. The CK1 enzyme, either recombinant human full-length CK1δ (Invitrogen #PR6695B) or CK1ε (Invitrogen #PR5147A), was added to the substrate mixture and titrated in a 5-fold serial dilution series starting at 200 nM in duplicate. [γ-^{33}P]ATP at 1 μM was added to initiate the reaction between CK1 enzyme and TDP-43 substrate. We included control conditions of reaction mixtures that contained only CK1 enzyme with [γ-^{33}P] ATP in buffer without TDP-43 substrate, which showed low levels of CK1δ and CK1ε autophosphorylation and these measurements were subtracted as background. The samples were analyzed after 1 hour and 2 hours of incubation. The activity was measured as the percentage ATP to ADP conversion using the company's proprietary filter-binding method. In this method, the reaction mixture was spotted on a phospho-cellulose paper (similar to P81) primed with phosphoric acid so the low pH would allow highly charge negative ATP to be repelled and only have the positively charged peptide bind to the paper. The paper was washed to remove radioactive ATP and the remaining radioactivity was measured as a direct reflection of the CK1 enzyme activity and the amount of phosphate transferred to the TDP-43 substrate.

Stable cell line generation

The stable cell lines were generated following standard lentivirus transduction methods as referenced on the Addgene webpage. U2OS and SH-SY5Y cells were transduced with lentivirus packaged from plasmid pHY189 (EF1a::rtTA3G-IRES neo) (Yu et al., 2021) to produce the TetON3G doxycycline-inducible stable cell lines. Two days after transduction, neomycin was added to the cells at concentration of 250ug/mL (G418, Thermo Fisher #10131027) for two weeks treatment incubation. Surviving stable U2OS and SH-SY5Y cells were then transduced with lentiviruses that were packaged from pHY265 (TRE3G::TDP-43-N50-Clover/PGK::BSD) or pHY266 (TRE3G::FKBP-N50-Clover/PGK::BSD). After two days of incubation, the cells were treated with 10ug/mL Blasticidin (Thermo Fisher # A1113903) for antibiotic selection over one week. The resulting stable U2OS and SH-SY5Y cells were treated with 1 μg/mL doxycycline for two days and then analyzed using flow cytometry to determine protein expression.

Cell culture

The U2OS-TDP43$^{N50\text{-}clover}$ and SH-SY5Y-TDP43$^{N50\text{-}clover}$ cell lines were provided by H.Y. of the Cleveland Lab at UCSD. Cells were maintained either in Dulbecco's modified Eagle's medium (DMEM) with F-12 or high glucose DMEM (Gibco) supplemented with 10% FBS (Gibco), 2 mM L-glutamine (Gibco), and 100 U/mL penicillin-streptomycin (Gibco). Cells were maintained in T75 flasks (Genesee Sci) and kept in incubators with a humidified atmosphere of 5% carbon dioxide at 37°C. Cells were detached using either Accutase (Invitrogen) for SH-SY5Y cells or 0.25% trypsin (Corning) for U2OS cells for maintenance passaging and plating for assays. Depending on the

assay, cells were plated in either 8-well chamber glass slides (Ibidi) for immunofluorescence staining, and either 6-well or 12-well plates (Corning) for all other RNA and protein biochemical assays. After 24 hours, the cells were cell-cycle arrested using palbociclib (APExBIO) and maintained as such throughout the experiment.

siRNA treatments

For knockdown experiments, U2OS-TDP43$^{N50\text{-clover}}$ cells were first seeded into 12-well plates and left to grow to 60% confluency overnight. The following day, a full media change using palbociclib-supplemented media was performed. Lipofectamine RNAiMAX Reagent (Thermo Fisher) was used to transfect siRNAs (Sigma Aldrich or Thermo Fisher) targeting the gene of interest, either a negative scramble control sequence, CSNK1D or CSNK1E, following the manufacturer's protocol. The siRNA-lipid complex was incubated with cells for 24 hours, and then a full media change using doxycycline-supplemented media was added to the cells for 48 hours of incubation before samples were collected for analysis. The siRNAs used were as follows: negative scramble control (Thermo fisher #4390843), CSNK1D (SASI_HS01_00040879, SASI_HS01_00040880, and s3629), and CSNK1E (SASI_HS01_00111724 and SIHK0513).

KINOME*scan*™ compound selectivity profiles

The KINOME*scan*™ compound selectivity assays were conducted by Eurofins Discovery Services following their manufacturer's proprietary protocol. The KINOME*scan*™ assay does not use ATP, so the data collected represents the true thermodynamic interaction affinities between the test compound and the kinase, unlike

IC_{50} values which would depend on ATP concentration in the assay. In the assay, binding reaction mixtures contained purified kinases, liganded affinity beads, and test compound. These mixtures were then incubated for one hour at room temperature on a shaker, and then the affinity beads were washed and resuspended in an elution buffer for 30 minutes of incubation before the kinase concentration in the eluates was measured by qPCR. The binding interaction to each kinase was reported as %Control, which is the percentage value of the test compound signal divided by the DMSO negative control signal. For this %Control value, a lower measure would indicate a stronger target hit out of the 468 human kinases tested. Any compound that bound to the active site of a kinase would prevent the kinase from binding to the immobilized ligand, so less kinase would be captured on the affinity beads and thus would result in a lower %Control value.

In vitro inhibitor treatment

For experiments testing inhibitor treatment in cells, either U2OS-TDP43$^{N50\text{-clover}}$ or SH-SY5Y-TDP43$^{N50\text{-clover}}$ cells were plated into 6-well TC treated plates and left to grow to 60% confluency overnight. The next day, a full media change with palbociclib-supplemented media was performed, then doxycycline was supplemented to the media after overnight incubation. The following day, the inhibitor compound was added at various doses for overnight incubation before samples were collected for analysis. The desired inhibitor doses were prepared in DMSO as a 1000X stock solution to ensure that the final DMSO concentration in cell culture media when added to cells was less than 0.1% in order to minimize the potential effects of DMSO-mediated toxicity. The inhibitors tested were commercially available and are as follows: CK1δ/ε-selective PF-05236216

(dosages 0.01 μM to 90 μM), CK1ε-selective PF4800567 (dosages 0.01 μM to 90 μM), CK2α-selective silmitasertib CX-4945 (dosages 0.1 μM to 30 μM), CDC7-selective simurosertib TAK-931 (dosages 0.1 μM to 30 μM), ERK1/2-selective ravoxertinib GDC-0994 (dosages 0.1 μM to 30 μM), p38α-MAPK14-selective neflamapimod VX-745 (dosages 0.1 μM to 30 μM), and TTBK1-selective TTBK 1-IN-1 (dosages 0.1 μM to 30 μM).

Real-time PCR (qRT-PCR)

RNA was extracted using the Direct-zol RNA miniprep kit (Bio-Rad) according to the manufacturer's protocol and samples were measured for RNA quantity (OD260/280) and purity (OD230/260) using a NanoDrop spectrophotometer (Thermo Fisher). qRT-PCR was performed with iTaq universal SYBR Green one-step kit (Bio-Rad) and CFX384 (Bio-Rad) as described in the manufacturer's protocol. Each 10 μL reaction contained iTaq universal SYBR Green reaction mix (2x), iScript reverse transcriptase, forward and reverse primers (300 nM), RNA (10 ng/μL), and nuclease-free H_2O. The PCR reactions were carried out as follows: 10 minutes at 50°C for the reverse transcription reaction, 1 minute at 95°C for the polymerase activation and initial DNA denaturation followed by 40 cycles of amplification at 95°C for 10 seconds and 60°C for 30 seconds. The primer sequences for genes detected were *Homo sapiens* casein kinase 1 delta (*CSNK1D*, NM_139062, forward 5'- CAGGAGAAGAGGTTGCCATCA -3', reverse 5'- CAAGCAGCAGGACGGTTTTG -3'), casein kinase 1 epsilon (*CSNK1E*, NM_152221, forward 5'- CGTGTGGGGAACAAGTACCG -3', reverse 5'- GATGTTGGCACCCAGGTAGAT -3'), TAR DNA binding protein (*TARDBP*, NM_007375,

forward 5’- CCGAACAGGACCTGAAAGAG -3’, reverse 5’- CAGTCACACCATCGTCCATC -3’), and glyceraldehyde-3-phosphate dehydrogenase (*GAPDH*, internal standard, NM_002046, forward 5’- GGAGCGAGATCCCTCCAAAAT -3’, reverse 5’- GGCTGTTGTCATACTTCTCATGG -3’).

Immunofluorescence (IF)

Cells were fixed with 4% PFA in PBS for 10 min at room temperature. After two washes with PBS, cells were permeabilized with 0.02% Triton-X in PBS for 15 minutes at room temperature and then blocked in 2% FBS in PBS for 1 hour at room temperature. Cells were then incubated overnight at 4°C with the primary antibodies diluted in blocking buffer. The primary antibodies used for staining were TDP-43 (1:2000, Proteintech #12892-1-AP) and pTDP-43 (S409/410) (1:1000, Cosmo Bio USA #TIP-PTD-M01). The following day, cells were washed three times with PBS for 10 minutes each and then incubated with fluorescently labeled secondary antibodies (Alexa Fluor 488 and 594, Thermo Fisher) diluted at 1:500 in blocking buffer for 1 hour at room temperature. Cells were then washed twice with PBS for 10 minutes each and stained with DAPI at 1:1000 for 5 minutes at room temperature. Cells were washed in PBS three times for 10 minutes each and then mounted with ProLong Gold Antifade Mountant with DAPI (Invitrogen). Slides were left at room temperature to dry completely before imaging. Imaging was performed using the UCSD Microscopy Core’s Zeiss LSM 880 Confocal with FAST Airyscan at 20X and 63X with oil. For quantification, three fields of view were captured by confocal microscopy for each condition and cells were manually counted. Each field of

view contained approximately 50-60 dox-induced TDP-43 positive cells (green channel), of which the pTDP-43 positive cells were counted using the red channel.

Protein extraction

To characterize pTDP-43 expression in samples, cells were homogenized in ice-cold RIPA buffer (Thermo Fisher) with protease and phosphatase inhibitors (Thermo Fisher) and then incubated on ice for 10 minutes. Samples were then centrifuged at 14,000 × g for 15 minutes at 4°C and the supernatant was saved in a new tube as the soluble fraction. The pellet was washed twice with RIPA buffer to remove residual soluble protein. The pellet was resuspended in 8 M urea + 3% SDS buffer and then sonicated, followed by incubation on ice for 15 minutes, then centrifuged at 14,000 rpm for 10 minutes at 10°C. The supernatant was then saved as the insoluble protein fraction.

Immunoblotting

To determine protein sample concentrations, Pierce BCA Protein Assay (Thermo Fisher) was used. Samples were loaded in equal volumes and normalized to 10 μg with PBS and then boiled with 4X Protein Loading Buffer (LI-COR) + β-mercaptoethanol for 5 minutes at 90°C. Samples were then loaded onto a 4-15% SDS–PAGE gel to run (80 V for 10 minutes, then 100 V for 50 minutes), then transferred to nitrocellulose membranes (85 V for 60 minutes on ice) using a Bio-Rad Mini-Protean Tetra Cell Electrophoresis System. Membranes were blocked using TBS Intercept blocking buffer (LI-COR) and then incubated with primary antibodies diluted in Intercept T20 Antibody Diluent (LI-COR) overnight at 4°C. The primary antibodies used were pTDP-43 (S409/410) (1:1000,

Proteintech #22309-1-AP), TDP-43 (1:500, Proteintech #12892-1-AP), CK1δ (1:500, Proteintech #14388-1-AP), CK1ε (1:500, Thermo Fisher #PA5-95934), β-actin (1:20,000, Proteintech #66009-1-Ig), and GAPDH (1:20,000, Proteintech #60004-1-Ig). The following day, the membranes were washed with TBST (0.1% Tween-20 in TBS) three times for 10 minutes each at room temperature and then incubated with secondary antibodies (1:20,000 IRDye 800CW and 1:20,000 IRDye 680RD, LI-COR) diluted in Intercept T20 Antibody Diluent (LI-COR) for 1 hour at room temperature. Membranes were then washed 3 times with TBST for 10 minutes each and then 2 times with TBS for 10 minutes each before imaging on the Odyssey® Fc Imaging System (LI-COR). ImageStudioLite was used to analyze signal intensity.

Statistical analyses

Data were analyzed using GraphPad Prism10 and are expressed as the mean ± standard error of the mean (SEM). Immunoblotting analysis was performed by normalizing bands of interest to the signal intensity for the internal sample control β-actin, and then a ratio for pTDP-43 (S409/410) over total TDP-43 levels was calculated and reported as a relative intensity measure compared to untreated doxycycline-induced condition (no addition of either siRNA or inhibitors). Statistics were performed with either one-way ANOVA or two-tailed t-test using GraphPad Prism 10 with p-values less than 0.05 considered significant.

Acknowledgements

This research was supported by grants from FightMND (Drug Development Grant); ALS Association (ALSA); Target ALS; UC Academic Senate; UCSD Microscopy Core (NINDS-P30NS047101); and National Institutes of Health (NIA-AG059358; NINDS-NS114162; NINDS-NS113517).

We thank Guruharsha Bhat and James Harvey at Biogen, Inc. for their assistance with the KINOME*scan*™ assays. Some figures, like schematics for experimental setups, were created with BioRender.com.

Chapter 2, in full, is a reformatted reprint of the material as it appears in Ko, V. I., Ong, K., Cleveland, D. W., Yu, H., & Ravits, J. M. (2024). CK1δ/ε kinases regulate TDP-43 phosphorylation and are therapeutic targets for ALS-related TDP-43 hyperphosphorylation. *Neurobiology of Disease*, *196*, 106516. https://doi.org/10.1016/j.nbd.2024.106516. The dissertation author was the primary investigator and author of this paper.

Chapter 3 : Targeting CK1ε-mediated phosphorylation of TDP-43 through *Csnk1e* genetic deletion *in vivo*

Abstract

A neuropathological signature of amyotrophic lateral sclerosis (ALS) is hyperphosphorylated aggregates in the cytoplasm of neurons. We previously showed that CK1δ and CK1ε phosphorylate TDP-43 at disease relevant S409/410 phosphorylation sites, and that genetic reduction and chemical inhibition could reduce pTDP-43 levels in cellular models. We advanced our previous findings into an *in vivo* mouse model of ALS and TDP-43 proteinopathy that possessed robust disease-relevant features of ALS, including TDP-43 nuclear depletion, cytoplasmic TDP-43 accumulation, pTDP-43 inclusions, motor behavior deficits, loss of body mass, and shortened survival. We tested the effect of homozygous genetic deletion of *Csnk1e* in the hTDP-43-ΔNLS mouse model on the phenotypes listed above. Overall, we established that targeting CK1ε-mediated phosphorylation via genetic knockout delayed the formation of pTDP-43, but long-term, was insufficient in ameliorating TDP-43 proteinopathy, behavior deficits, and disease progression *in vivo*. In addition, our results suggested the role of CK1-mediated phosphorylation in this particular disease context may be to promote TDP-43 solubility and either prevent the formation of TDP-43 inclusions or alter existing insoluble TDP-43 inclusions into soluble TDP-43. This work adds to a growing body of literature underpinning the role of phosphorylation in affecting TDP-43 solubility and aggregation.

Introduction

Post-translational modifications (PTMs) serve important roles in regulating normal protein functions in signaling pathways (Buratti, 2018; T. J. Cohen et al., 2012, 2015; Ikeda & Tsuchiya, 2004; McGurk et al., 2018). Abnormal PTMs have been observed in disease contexts, but the contribution of PTMs to disease mechanisms remains poorly understood. In ALS cases, numerous abnormal post-translational modifications of TDP-43 have been observed in neuropathological studies, including acetylation, liquid–liquid phase separation (LLPS), mislocalization, phosphorylation, solubilization, proteolytic cleavage, truncation, and ubiquitination (Buratti, 2018; Prasad et al., 2019; Sternburg et al., 2022). The roles of each modification may influence each other and contribute to a mixture of dynamic interactions or be completely independent of each other.

Phosphorylation of TDP-43, in particular, is still being studied to determine whether it is a protective or toxic mechanism in ALS and related TDP-43 proteinopathies (Eck et al., 2021). Further, TDP-43 protein solubility and insolubility, phase changes, and aggregation have been implicated alongside phosphorylation and add complexity to the overall disease mechanism. Attempts to characterize the phosphorylation sites on TDP-43 using bioinformatic and biochemical *in vitro* studies revealed 64 predicted potential phosphorylation sites, of which there are 41 serine (S), 15 threonine (T), and 8 tyrosine (Y) residues. The most common serine sites observed to be hyperphosphorylated in postmortem ALS cases have been S369, S379, S403/404, and S409/410, all within the C-terminal glycine-rich domain of TDP-43 (Hasegawa et al., 2008; Inukai et al., 2008; Kametani et al., 2016; Neumann et al., 2009, 2020, 2021). Of these sites, the most implicated and studied phosphorylation site in ALS is S409/410. The S409/410 site is

commonly examined due to its striking and robust presence in patient neuropathology, but also because antibody tools to detect other phosphorylation sites are limited and largely ineffective.

Studies have proposed phosphorylation as a mechanism that regulates the phase separation of TDP-43 to alter its solubility and polymerization, thus, affecting TDP-43's resistance to proteasomal degradation or localization (Eck et al., 2021; Gasset-Rosa et al., 2019; Newell et al., 2019; Nonaka et al., 2013; A. Wang et al., 2018; Yamashita et al., 2016). Phosphorylation of serine sites within TDP-43's C-terminal domain has been shown to contribute to cell toxicity and attenuate TDP-43 oligomer aggregates in cells, fruit flies, and nematode models (Chiang et al., 2022; Choksi et al., 2014; Hicks et al., 2020; Kim et al., 2015; Liachko et al., 2010; Nonaka et al., 2016; Zhang et al., 2010). On the other hand, phosphorylation may serve a protective compensatory role to regulate the solubility of TDP-43 aggregates towards a more liquid-like phase separated state in response to protein aggregation (Brady et al., 2011; Gruijs Da Silva et al., 2022; H.-Y. Li et al., 2011). For example, when cells were treated with a heat shock stressor, TDP-43 was found to be phosphorylated at non-serine sites (T153 and Y155) by MEK, a heat shock response-dependent kinase responsible for protein homeostasis, and this pTDP-43 species remained soluble and not aggregate prone, suggesting the role of phosphorylation to be non-pathogenic and help restore TDP-43 homeostasis (W. Li et al., 2017). The field still lacks consensus and knowledge of the temporal dynamics of TDP-43 phosphorylation, such as whether it precedes or is a consequence of TDP-43 aggregation. Generally, the mechanism responsible for TDP-43 phosphorylation and its

influence on the formation of cytoplasmic, aggregated, and pathological TDP-43 remains understudied.

Many ALS-related studies conducted in cellular models fail to capture progressive cell death that is observed in human patients with motor neuron degeneration as a result of ALS. Our cellular models described in Chapter 2 have their own set of limitations, which has directed us towards *in vivo* testing of CK1-dependent TDP-43 phosphorylation and its effect on TDP-43 proteinopathy. Ultimately, using a mouse model will allow us to incorporate the complexities of mammalian biology into our studies of neurodegenerative diseases mechanisms. There are numerous mouse models available for the study of ALS and motor neuron degeneration, some with genetic mutations of ALS-disease causing genes like *SOD1*, *TARDBP*, *C9orf72*, and others. We selected a model of TDP-43 overexpression (hTDP-43-ΔNLS) where mice generated cytoplasmic phosphorylated TDP-43 inclusions in neurons and exhibited significant motor behavior deficits and shortened survival (Alfieri et al., 2014; Igaz et al., 2011; Walker et al., 2015).

In the previous chapter, we demonstrated that CK1δ and CK1ε are the primary kinases to regulate TDP-43 phosphorylation, and that we can significantly reduce pTDP-43 levels by genetic siRNA interference methods and small molecule chemical inhibitors that target CK1δ and CK1ε (Ko et al., 2024). Studies of the CK1 kinase family showed that CK1δ and CK1ε shared significant homology in their kinase domains which suggested potential redundant roles , depending on the biological pathway (Cheong & Virshup, 2011; Fish et al., 1995; Fulcher & Sapkota, 2020). Genetic deletion studies in mice revealed that CK1ε may be dispensable, but CK1δ was indispensable and a critical

component for cell viability since homozygous deletion was perinatal lethal (Etchegaray et al., 2009).

In the present study, we tested whether homozygous deletion of *Csnk1e* in the inducible hTDP-43-ΔNLS mouse model of ALS would affect behavioral motor impairments and TDP-43 proteinopathy phenotypes. We validated the specificity of genetic knockout to *Csnk1e,* which did not result in altered expression of *Csnk1d* or *Tardbp/TARDBP* in our mouse experimental system. Overall, we found that targeting CK1ε-mediated phosphorylation via genetic knockout in mice delayed the formation of pTDP-43 but was insufficient in reducing TDP-43 proteinopathy and ameliorating behavior deficits. Our analysis of soluble and insoluble protein fractions throughout disease progression suggested the role of phosphorylation, in this particular experimental system, may be to promote TDP-43 solubility and either prevent the formation of TDP-43 inclusions or alter existing insoluble TDP-43 inclusions into soluble TDP-43. This work adds to a growing body of literature underpinning the role of phosphorylation in altering TDP-43 solubility and aggregation.

Results

Mouse model of inducible TDP-43 proteinopathy has ALS disease-relevant phenotypes

To translate our previous studies into a relevant mammalian disease model, we used hTDP-43-ΔNLS mice, which is a tet-off doxycycline (dox) inducible system with overexpression of human TDP-43 containing a defective nuclear localization signal (NLS) (Figure 3.1A-B). When dox is removed during adulthood, allowing transgene expression,

mice develop hallmark ALS phenotypes of motor neuron degeneration in brain and spinal cord, motor behavior deficits, declining health measures, and premature death with median survival of 8-10 weeks (Alfieri et al., 2014; Igaz et al., 2011; Walker et al., 2015). In our study to characterize and validate the disease mouse model (Figure 3.2A), we found that observable symptom onset of deficits for rotarod and forelimb grip strength tasks were significant by 14 days (Figure 3.2B) and 32 days (Figure 3.2C) of induced TDP-43 expression, respectively, as compared to littermate wild-type control mice. As disease progressed, their body mass significantly declined (Figure 3.2D) and the median survival was reached by day 50 (Figure 3.2E).

As mice progressed, there was observable TDP-43 nuclear clearance and cytoplasmic pTDP-43 expression in neurons of both brain and spinal cord (Figure 3.3A-B), recapitulating neuropathic observations of ALS postmortem tissue. The confocal imaging of immunostained tissue showed distinct nuclear depletion of TDP-43 as well as robust diffused TDP-43 signal in the cytoplasm of motor neurons, as visualized by the green channel. A significant portion of the cytoplasmic TDP-43 was observed to be phosphorylated, as visualized in the red channel utilizing an antibody that detected the S409/410 phosphosites. These robust phenotypes justified using the hTDP-43-ΔNLS mouse model to study the effects of CK1ε-mediated phosphorylation on TDP-43 proteinopathy.

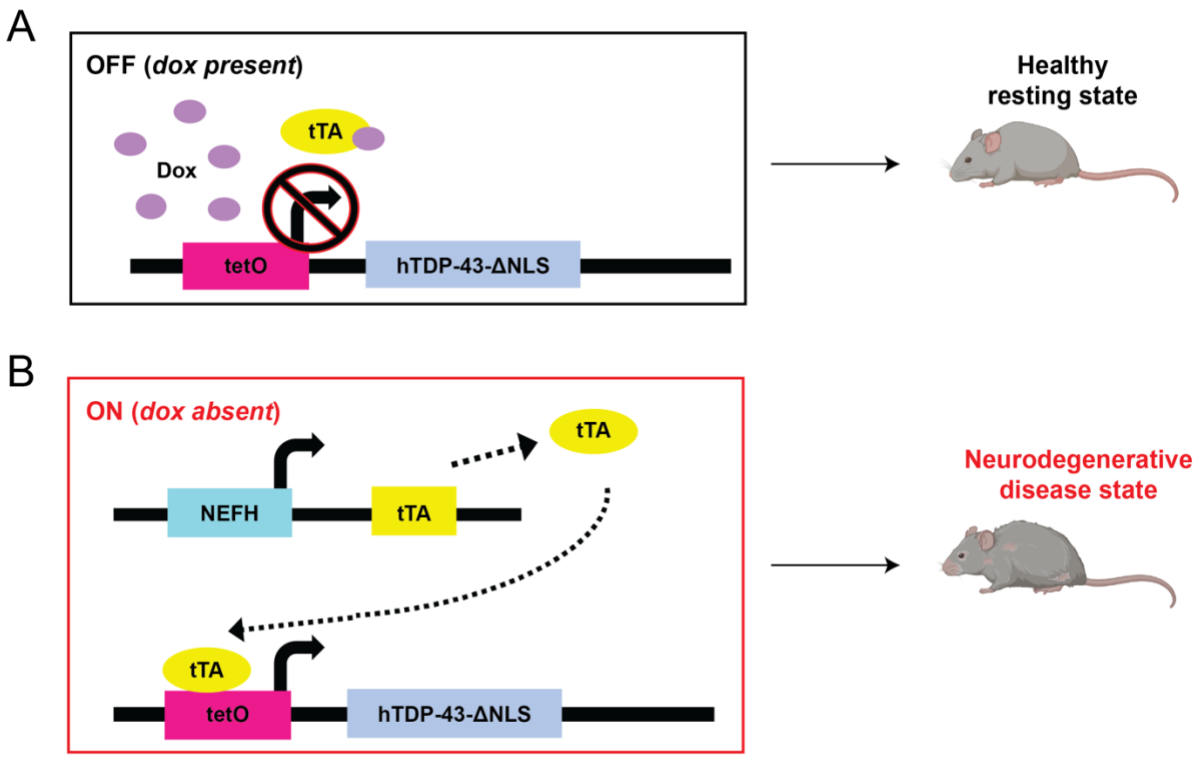


Figure 3.1 Mouse disease model is a tet-off dox inducible system.

(A) When hTDP-43-ΔNLS mice were fed dox chow, the hTDP-43-ΔNLS transgene was suppressed, and mice grew normally into adulthood. (B) The neurofilament heavy chain (NEFH) promoter line drove cell-specific expression in neurons with large caliber exons, which were primarily motor neurons of the brain and spinal cord. When dox chow was replaced with normal chow, the tetracycline activator protein (tTA) activated the transcription of the hTDP-43-ΔNLS transgene, which encoded the human TARDBP gene that contained a defective nuclear localization signal (ΔNLS). This initiated the progressive TDP-43 proteinopathy disease phenotypes and neurodegeneration in mice.

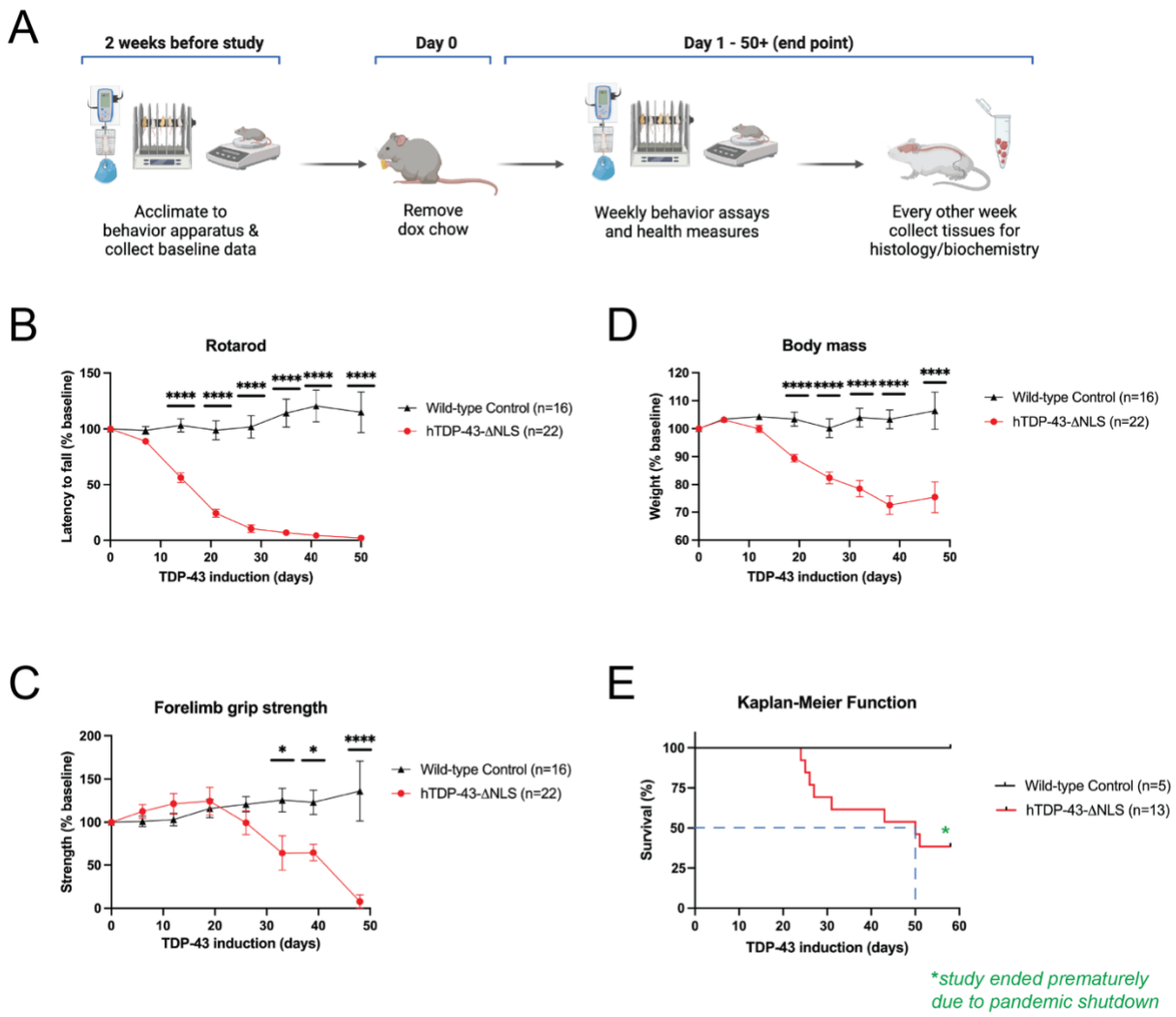


Figure 3.2 hTDP-43-ΔNLS mice display significant motor deficits and degenerative health.

(A) Experimental design used to characterize and validate the hTDP-43-ΔNLS mouse model. Mice were trained on behavior tasks in the weeks prior to the study start date, and the baseline data was collected before dox chow was changed to regular chow. Data on motor behavior and health measures was collected weekly. Satellite mice were run in parallel for tissue collection to have samples that represented early, middle, and late stages of disease progression. (B) Rotarod performance for hTDP-43-ΔNLS mice was significantly decreased by 14 days. (C) Forelimb grip test strength declined significantly by 32 days. (D) Body mass quickly declined as disease progressed in hTDP-43-ΔNLS mice. (E) The median survival was reached by day 50, as indicated by the blue dashed lines. The study ended prematurely in 2020 due to the COVID pandemic shutdown. Two-way ANOVA, *p < 0.03, **p < 0.002, ***p < 0.0002, ****p < 0.0001. Error bars represent SEM.

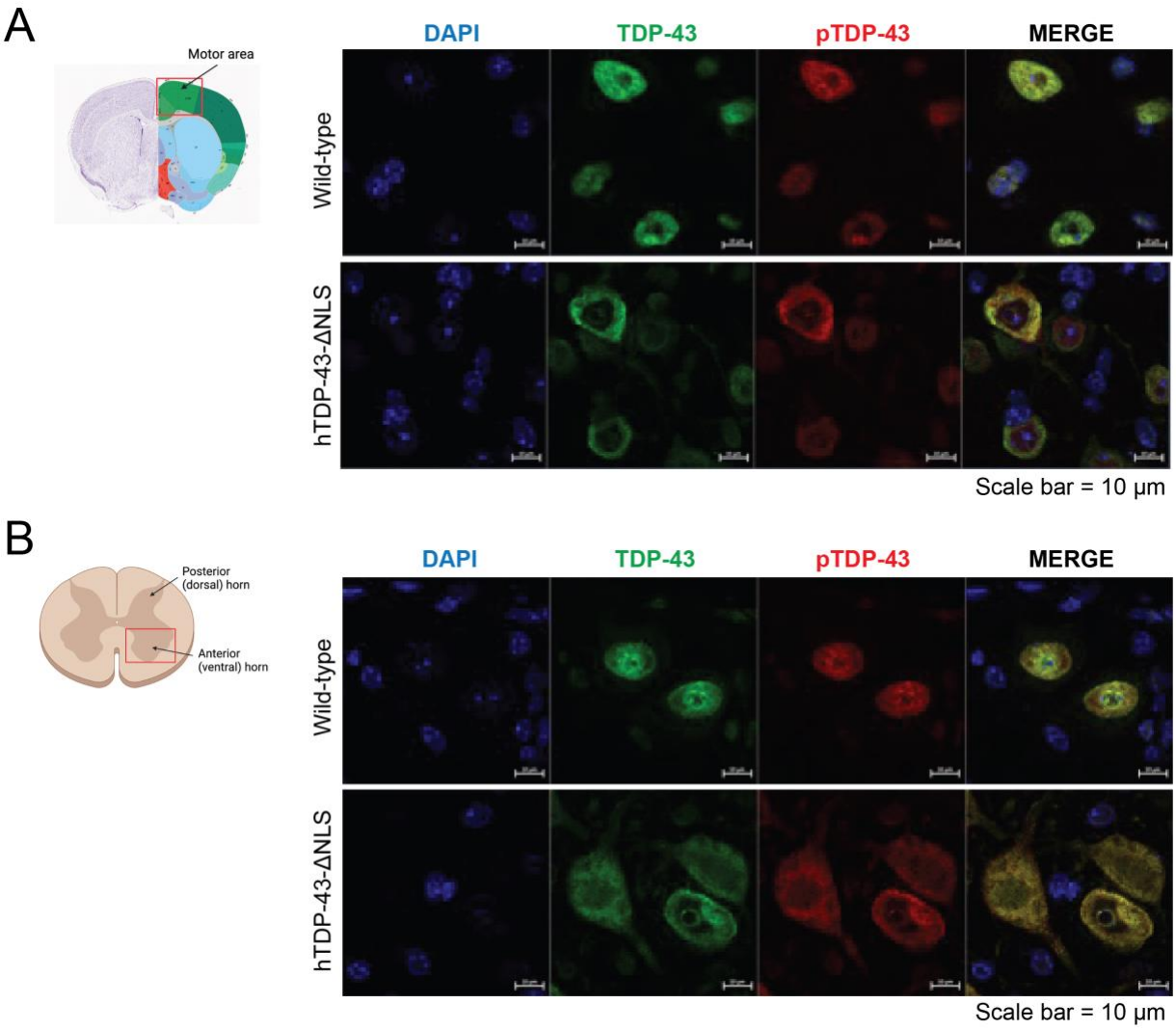


Figure 3.3 hTDP-43-ΔNLS mice display TDP-43 nuclear clearance and cytoplasmic pTDP-43 expression in neurons.

(A) Representative immunofluorescence images of neurons in cortex of wild-type control and hTDP-43-ΔNLS mice with staining for TDP-43 (green), pTDP-43 (red), and DAPI (blue). TDP-43 remained nuclear in wild-type cells while it became translocated and mislocalized to the cytoplasm in hTDP-43-ΔNLS samples. Much of the mislocalized TDP-43 was also found to be phosphorylated. Scale bars represent 10 μm. (B) Similar observations of altered TDP-43 expression was also observed in lumbar spinal cord tissue sections. Scale bars represent 10 μm.

Deletion of *Csnk1e* is gene-specific and does not alter the regulation of *Csnk1d*

To test whether removal of the *Csnk1e* gene would affect TDP-43 phosphorylation *in vivo*, we generated homozygous *Csnk1e* knockout (KO) in the hTDP-43-ΔNLS mouse model. Homozygous *Csnk1e*-KO mice displayed no behavioral deficits or overt phenotypes and bred normally. To produce homozygous *Csnk1e*-KO x hTDP-43-ΔNLS mice, homozygous *Csnk1e*-KO mice were bred with each parent line of the hTDP-43-ΔNLS mouse model which were the hemizygous NEFH-tTA mice and hemizygous tetO-hTDP-43-ΔNLS mice. Offspring with the desired genotypes were then crossed to create homozygous *Csnk1e*-KO x hTDP-43-ΔNLS mice, which will be referred to as *Csnk1e*-KO mice for the remainder of this chapter (Figure 3.4A). The homozygous *Csnk1e*-WT x hTDP-43-ΔNLS littermate controls will be referred to as *Csnk1e*-WT moving forward in this chapter. In this final crossing, mating pairs were fed dox chow to suppress transgene expression so pups could develop properly and grow into adulthood. The homozygous knockout of *Csnk1e* on both alleles was accomplished using the Cre-*loxP* recombination system, where *LoxP* sites were inserted into introns 1 and 4 and Cre-mediated excision of exons 2-3 of *Csnk1e* resulted in deletion of a part of the ATP binding domain essential for CK1ε kinase activity (Etchegaray et al., 2009). Due to Mendelian genetics where only 6.25% of offspring in our breeding scheme would have the desired genotypes, over 450 mice were bred to achieve the necessary sample size for experiments.

Given that *Csnk1d* shared 85% homology with *Csnk1e* by comparing their nucleotide sequences using the Basic Local Alignment Search Tool (BLAST) on NCBI (https://blast.ncbi.nlm.nih.gov/Blast.cgi), we validated and characterized the *Csnk1e*-KO and *Csnk1e*-WT mice for genetic deletion specificity and potential compensatory gene

regulation. Additionally, BLAST alignment comparisons revealed that human *CSNK1D* and *CSNK1E* shared 98% homology with respective mouse *Csnk1d* and *Csnk1e*, thus the results from our study in mice would likely be relevant and applicable to human contexts. Studies that have tested *Csnk1d* gene deletion in mice found the homozygous knockout to be perinatal lethal, so we were unable to pursue studies of *Csnk1d* via genetic knockout in our hTDP-43-ΔNLS disease mouse model (Etchegaray et al., 2009).

Homozygous deletion of *Csnk1e* was found to be gene-specific, without significant changes to *Csnk1d* RNA expression when compared to *Csnk1e*-WT littermate controls (Figure 3.4B-C). Furthermore, immunoblots of immunoprecipitated samples for the low expressing CK1ε and CK1δ kinases showed lack of CK1ε protein in *Csnk1e*-KO mice, while CK1δ was still detected at similar levels to controls (Figure 3.4D-E). The CK1 antibodies used for immunoprecipitation and immunoblotting were validated using recombinant proteins and found to be specific for solely either CK1δ or CK1ε, not both, providing confidence that there was no observable significant compensatory *Csnk1d* expression in *Csnk1e*-KO mice (data not shown). In addition, the RNA expressions of both endogenous mouse *Tardbp* gene and the overexpressed human *TARDBP* transgene in *Csnk1e*-KO mice indicated no significant change compared to *Csnk1e*-WT controls (Figure 3.4F-G). These characterizations and validations allowed the results of our study to be reasonably attributed to the specificity of the *Csnk1e* knockout.

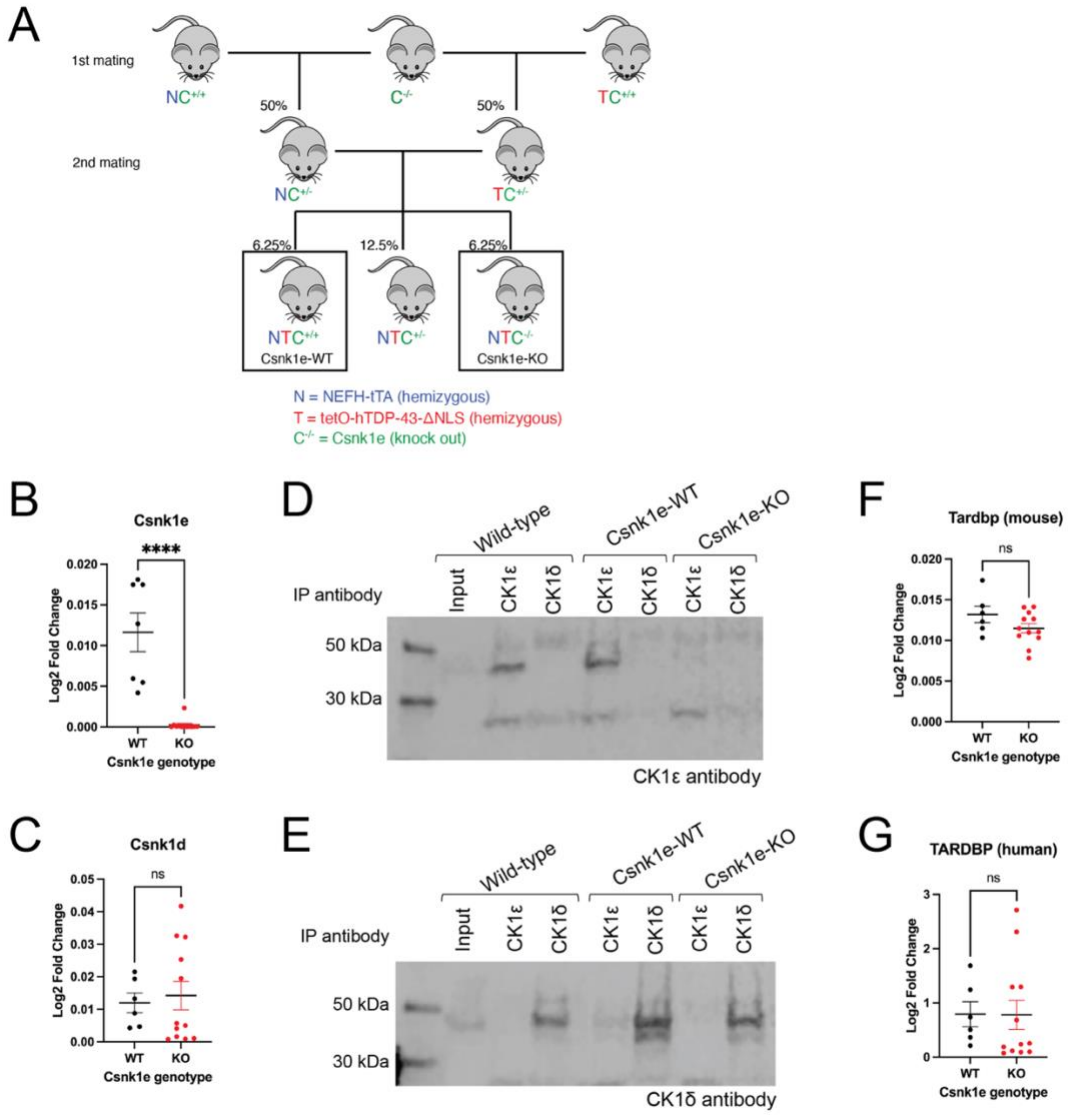


Figure 3.4 Characterization and validation of Csnk1e-KO mice.

(A) Breeding scheme used to generate *Csnk1e*-KO mice and *Csnk1e*-WT control litter mates. (B-C) qRT-PCR data of gene expression for *Csnk1e* and *Csnk1d* mRNA levels in mice. *GAPDH* mRNA was used as endogenous control. Deletion of *Csnk1e* in mice was successful, with no significant effect on *Csnk1d* gene expression. Mann-Whitney t-test, *p < 0.03, **p < 0.002, ***p < 0.0002, ****p < 0.0001. Error bars represent SEM. (D, E) Immunoblots of brain cortex lysate after immunoprecipitation (due to low expression levels of CK1ε and CK1δ) showed *Csnk1e* specific knockout in mice where CK1ε was not detected in *Csnk1e*-KO samples (D) but CK1δ could still be detected (E). (F-G) qRT-PCR data of gene expression for mouse-specific *Tardbp* and human-specific *TARDBP* mRNA levels in mice. *GAPDH* mRNA was used as endogenous control. Deletion of *Csnk1e* in mice resulted in no significant effect on TDP-43 gene expression. Mann-Whitney t-test, *p < 0.03, **p < 0.002, ***p < 0.0002, ****p < 0.0001. Error bars represent SEM.

Deletion of *Csnk1e* delayed pTDP-43 formation, but was insufficient in reducing TDP-43 proteinopathy

Following the same experimental design as discussed above (Figure 3.2A), we assayed the mice for general health measures, motor behavior tests, and analyzed tissue samples afterwards. Biochemical analysis of immunoblots showed that *Csnk1e*-KO mice had generally reduced pTDP-43 levels across all timepoints collected (Figure 3.5A). We then grouped the data into early stage (less than 21 days) and late stage (more than 21 days) of disease progression based upon the onset of motor deficits and declining health (Figure 1C-H). This analysis revealed a decrease of pTDP-43 only observed in early stages (Figure 3.5B). This effect was no longer seen in later stages, where pTDP-43 levels of *Csnk1e*-KO mice were similar to that of *Csnk1e*-WT control mice (Figure 3.5C).

Because we detected a difference in pTDP-43 levels depending on whether *Csnk1e*-KO mice were early or late stage, we pursued protein fractionation of cortical tissue into RIPA-soluble and RIPA-insoluble/urea-soluble fractions for further analysis. Despite being an underpowered study due to sample tissue availability, the results of protein fractionation revealed some striking differences. The immunoblots showed a delay in soluble pTDP-43 formation from early to late stage, where the late-stage mice had comparable soluble pTDP-43 levels as controls (Figure 3.5D). The emergence of pTDP-43 levels while CK1ε was no longer present may be due to other kinases, like CK1δ or others, that could phosphorylate TDP-43. More interestingly, pTDP-43 was not detected in the insoluble protein fractions either in the early and late stages in the *Csnk1e*-KO mice. Our results suggest that deletion of *Csnk1e* delayed pTDP-43 formation. Further, they

suggest that phosphorylation of TDP-43 may actually be a mechanism that promotes protein solubility and drives TDP-43 into a soluble state (Figure 3.5D).

In our motor behavior studies, we did not observe an improvement on either rotarod or forelimb grip strength tests (Figure 3.6A-B) and the *Csnk1e*-KO group performed similarly as the control *Csnk1e*-WT group. Body mass yielded no significant difference between groups, which also indicated that *Csnk1e* deletion was not detrimental to accelerate or worsen the overall health of mice (Figure 3.6C). Analyzing the tissues collected for immunohistochemistry and fluorescent confocal imaging revealed that neurons of *Csnk1e*-KO mice still developed hallmarks of TDP-43 proteinopathy with TDP-43 nuclear clearance and cytoplasmic pTDP-43 expression in the brain and spinal cord (Figure 3.7A-B). However, we observed a brief period between days 25 to 45 where the Kaplan-Meier curve suggested an extension of survival (Figure 3.6D), and this was likely a result of the reduced and delayed pTDP-43 formation (Figure 3.5B and D). Despite this temporary extension of survival, there was no accompanied change in reducing or slowing disease symptoms or progression. Both *Csnk1e*-KO and *Csnk1e*-WT groups reached their end points in a similar amount of time. Thus, we concluded *Csnk1e*-KO was overall insufficient in reducing hallmark phenotypes of TDP-43 proteinopathy in the hTDP-43-ΔNLS mouse model.

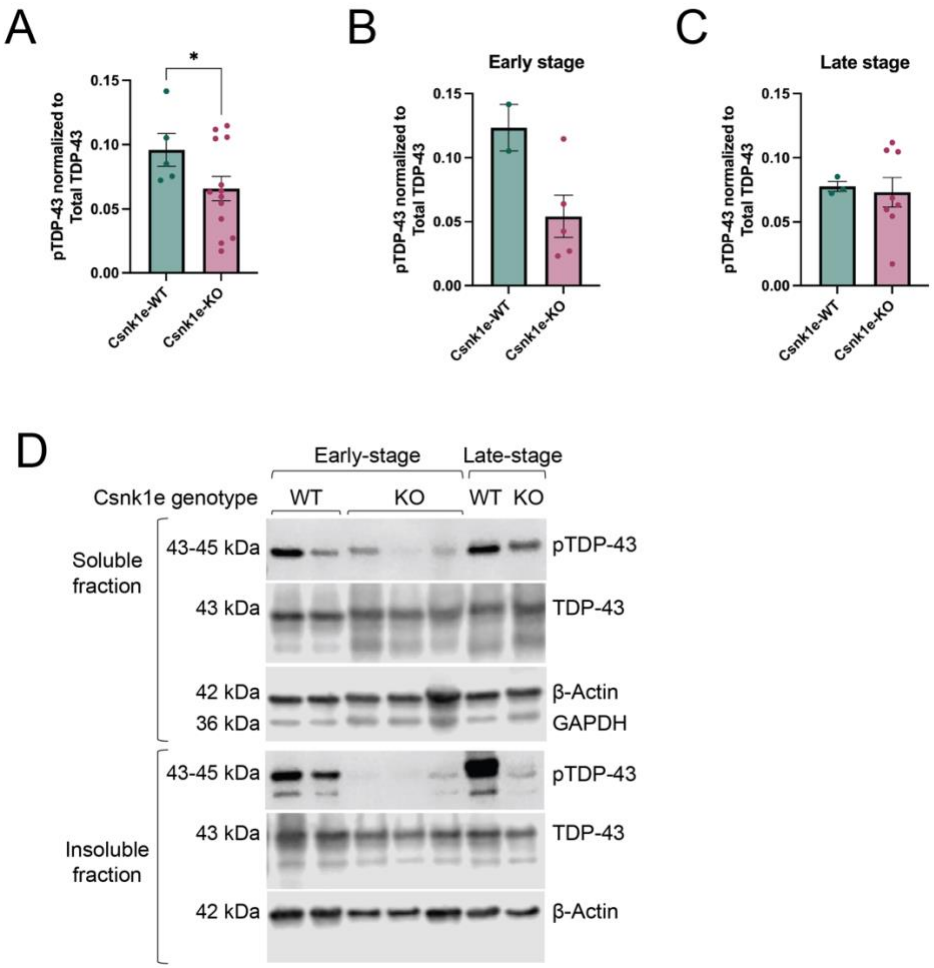


Figure 3.5 TDP-43 phosphorylation was delayed in *Csnk1e*-KO mice and may be a mechanism that promotes protein solubility.

A) *Csnk1e*-KO mice had generally reduced pTDP-43 levels across all timepoints collected. (B-C) Data was grouped into early (less than 21 days) and late (more than 21 days) stages of disease progression. Only samples from early stage *Csnk1e*-KO mice demonstrated pTDP-43 reduction. Quantification of pTDP-43 reduction in soluble and insoluble protein fractions was computed as a normalized ratio between pTDP-43 and total TDP-43 signals. The signal intensity for each pTDP-43 band was first normalized to β-Actin, then calculated as a ratio relative to total TDP-43 levels (which was also normalized to β-Actin). Mann-Whitney t-test, *$p < 0.03$, **$p < 0.002$, ***$p < 0.0002$, ****$p < 0.0001$. Error bars represent SEM. (D) Fractionating the protein into soluble and insoluble compartments demonstrated a delay in soluble pTDP-43 formation in *Csnk1e*-KO mice from early to late stage as compared with *Csnk1e*-WT mice which had detectable pTDP-43 at both stages of disease progression. There was no pTDP-43 detected in insoluble protein fractions of both early and late stage *Csnk1e*-KO mice. There were high levels of pTDP-43 signal detected in *Csnk1e*-WT control mice for both early and late stages of disease progression. GAPDH signal was used to indicate the quality of fractionation between insoluble and soluble protein fractions.

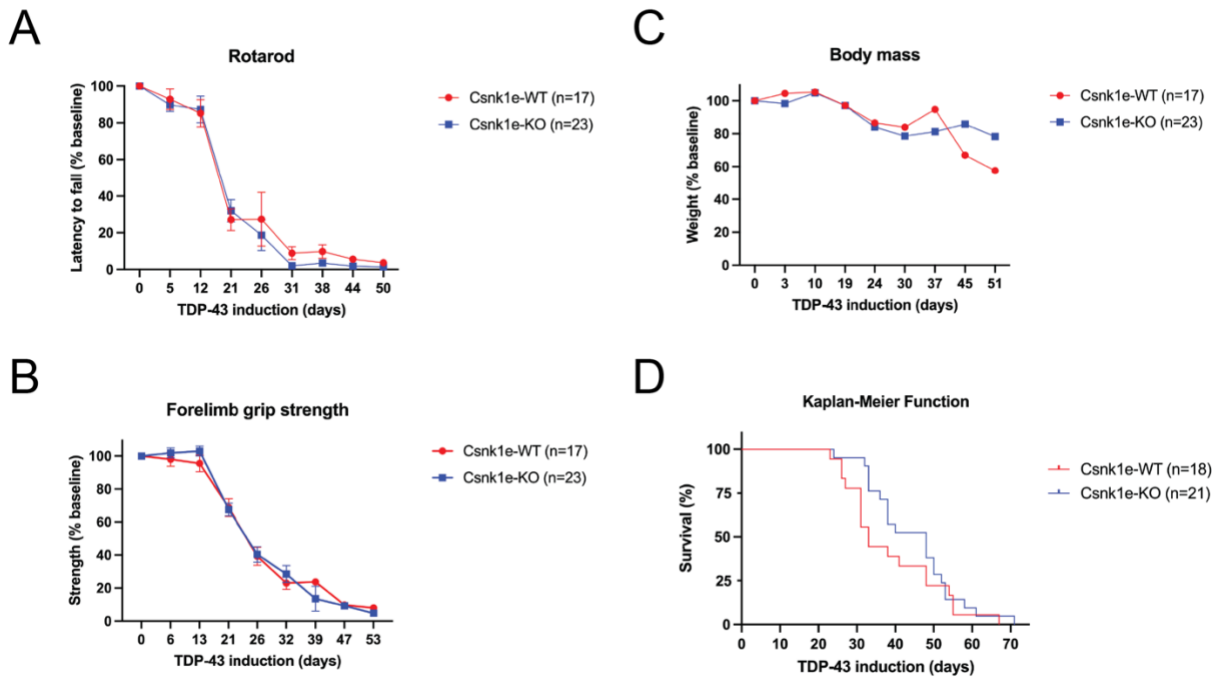


Figure 3.6 Deletion of *Csnk1e* did not exacerbate motor impairments or overall health of mice.

A) Rotarod performance for *Csnk1e*-KO mice did not improve as compared to *Csnk1e*-WT control mice. (B) Forelimb grip strength test also did not display improvements. (C) *Csnk1e* deletion did not exacerbate the overall health of mice and the body mass declined similarly in both groups. (D) There was a modest extension of median survival for *Csnk1e*-KO mice, but the effect was not sustained long-term, and mice of both groups reached end points at similar times.

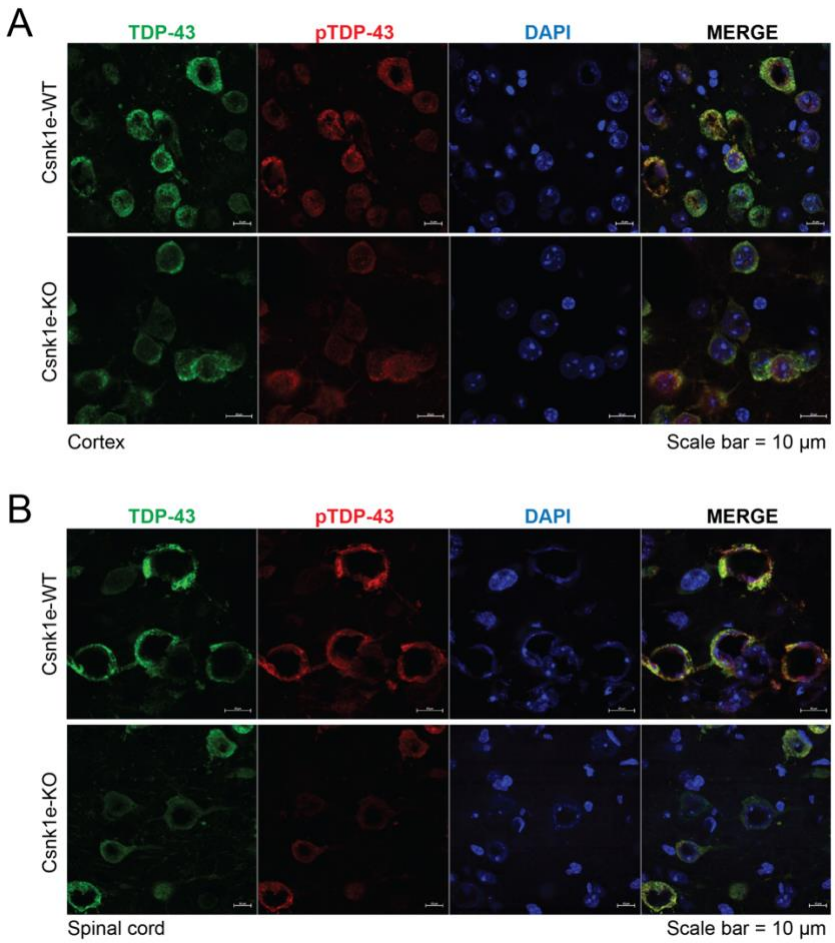


Figure 3.7 *Csnk1e*-KO mice developed hallmarks of cellular TDP-43 proteinopathy in the brain and spinal cord.

((A-B) Representative immunofluorescence images of cortex and spinal cord tissue with TDP-43 (green), pTDP-43 (red), and DAPI (blue). No difference in TDP-43 nuclear clearance or cytoplasmic pTDP-43 accumulation was observed in neurons in brain or spinal cord tissue from *Csnk1e*-KO mice as compared to *Csnk1e*-WT control mice. Scale bars represent 10 μm.

Discussion

In this study, we advanced our previous findings from *in vitro* and cellular experimental systems into an *in vivo* mammalian disease model. Specifically, we focused the present study on testing the effects of genetic deletion of *Csnk1e* in the inducible

hTDP-43-ΔNLS mouse model of ALS and related TDP-43 proteinopathies. We selected this particular ALS mouse model due to its robust disease-relevant hallmarks of ALS progression, including TDP-43 nuclear depletion, cytoplasmic pTDP-43 inclusions, motor behavior deficits, loss of body mass, and shortened survival. In our intricate breeding scheme to generate hTDP-43-ΔNLS mice with homozygous deletion of *Csnk1e*, we were able to validate the specificity of genetic knockout to *Csnk1e*, which was accompanied with no significant disruption or alterations to *Csnk1d* or *Tardbp/TARDBP* gene expressions. Overall, we found that targeting CK1ε-mediated phosphorylation via genetic knockout in hTDP-43-ΔNLS mice delayed the formation of pTDP-43 but was ultimately insufficient in reducing pTDP-43 levels and TDP-43 proteinopathy long-term and ameliorating behavior deficits and disease progression.

A limitation of this study and important consideration when interpreting these results was that the presence and functional contribution of CK1δ still remained in our experimental system. We had thoroughly characterized the *Csnk1e*-KO mice for *Csnk1d* expression, which indicated no significant alterations when *Csnk1e* was removed. Despite the lack of expression change, CK1δ may have increased its functional kinase activity to compensate for the lack of CK1ε *in vivo*. Ideally, an *in vivo* kinase assay would be used to determine if CK1δ activity was increased but identifying and developing the assay for a CK1δ-specific sensitive biomarker as a readout was complicated and challenging. We also attempted immunoblotting, global proteomic mass spectrometry profiling, and phospho-proteomic approaches to see if we could detect increased phosphorylation of downstream CK1δ targets (i.e. PER1, PER2, etc.), but the antibody tools were inadequate and mass spectrometry protein phosphorylation detection lacked

sensitivity and was highly variable. Thus, we intended to leverage pharmacologic strategies and pursue testing CK1 kinase inhibitors in hTDP-43-ΔNLS mice to study the contribution of CK1δ-mediated phosphorylation of TDP-43 in addition to that of CK1ε-mediated phosphorylation.

Despite a lack of significant rescue of behavior deficits or health measures in *Csnk1e*-KO mice, our biochemical analysis showed delayed pTDP-43 formation when *Csnk1e* was removed. Notably, the observations of pTDP-43 levels between the soluble and insoluble fractions, and acknowledgement that the presence of other kinases could phosphorylate TDP-43, suggested that phosphorylation in this particular *in vivo* experimental system may be a mechanism intended to promote the solubility of accumulated TDP-43 and abnormal insoluble TDP-43 protein. In *Csnk1e*-KO mice, phosphorylation did not contribute to the formation of insoluble TDP-43 and may have potentially suppressed the phase separation or aggregation of TDP-43 by disrupting the self-self-interaction of the C-terminal glycine-rich domain on TDP-43. Studies have suggested that phosphorylation of TDP-43 occurred after aggregate formation and that the modification was not a prerequisite for aggregation (Dormann et al., 2009; Iguchi et al., 2012). Taken together, phosphorylation may act as a mechanistic switch for TDP-43 cytoplasmic accumulation and either prevent the initial formation of TDP-43 inclusions or alter the existing insoluble TDP-43 inclusions into soluble TDP-43. Nevertheless, our work adds to a growing body of literature underpinning the role of phosphorylation in altering TDP-43 solubility and aggregation.

Methods

Mouse breeding and maintenance of hTDP-43-ΔNLS mice

Bigenic transgenic mice for the hTDP-43-ΔNLS model (JAX Stock No. 028412) were generated by crossing monogenic NEFH-tTA mice (JAX Stock No. 025397) with monogenic tetO-hTDP-43-ΔNLS mice (JAX Stock No. 014650) obtained from the Jackson Laboratory (Bar Harbour, Maine, USA). Parent lines were maintained on a B6C3F1/J (JAX Stock No. 100010) background. Mice were fed with 200 mg/kg doxycycline (dox) supplemented chow (Envigo TD.08541) throughout breeding and weaning to suppress the hTDP-43-ΔNLS transgene. To induce hTDP-43-ΔNLS transgene expression, mice were switched to and fed standard chow without dox (PicoLab Rodent Diet 20 #5053). Genotyping was performed using tail DNA and sent to the commercial vendor Transnetyx for automated test results. All procedures were formed in accordance with NIH Guide for the Care and Use of Experimental Animals and Studies were approved by the Institutional Animal Care and Use Committee (IACUC) of the University of California, San Diego.

Generation of *Csnk1e* knockout mouse line breeding with NEFH-hTDP-43ΔNLS mice

Transgenic heterozygote *Csnk1e* mutant mice were donated by Dr. David Weaver of University of Massachusetts Medical School. These mice were maintained on a C57BL/6J (JAX Stock No. 000664) background. For *Csnk1e* knockout mouse studies, *Csnk1e* mutant mice were bred with each parent line of the hTDP-43-ΔNLS mouse model, and then were subsequently crossed to create homozygous *Csnk1e*-KO x hTDP-43-ΔNLS mice. Double knockout of *Csnk1e* on both alleles was accomplished using the Cre-

loxP system. *LoxP* sites were inserted into introns 1 and 4, where Cre-mediated excision of exons 2-3 of *Csnk1e* resulted in removal of a portion of the ATP binding domain essential for CK1ε kinase activity (Etchegaray et al., 2009). In the final crossing, mice were fed with 200 mg/kg doxycycline (dox) supplemented chow (Envigo TD.08541) throughout breeding and weaning to suppress the hTDP-43-ΔNLS transgene. To induce hTDP-43-ΔNLS transgene expression, mice were switched to and fed standard chow without dox (PicoLab Rodent Diet 20 #5053). Genotyping was performed using tail DNA and sent to the commercial vendor Transnetyx for automated test results. All procedures were formed in accordance with NIH Guide for the Care and Use of Experimental Animals and Studies were approved by the Institutional Animal Care and Use Committee (IACUC) of the University of California, San Diego. Littermates were grouped into indicated cohorts based upon genotype in a gender-balanced way. Experimenters were blinded to genotype assignment throughout the study.

Rotarod behavior

To assay motor coordination and balance, the rotarod (Ugo Basile) rotated at a speed of 4 rpm and accelerated to 40 rpm over 300 seconds. The time to fall was recorded with a maximum score of 300 seconds if the mouse was still running on the rod at the end of the session. There was one training session and three test sessions for each mouse with at least 30 minutes of rest in between sessions. The final score for each mouse was the average time of the three test sessions.

Grip test behavior

Mice were lowered onto a triangular bar of the grip meter (Columbus Instruments) until they gripped the bar with their hindlimbs. Then, mice were pulled backwards by their tail until they released their grip and the maximum force in kilograms was recorded. One training session and five testing sessions were performed, with at least 5 minutes of rest in between sessions. The final score for each mouse was an average of the five test sessions.

Tissue collection for biochemistry assays

Mice were anesthetized by isoflurane vapors in a glass chamber box. Toe pinch was used to test depth of anesthesia. Once anesthetized, scissors were used to decapitate the mouse, and then the brain and spinal cord tissues were extracted and partitioned into 1.5 mL Eppendorf tubes. Once tissues were collected, tubes were flash frozen onto dry ice and stored in -80°C until use.

Tissue collection for histology assays

Mice were injected via intraperitoneal (IP) with avertin, and toe pinch was used to test depth of anesthesia. Once anesthetized, mice were perfused with freshly prepared ice-cold PBS and 4% paraformaldehyde (PFA) using a peristaltic pump. When sufficiently fixed, brain and spinal cord tissues were extracted and put into conical tubes containing 4% PFA for overnight fixation at 4°C. The following day, the solution was changed to 30% sucrose. Once the tissue was saturated with sucrose, it was embedded into OCT blocks

for cryosectioning at the desired thickness (35 μm) and stored in cryoprotectant solution until use for immunofluorescent staining.

Real-time PCR (qRT-PCR)

RNA was extracted using the Direct-zol RNA miniprep kit (Bio-Rad) according to the manufacturer's protocol and samples were measured for RNA quantity (OD260/280) and purity (OD230/260) using a NanoDrop spectrophotometer (Thermo Fisher). qRT-PCR was performed with iTaq universal SYBR Green one-step kit (Bio-Rad) and CFX384 (Bio-Rad) as described in the manufacturer's protocol. Each 10 μL reaction contained iTaq universal SYBR Green reaction mix (2x), iScript reverse transcriptase, forward and reverse primers (300 nM), RNA (10 ng/μL), and nuclease-free H_2O. The PCR reactions were carried out as follows: 10 minutes at 50°C for the reverse transcription reaction, 1 minute at 95°C for the polymerase activation and initial DNA denaturation followed by 40 cycles of amplification at 95°C for 10 seconds and 60°C for 30 seconds. The primer sequences for genes detected were *Mus musculus* casein kinase 1 delta (*Csnk1d*, NM_027874, forward 5'- CTGAGGGTCGGGAACAGGTA -3', reverse 5'- TGAGGATGTTTGGTTTTGACACA -3'), *Mus musculus* casein kinase 1 epsilon (*Csnk1e*, NM_013767, primer set 1 forward 5'- AAGCTCGAATGTGTGAAGACG -3', primer set 1 reverse 5'- TGACCATCACGTTATAGTCTCCC -3', primer set 2 forward 5'- AGGTTGAAGCATGGAGTTGC -3', primer set 2 reverse 5'- TGGGGATGTTTCGTCTTCAC -3'), *Mus musculus* TAR DNA binding protein (*Tardbp*, NM_145556, forward 5'- ATGAGAACGATGAACCCATTGAA -3', reverse 5'- TGAGACACGGGATTCCGGTAG -3'), *Homo sapiens* TAR DNA binding protein

(*TARDBP*, NM_007375, forward 5'- CCGAACAGGACCTGAAAGAG -3', reverse 5'- CAGTCACACCATCGTCCATC -3'), and *Mus musculus* glyceraldehyde-3-phosphate dehydrogenase (*Gapdh*, internal standard, NM_008084, forward 5'- AGGTCGGTGTGAACGGATTTG -3', reverse 5'- TGTAGACCATGTAGTTGAGGTCA -3').

Protein extraction

To characterize pTDP-43 expression in samples, brain tissue was homogenized in ice-cold N-PER buffer (Thermo Fisher) with protease and phosphatase inhibitors (Thermo Fisher) and then incubated on ice for 10 minutes. Samples were then centrifuged at 13,500 rpm for 20 minutes at 4°C and the supernatant was saved in a new tube as the soluble fraction. The pellet was washed twice with N-PER buffer to remove residual soluble protein. The pellet was resuspended in lysis buffer + 8 M urea + 3% SDS and then sonicated, followed by incubation on ice for 15 minutes, then centrifuged at 14,000 rpm for 10 minutes at 10°C. The supernatant was then saved as the insoluble protein fraction.

Immunoprecipitation (IP)

SureBeads Magnetic Beads (BioRad) were vortexed in their solution to resuspend, and 100 uL was transferred into a tube. Beads were magnetized and the supernatant was discarded. Beads were then washed 3 times with 1 mL PBST (PBS + 0.1% Tween-20) by vortexing and magnetizing to discard the supernatant. The IP antibody was then diluted in PBST and added to the beads for resuspension. Antibodies used were CK1δ

(Thermo Fisher #MA5-17243) and CK1ε (Thermo Fisher #MA5-517231). The mixture was rotated at room temperature for 10 minutes, then vortexed, magnetized, and the supernatant was discarded. The beads (with antibody bound to them at this stage) were washed 3 times with 1 mL PBST and then protein lysate was added to incubate with breads and antibody for rotation at room temperature for 1 hour. After the incubation, the beads were washed 3 times with PBST by vortexing, magnetizing, and discarding the supernatant. The protein was eluted into 1X orange loading buffer by incubation at 70°C for 10 minutes. Beads were then magnetized, and the eluent was moved to a new vial for immunoblotting.

Immunoblotting

To determine protein sample concentrations, Pierce BCA Protein Assay (Thermo Fisher) was used. Samples were loaded in equal volumes and normalized to 10 μg with PBS and then boiled with 4X Protein Loading Buffer (LI-COR) + β-mercaptoethanol for 5 minutes at 90°C. Samples were then loaded onto a 4-15% SDS–PAGE gel to run (80 V for 10 minutes, then 100 V for 50 minutes), then transferred to PVDF membranes (85 V for 60 minutes on ice) using a Bio-Rad Mini-Protean Tetra Cell Electrophoresis System. Membranes were blocked using TBS Intercept blocking buffer (LI-COR) and then incubated with primary antibodies diluted in Intercept T20 Antibody Diluent (LI-COR) overnight at 4°C. The primary antibodies used were pTDP-43 (S409/410) (1:1000, Proteintech #22309-1-AP), TDP-43 (1:500, Proteintech #12892-1-AP), CK1δ (1:1000, Thermo Fisher #MA5-17243), CK1ε (1:1000, Thermo Fisher #MA5-517231), β-actin (1:20,000, Proteintech #66009-1-Ig), and GAPDH (1:20,000, Proteintech #60004-1-Ig).

The following day, the membranes were washed with TBST (0.1% Tween-20 in TBS) three times for 10 minutes each at room temperature and then incubated with secondary antibodies (1:20,000 IRDye 800CW and 1:20,000 IRDye 680RD, LI-COR) diluted in Intercept T20 Antibody Diluent (LI-COR) for 1 hour at room temperature. Membranes were then washed 3 times with TBST for 10 minutes each and then 2 times with TBS for 10 minutes each before imaging on the Odyssey® Fc Imaging System (LI-COR). ImageStudioLite was used to analyze signal intensity. Quantification of band intensity was based upon immunoblot densitometry values. The pTDP-43 band signal was first normalized to β-Actin, as was the total TDP-43 band signal. These two normalized values were then computed as a ratio with pTDP-43 relative to total TDP-43. This analysis incorporated normalization not only to an internal protein control within each sample using the housekeeping gene β-Actin, but also considered the expression of the total TDP-43 (hTDP-43-ΔNLS transgene) since there may have been inherent genetic regulatory variability between samples.

Immunofluorescence (IF)

Tissue sections were removed from cryoprotectant solution and washed in PBS 3 times for 10 minutes each. Sections were then blocked in 5% horse serum with 0.2% TritonX in PBS for 1 hour at room temperature. Tissue sections were then incubated overnight at 4°C with the primary antibodies diluted in blocking buffer. The primary antibodies used for staining were TDP-43 (1:500, BioLegend #808301) and pTDP-43 (S409/410) (1:500, Proteintech #22309-1-AP). The following day, tissues were washed three times with PBS for 10 minutes each and then incubated with fluorescently labeled

secondary antibodies (Alexa Fluor 488 and 594, Thermo Fisher) diluted at 1:500 in blocking buffer for 2 hours at room temperature. Tissues were then washed twice with PBS for 10 minutes each and stained with DAPI at 1:1000 for 5 minutes at room temperature. Tissues were washed in PBS three times for 10 minutes each and then mounted with ProLong Gold Antifade Mountant with DAPI (Invitrogen). Slides were left at room temperature to dry completely before imaging. Imaging was performed using the UCSD Microscopy Core's Zeiss LSM 880 Confocal with FAST Airyscan at 20X and 63X with oil.

Statistical analyses

Data were analyzed using GraphPad Prism10 and are expressed as the mean ± standard error of the mean (SEM). Immunoblotting analysis was performed by normalizing bands of interest to the signal intensity for the internal sample control β-actin, and then a ratio for pTDP-43 (S409/410) over total TDP-43 levels was calculated and reported as a relative intensity measure. Statistics were performed with either two-way ANOVA or Mann-Whitney t-test using GraphPad Prism 10 with p-values less than 0.05 considered significant.

Acknowledgements

We thank Dr. David Weaver of University of Massachusetts Medical School for donating the transgenic heterozygote *Csnk1e* mutant mice for our experiments. In addition, we thank Melissa McAlonis from the Cleveland lab for sharing her expert knowledge on *in vivo* experimental design and assistance with the mouse husbandry and IACUC approvals. Some figures, like schematics for experimental setups, were created with BioRender.com.

This research was supported by grants from FightMND (Drug Development Grant); ALS Association (ALSA); Target ALS; UC Academic Senate; and UCSD Microscopy Core (NINDS-P30NS047101).

Chapter 3, in part, is being prepared for submission for publication of the material as “Manipulation of the S409/410 site on TDP-43 by selective CK1δ/ε inhibition as a candidate therapeutic target”. Other co-authors will be Kailee Ong, Deborah Y. Kwon, Xueying Li, Alicia Pietrasiewicz, James Harvey, Mukesh Lulla, Guruharsha Bhat, Don W. Cleveland, and senior author John M. Ravits. The dissertation author will be the primary investigator and author of this paper.

Chapter 4 : Manipulation of the S409/410 site on TDP-43 by selective CK1δ/ε inhibition as a candidate therapeutic target

Abstract

Hyperphosphorylated TDP-43 aggregates in the cytoplasm of motor neurons is a neuropathological hallmark of amyotrophic lateral sclerosis (ALS). These inclusions have been proposed to possess a toxic disease driving role in ALS pathogenesis and progression, however, the contribution of phosphorylation to TDP-43 aggregate formation and ALS disease mechanisms remains poorly understood. In previous chapters, we demonstrated that siRNA-mediated knockdown and chemical inhibitors targeting CK1δ and CK1ε resulted in reduced pTDP-43 in cellular models. We then tested genetic deletion of *Csnk1e* in the hTDP-43-ΔNLS disease mouse model of ALS and observed a delay in the formation of pTDP-43 but was insufficient in reducing TDP-43 proteinopathy and disease progression. Our work suggested phosphorylation as a mechanism that facilitated TDP-43 solubility to either prevent the formation of TDP-43 inclusions or modify the existing insoluble TDP-43 inclusions into soluble TDP-43. In this present study, we tested the preclinical efficacy of targeting CK1δ and CK1ε kinases by way of CK1δ/ε-selective inhibitors in the hTDP-43-ΔNLS mouse model. We characterized the pharmacokinetic and pharmacodynamic profiles for the two compounds of interest, CK1δ/ε-specific PF-05236216 inhibitor and CK1ε-specific PF-4800567 inhibitor and selected the CK1δ/ε-specific PF-05236216 inhibitor to advance into preclinical efficacy studies. We were able to reduce TDP-43 phosphorylation and lower Nf-L levels, indicating

neurodegeneration reduction, but not sufficiently to fully eliminate toxicity or result in functional benefit. Our results demonstrated that manipulation of the S409/410 site on TDP-43 by selective CK1δ/ε inhibition may not be a suitable candidate therapeutic target on its own for ALS therapy.

Introduction

Amyotrophic lateral sclerosis (ALS) is a devastating and rapidly fatal adult-onset neurodegenerative disease with progressive cell death of upper motor neurons of the brain's motor cortex and the lower motor neurons of the spinal cord. Its progression is severely debilitating and quick, with patients surviving on average 3-5 years from diagnosis. A defining neuropathological feature found in 97% of all sporadic and familial ALS cases is TDP-43 proteinopathy, which is the altered expression and function of transactive response DNA-binding protein 43 (TDP-43) in cells, primarily in motor neurons (R. H. Brown & Al-Chalabi, 2017; S.-C. Ling et al., 2013; Polymenidou et al., 2012; Swinnen & Robberecht, 2014). Specifically, TDP-43 is mislocalized from the nucleus to the cytoplasm, where TDP-43 accumulates into inclusions containing various aberrant post-translational modifications, like phosphorylation, ubiquitination, and acetylation, to name a few (Buratti, 2018; Prasad et al., 2019; Sternburg et al., 2022). Currently, the field lacks consensus as to the extent of contributions that TDP-43 nuclear loss-of-function or TDP-43 cytoplasmic gain-of-toxicity has on ALS disease pathogenesis.

In healthy cells, TDP-43 remains localized to the nucleus where it regulates gene expression and RNA splicing and processing. The C-terminal end of TDP-43 contains a low-complexity glycine-rich region which is where a majority of ALS disease-causing

genetic mutations have been found. This region also contains multiple serine residues that have been observed to be abnormally phosphorylated in ALS cases. Neuropathological studies of ALS samples have revealed S369, S379, S403/404, and S409/410 to be most commonly observed, of which S409/410 is most thoroughly studied due to limited detection methods and consistent technical antibody quality (Hasegawa et al., 2008, 2011; Inukai et al., 2008; Kametani et al., 2016; Neumann et al., 2009, 2020, 2021).

Studies have implicated phosphorylation of TDP-43 as a toxic gain-of-function mechanism, where increased TDP-43 aggregate formation and cell toxicity was observed in various models such as cells, fruit flies, and nematode models (Choksi et al., 2014; Hicks et al., 2020; Kim et al., 2015; Liachko et al., 2010; Nonaka et al., 2016; Zhang et al., 2010). There is also a set of studies that has proposed phosphorylation as a protective compensatory mechanism to solubilize the TDP-43 aggregates (Brady et al., 2011; Gruijs Da Silva et al., 2022; H.-Y. Li et al., 2011). Nevertheless, phosphorylation appeared to have some regulatory role for TDP-43 solubility, phase separation, and polymerization and affected TDP-43's susceptibility for protein degradation pathways in disease states (Gasset-Rosa et al., 2019; Newell et al., 2019; Nonaka et al., 2013; A. Wang et al., 2018; Yamashita et al., 2016).

Given the lack of consensus within the field on the role of TDP-43 phosphorylation in disease mechanisms, we sought to identify the primary kinase responsible for phosphorylating TDP-43 in ALS and study its influence on the formation of cytoplasmic, aggregated, and pathological TDP-43. Our previously published work identified *CSNK1E* as being strongly correlated with pTDP-43 pathology in ALS patient samples (Krach et

al., 2018). *CSNK1E* (gene encoding CK1ε protein) and *CSNK1D* (gene encoding CK1δ protein) are closely related family members that share 84% homology and were found to contribute to circadian rhythm biology to different magnitudes (Cheong & Virshup, 2011; Etchegaray et al., 2009, 2010; Fish et al., 1995; Fulcher & Sapkota, 2020; Walton et al., 2009). Our *in vitro* and cellular studies revealed CK1δ and CK1ε as principal kinases that regulated TDP-43 phosphorylation at disease relevant S409/410 phosphorylation sites, and that genetic siRNA interference reduction and selective small molecule chemical inhibition targeting CK1δ and CK1ε reduced pTDP-43 levels effectively (Ko et al., 2024). We then advanced our studies into an *in vivo* mammalian mouse model of TDP-43 proteinopathy (hTDP-43-ΔNLS) where mice generated cytoplasmic phosphorylated TDP-43 inclusions in neurons and exhibited significant motor behavior deficits and shortened survival. We found that targeting CK1ε-mediated phosphorylation via *Csnk1e* genetic knockout delayed the formation of pTDP-43 but was ineffective in reducing TDP-43 proteinopathy phenotypes and ameliorating behavior deficits and disease progression. However, CK1δ still remained functional in the experimental system tested, and therefore, may have contributed to the results.

In this present study, we tested the preclinical efficacy of targeting CK1δ and CK1ε kinases by way of small molecule chemical inhibitors in the hTDP-43-ΔNLS mouse model. First, we performed dose-finding studies and characterized the pharmacokinetic profiles for both CK1δ/ε-selective PF-05236216 and CK1ε-selective PF-4800567 inhibitors. We also provided pharmacodynamic target engagement evidence for utilizing CK1 inhibitors *in vivo* to reduce pTDP-43 levels in soluble and insoluble TDP-43 protein fractions. In our preclinical efficacy study, we showed that we were able to reduce TDP-43

phosphorylation and lower Nf-L levels, but not sufficiently to fully eliminate toxicity or result in functional benefit. Our results demonstrated that manipulation of the S409/410 site on TDP-43 by selective CK1δ/ε inhibition may not be a suitable candidate target on its own for ALS therapy.

Results

Novel characterization of mouse model reveals supplementary measures of neurodegenerative phenotypes

Expanding upon the established phenotypes of the hTDP-43-ΔNLS mouse model introduced in Chapter 3, we included the following assays and further characterized these mice for neurofilament light chain (Nf-L) levels and compound muscle action potentials (CMAP). Nf-L is a common non-specific early-stage biomarker of neurodegeneration and neuronal damage, and is increasingly used as a biomarker of therapeutic efficacy in clinical trials, which can be measured in biofluids like CSF or blood plasma (Benatar et al., 2016, 2020). Increases in Nf-L levels has been shown to be correlated with neurodegenerative disease progression. The Nf-L levels in this mouse model was increased by day 14 and significantly elevated by day 28 of induced TDP-43 expression (Figure 4.1A). CMAP recordings were conducted for both right and left hindlimb tibialis anterior (TA) muscles via stimulation of the sciatic nerve as a proxy for muscle neurophysiology and motor neuron degeneration (McCampbell et al., 2018). The CMAP recordings showed significant decline in peak-to-peak amplitude by day 25 of induced TDP-43 expression (Figure 4.1B). These additional phenotypes that can be measured in our mouse model, which are assays used in humans and reflect the ALS disease

progression in patients, will be valuable in our studies testing the preclinical efficacy of CK1 inhibitors *in vivo*.

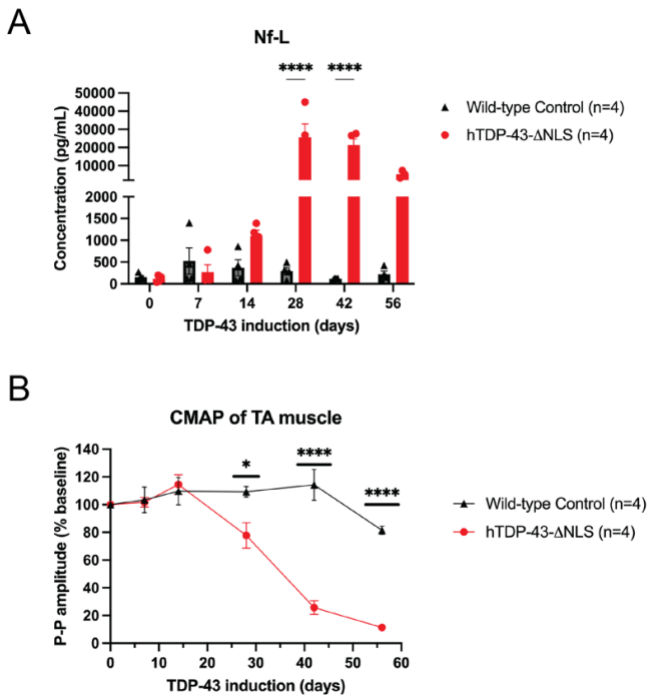


Figure 4.1 Nf-L and CMAP assays demonstrate robust neurodegeneration phenotypes.

(A) hTDP-43-ΔNLS mice displayed elevated Nf-L levels by 14 days of induced TDP-43 expression, with significant increases by day 28. (B) CMAP recordings showed significant decline in the peak-to-peak amplitude in TA muscles by day 25 of induced TDP-43 expression. Two-way ANOVA, *p < 0.03, **p < 0.002, ***p < 0.0002, ****p < 0.0001. Error bars represent SEM.

TDP-43 hyperphosphorylation and cytoplasmic accumulation precedes motor behavior deficits in hTDP-43-ΔNLS mice

To capture the TDP-43 phosphorylation dynamics in this mouse model, we characterized pTDP-43 accumulation in soluble and insoluble protein fractions via detection in immunoblots. We found that 7 days of TDP-43 induction was sufficient to begin detecting pTDP-43 levels in both soluble and insoluble protein fractions, with

maximal signal intensity by day 10 (Figure 4.2A). This data indicated that TDP-43 phosphorylation preceded motor deficits, which were observable at day 14 of induced TDP-43 expression. The insoluble protein fraction contained detectable pTDP-43 before the soluble protein fraction, suggesting phosphorylation as a modification that occurred after insoluble TDP-43 formation. Further, accumulation of a higher molecular weight (>43 kDa) hyperphosphorylated TDP-43 species was detected exclusively in the insoluble protein fraction at later timepoints (Figure 4.2A).

These biochemical observations support phosphorylation as a mechanism that occurred earlier in disease pathogenesis before behavioral symptoms could be detected, allowing us a window of approximately 10 days to examine how CK1δ- and CK1ε-mediated phosphorylation would affect pTDP-43 accumulation and protein solubility during disease progression. Additionally, this model sufficiently generated an altered higher molecular weight insoluble hyperphosphorylated TDP-43 species later in disease progression, which was reflective of the neuropathological observations of TDP-43 protein recovered from human samples (Hasegawa et al., 2008), and would allow us to study the short- and long-term effects of CK1δ- and CK1ε-mediated phosphorylation on disease progression.

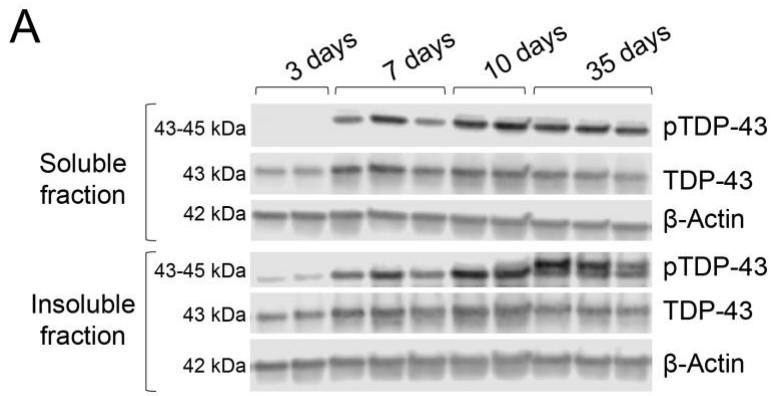


Figure 4.2 pTDP accumulation precedes motor deficits.

(A) Representative immunoblots demonstrate that pTDP-43 was detected in soluble and insoluble protein fractions after 7 days of induced TDP-43 expression, with maximal signal intensity by day 10. pTDP-43 accumulated and was detected in the insoluble fraction before it could be detected in the soluble fraction. Later into the disease course, a higher molecular weight hyperphosphorylated TDP-43 species (top band) could be detected in the insoluble fraction.

Characterization of CK1 inhibitors as an *in vivo* tool

We previously used CK1δ/ε-specific PF-05236216 inhibitor and CK1ε-specific PF-4800567 inhibitor *in vitro* to demonstrate their efficacy in reducing pTDP-43 levels in U2OS and SH-SY5Y cell models that generated phosphorylated TDP-43 (Ko et al., 2024). To use these inhibitors *in vivo*, we conducted early dose-finding studies to characterize the pharmacokinetic (PK) and pharmacodynamic (PD) properties for both CK1 inhibitors in mice and identify the inhibitor dose and dosing route and regimen. These studies allowed us to explore the exposure-response relationship between compound exposure concentrations in the brain and the compound's target engagement effectiveness. They also helped to indicate whether there were any immediate concerns for organ impairment or toxicity and safe use. We identified the maximal tolerated dose (MTD) for CK1δ/ε-specific PF-05236216 inhibitor was 80 mg/kg from the range of doses we tested at 20,

40, 80, 120 mg/kg. We did not encounter a MTD for CK1ε-specific PF-4800567 inhibitor with the range of doses we tested at 25, 50, 100, and 150 mg/kg.

In our PK study, we sought to characterize the drug metabolism and half-life profile for both CK1 inhibitors. We performed a single intraperitonially (IP) injection of the inhibitors into wild-type mice and collected brain tissue and plasma at multiple timepoints, which included 1-, 2-, 4-, 8-, and 24-hours post-injection (n = 6, 3 females and 3 males for each timepoint). The doses tested were 40 mg/kg for CK1δ/ε-specific PF-05236216 and 100 mg/kg for of CK1ε-specific PF-4800567, which were selected from our MTD study and published circadian studies utilizing these compounds or similar ones (Walton et al., 2009). Our PK analysis of unbound compound concentrations in brain tissue revealed that the half-life for CK1δ/ε-specific PF-05236216 inhibitor was approximately 4-6 hours (Figure 4.3A), which was longer than the 1–2-hour half-life for CK1ε-specific PF-4800567 inhibitor (Figure 4.3B). The longer half-life for compound CK1δ/ε-specific PF-05236216 inhibitor was a more favorable PK profile for us to advance into preclinical efficacy studies since it would allow us to have the temporal resolution to study CK1-dependent TDP-43 phosphorylation *in vivo*.

Next, we sought to demonstrate whether *in vivo* target engagement by the inhibitors could be achieved in hTDP-43-ΔNLS mice to establish a robust PD readout. Mice began treatment simultaneously as dox chow was removed to allow for transgene expression. Either CK1δ/ε-specific PF-05236216 inhibitor or CK1ε-specific PF-4800567 inhibitor was injected via IP at the pre-symptomatic stage once daily for 10 consecutive days at doses of 20 and 40 mg/kg and 50 and 100 mg/kg, respectively. The doses were selected upon our MTD study and from referencing published circadian studies utilizing

these compounds or similar ones (Walton et al., 2009). The 10-day treatment length was selected based upon maximal pTDP-43 signal detection in immunoblots as previously mentioned (reference Figure 4.2A). On the final 10th day, samples were collected 2-4 hours after the last injection to account for the compound's half-life (Figure 4.4A) and processed for immunoblotting.

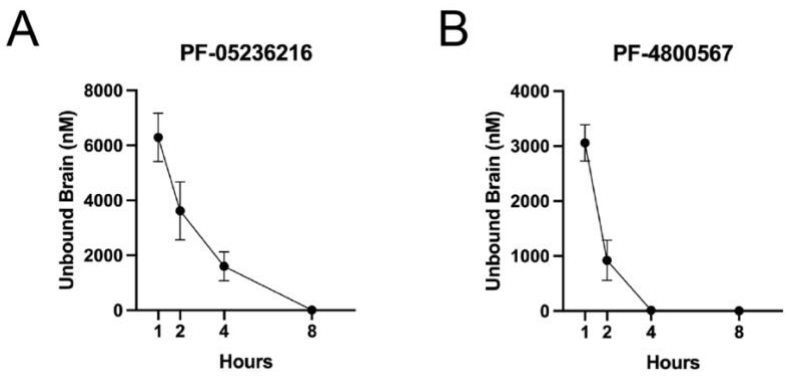


Figure 4.3 Pharmacokinetic (PK) profiles of CK1 inhibitors indicate half-lives and exposure levels.

(A) The PK profile for 40mg/kg dose of CK1δ/ε-specific PF-05236216 inhibitor measured as unbound compound concentrations in the brain demonstrated a half-life approximately 4-6 hours long. (B) The PK profile for 100 mg/kg dose of CK1ε-specific PF-4800567 inhibitor measured as unbound compound concentrations in the brain demonstrated a half-life of approximately 1-2 hours long. Samples were collected 1-, 2-, 4-, 8-, and 24-hours after a single IP injection. Group sizes were n = 6, with 3 females and 3 males for each timepoint.

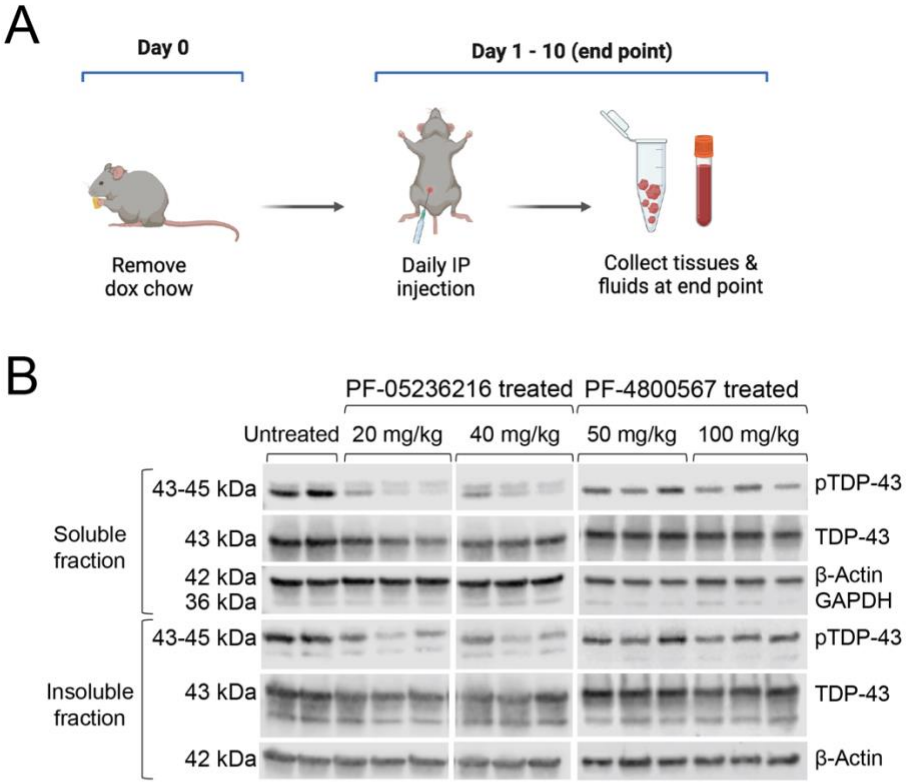
Generally, hTDP-43-ΔNLS mice treated for 10 days with CK1 inhibitor daily demonstrated target engagement of mechanism at both doses for each inhibitor tested with reduced pTDP-43 protein levels as observed in immunoblots (Figure 4.4B). While pTDP-43 reduction was observed in mice treated with 100 mg/kg of CK1ε-specific PF-4800567 inhibitor, the effect was much more significant in mice treated with 20 mg/kg and

40 mg/kg of CK1δ/ε-specific PF-05236216 inhibitor, with 50% or more reduction observed in the soluble protein fraction (Figure 4.4C). Notably, the reduced phosphorylation was more prominent in soluble protein fractions as opposed to insoluble protein fractions in hTDP-43-ΔNLS mice, suggesting the soluble pTDP-43 was more amenable to effects of the CK1 inhibitor, which was similar to results observed in our cellular models (Figure 4.4C-D and Figure 2.7E-F of Chapter 2).

Altogether, these PK and PD data provided proof-of-concept for testing the long-term efficacy of CK1 inhibitors, particularly the CK1δ/ε-specific PF-05236216 inhibitor at a dosage of 40 mg/kg via IP injection, given its favorable profiles for longer PK half-life and effective PD target engagement of mechanism to reduce pTDP-43 levels in both soluble and insoluble protein fractions, and determine whether there would be a difference in TDP-43 proteinopathy, behavioral deficits, and other health metrics of hTDP-43-ΔNLS mice.

Figure 4.4 Characterization of target engagement to TDP-43.

(A) Schematic of the study design to test the target engagement for CK1δ/ε-specific PF-05236216 and CK1ε-specific PF-4800567 inhibitors in hTDP-43-ΔNLS mice. (B) Representative immunoblot images demonstrated reduced pTDP-43 levels in both soluble and insoluble protein fractions when mice were treated with either of the CK1 inhibitors at both doses tested. GAPDH signal was used to indicate the quality of fractionation between insoluble and soluble protein fractions. (C-D) Quantification of immunoblots showed pTDP-43 reduction in both soluble and insoluble protein fractions, with greater reduction observed in the soluble portion. Quantification of pTDP-43 reduction in soluble and insoluble protein fractions was computed as a normalized ratio between pTDP-43 and total TDP-43 signals. The signal intensity for each pTDP-43 band was first normalized to β-Actin, then calculated as a ratio relative to total TDP-43 levels (which was also normalized to β-Actin). Ratios were then compared to the untreated control group. This analysis incorporated normalization not only to an internal gene control within each sample using the housekeeping gene β-Actin, but also took into account the expression of the total TDP-43 (hTDP-43-ΔNLS transgene) since there may have been inherent genetic regulatory variability between samples. Two-way ANOVA, *p < 0.03, **p < 0.002, ***p < 0.0002, ****p < 0.0001. Error bars represent SEM.


A
Day 0
Day 1 - 10 (end point)
Remove dox chow
Daily IP injection
Collect tissues & fluids at end point
B
PF-05236216 treated
PF-4800567 treated
Untreated
20 mg/kg
40 mg/kg
50 mg/kg
100 mg/kg
Soluble fraction
43-45 kDa
43 kDa
42 kDa
36 kDa
pTDP-43
TDP-43
β-Actin
GAPDH
Insoluble fraction
43-45 kDa
43 kDa
42 kDa
pTDP-43
TDP-43
β-Actin
C
Soluble fraction
Relative Intensity pTDP(409/410) / TDP-43
*
****
**
Untreated
20 mg/kg
40 mg/kg
50 mg/kg
100 mg/kg
PF-05236216
PF-4800567
D
Insoluble fraction
Relative Intensity pTDP(409/410) / TDP-43
Untreated
20 mg/kg
40 mg/kg
50 mg/kg
100 mg/kg
PF-05236216
PF-4800567

Selective inhibition of CK1δ/ε reduces TDP-43 phosphorylation and Nf-L levels

With the inhibitor's target engagement established, we then tested the preclinical efficacy of long-term treatment with CK1δ/ε-specific PF-05236216 inhibitor in hTDP-43-ΔNLS mice. Mice began treatment simultaneously as dox chow was removed to allow for transgene expression. The inhibitor was injected intraperitonially (IP) once daily at a dose of 40 mg/kg until mice reached either a natural humane endpoint or median survival, which was 47 days for the study (Figure 4.5A). Mice were recorded and tested weekly for general health measures (body mass and survival), motor behavior assays (rotarod and forelimb grip strength tests), and muscle neurophysiology CMAP recordings. We also included in parallel, satellite cohorts for intermediary timepoint collections at days 14 and 22 throughout the treatment duration, which was determined based upon early-stage and late-stage observations in our *Csnk1e*-KO mouse study (reference Chapter 3). The samples collected for biochemical assays included plasma for Nf-L measures, brain tissue and plasma for PK analysis of unbound inhibitor exposure levels, and brain and spinal cord tissues for immunoblotting soluble and insoluble protein fractions (Figure 4.5A).

In our study, we measured unbound inhibitor concentrations in the brain across 14, 22, and 47 days of treatment. Samples were collected 2-4 hours after IP injection. We confirmed the 40 mg/kg dose of CK1δ/ε-specific inhibitor PF-05236216 had sufficient CNS penetration and distribution past the blood brain barrier, with some inhibitor availability in the brain tissues still remaining (Figure 4.5B). The nanomolar (nM) concentrations for unbound inhibitor in the brain was approximately 20-fold lower than the measurements from our PK study (Figure 4.3A). This difference was likely due to the

length of treatment, where the PK characterization was a single non-repeated dose on the first day in wild-type mice and our efficacy samples were from hTDP-43-ΔNLS mice treated daily for multiple days. It can take approximately four to five half-lives for a compound to reach steady state when given at a regular interval. The measures for unbound inhibitor concentration in brains of mice treated for 14, 22, and 47 days likely represented steady state concentrations where a dynamic equilibrium was reached, and the inhibitor concentrations remained consistent throughout the duration of the efficacy study.

Measuring Nf-L levels from plasma as a biomarker for neurodegeneration progression revealed a significant 2-fold reduction of Nf-L in mice treated for 14 days with CK1δ/ε-specific inhibitor PF-05236216 (Figure 4.5C). This effect was not sustained with longer treatment durations of 22 or 47 days as treated mice had Nf-L levels similar to untreated control mice (Figure 4.5D-E). The changes in Nf-L measurements strongly suggested that reducing TDP-43 phosphorylation via CK1 inhibition was sufficient to reduce neurodegeneration and delay disease progression.

Immunoblot analysis of brain protein lysates revealed that inhibitor treatment of 14 days resulted in decreased pTDP-43 levels in both soluble and insoluble protein fractions (Figure 4.6A). Quantifying the immunoblots showed pTDP-43 reduction in soluble and insoluble protein fractions for 14-day treated mice (Figure 4.6D). However, the effect was not sustained over longer periods of 22-day or 47-day inhibitor treatment Figure 4.6B-C), and no differences were detected between treated and untreated mice for 22-day or 47-day groups (Figure 4.6E-F). The reduced pTDP-43 levels may correlate with the decreased Nf-L that was observed in 14-day treated mice, adding support to the

suggestion that CK1δ/ε inhibitor treatment was sufficient to reduce neurodegeneration and delay disease progression in hTDP-43-ΔNLS mice temporarily. While targeting CK1δ/ε-mediated phosphorylation of TDP-43 demonstrated an effect with short-term inhibitor treatment, the longer treatment periods also did not exacerbate Nf-L levels or pTDP-43 levels.

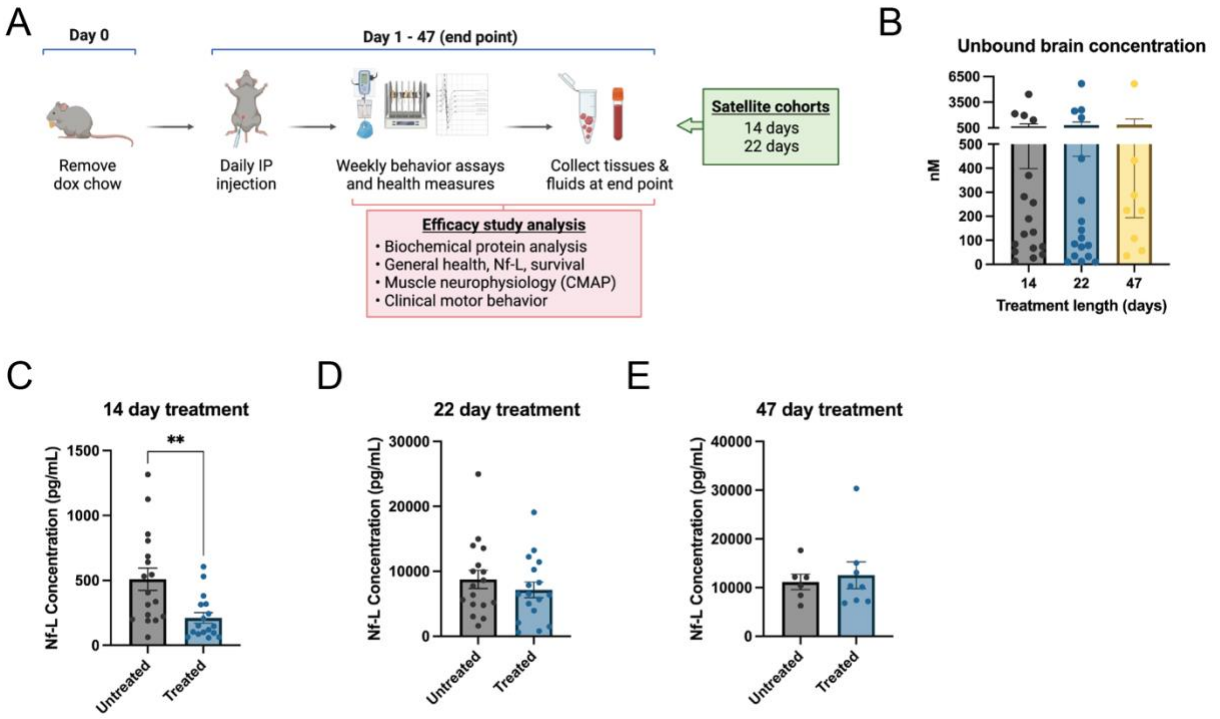
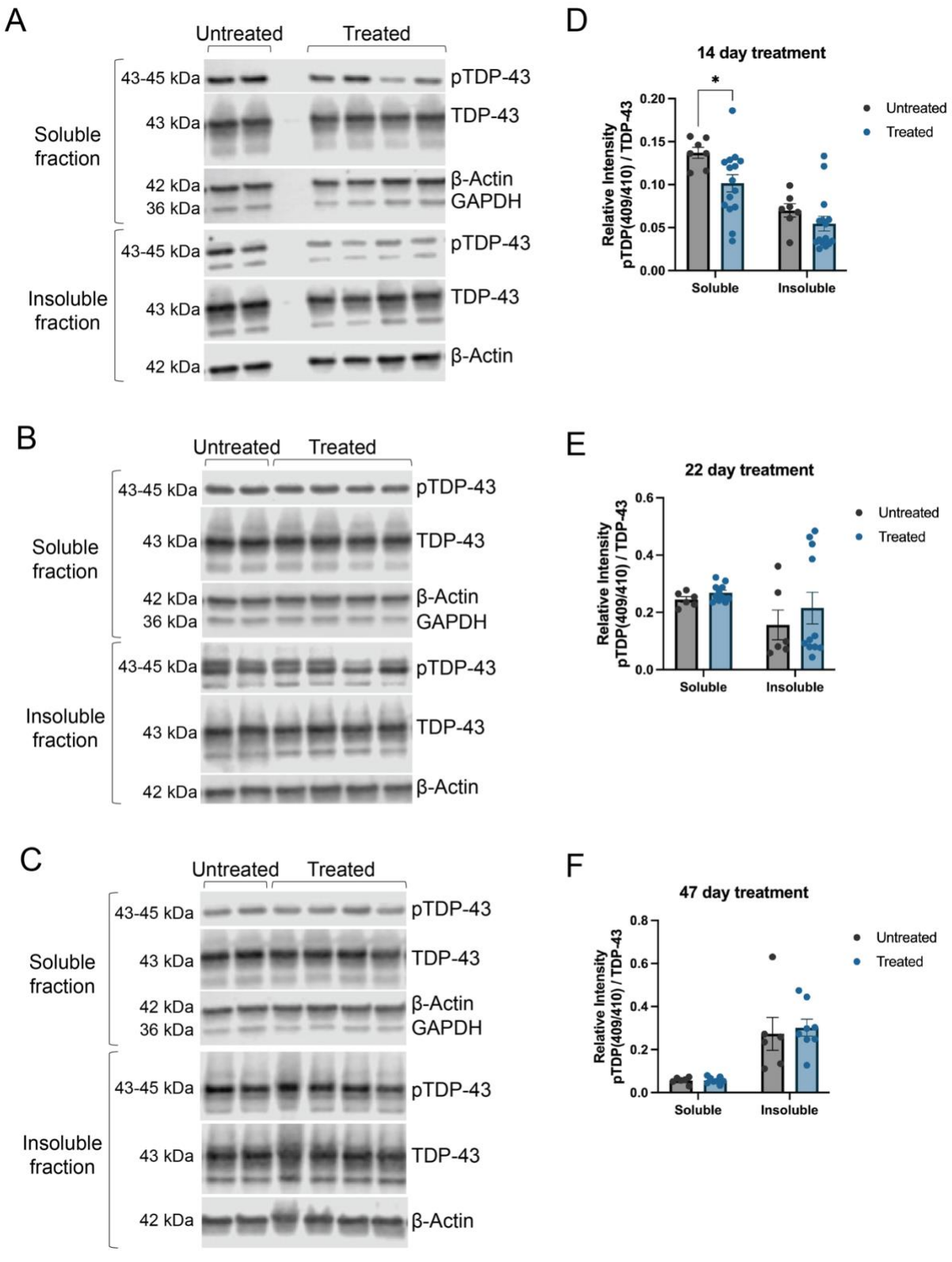


Figure 4.5 Treated mice had sufficient compound exposure levels and showed changes in Nf-L levels.

(A) Schematic of experimental design to test the efficacy of CK1δ/ε-specific inhibitor PF-05236216 in hTDP-43-ΔNLS mice. (B) Unbound inhibitor concentrations were detected and measured in the brain across 14, 22, and 47 days of inhibitor treatment, confirming the inhibitor could cross the blood brain barrier well. (C-E) Nf-L measurements from plasma samples across 14, 22, and 47 days of inhibitor treatment. Nf-L was significantly reduced by 2-fold in mice treated for 14 days. Mice treated for longer time frames did not show a difference compared to untreated mice. Mann-Whitney t-test, *p < 0.03, **p < 0.002, ***p < 0.0002, ****p < 0.0001. Error bars represent SEM.

Figure 4.6 Treated mice showed reduced pTDP-43 with short-term inhibitor treatment.

(A) Representative immunoblot images demonstrated reduced pTDP-43 levels in both soluble and insoluble protein fractions when hTDP-43-ΔNLS mice were treated with CK1δ/ε-specific PF-05236216 inhibitor for 14 days. (B-C) 22-day and 47-day inhibitor treatment did not show a difference between treated and untreated groups. (D-F) Quantification of immunoblots showed greater pTDP-43 reduction in soluble protein fractions for 14-day long treated mice. No significant differences were detected in mice treated for either 22 or 47 days. Quantification of pTDP-43 reduction in soluble and insoluble protein fractions was computed as a normalized ratio between pTDP-43 and total TDP-43 signals. The signal intensity for each pTDP-43 band was first normalized to β-Actin, then calculated as a ratio relative to total TDP-43 levels (which was also normalized to β-Actin). GAPDH signal was used to indicate the quality of fractionation between insoluble and soluble protein fractions. This analysis incorporated normalization not only to an internal gene control within each sample using the housekeeping gene β-Actin, but also took into account the expression of the total TDP-43 (hTDP-43-ΔNLS transgene) since there may have been inherent genetic regulatory variability between samples. Two-way ANOVA, *$p < 0.03$, **$p < 0.002$, ***$p < 0.0002$, ****$p < 0.0001$. Error bars represent SEM.


A
Untreated
Treated
Soluble fraction
43-45 kDa
pTDP-43
43 kDa
TDP-43
42 kDa
β-Actin
36 kDa
GAPDH
Insoluble fraction
43-45 kDa
pTDP-43
43 kDa
TDP-43
42 kDa
β-Actin
B
Untreated
Treated
Soluble fraction
43-45 kDa
pTDP-43
43 kDa
TDP-43
42 kDa
β-Actin
36 kDa
GAPDH
Insoluble fraction
43-45 kDa
pTDP-43
43 kDa
TDP-43
42 kDa
β-Actin
C
Untreated
Treated
Soluble fraction
43-45 kDa
pTDP-43
43 kDa
TDP-43
42 kDa
β-Actin
36 kDa
GAPDH
Insoluble fraction
43-45 kDa
pTDP-43
43 kDa
TDP-43
42 kDa
β-Actin
D
14 day treatment
*
Relative Intensity pTDP(409/410) / TDP-43
0.20
0.15
0.10
0.05
0.00
Soluble
Insoluble
Untreated
Treated
E
22 day treatment
Relative Intensity pTDP(409/410) / TDP-43
0.6
0.4
0.2
0.0
Soluble
Insoluble
Untreated
Treated
F
47 day treatment
Relative Intensity pTDP(409/410) / TDP-43
0.8
0.6
0.4
0.2
0.0
Soluble
Insoluble
Untreated
Treated

Selective inhibition of CK1δ/ε is insufficient to rescue motor deficits for functional benefit

In our preclinical efficacy study testing CK1δ/ε-specific PF-05236216 inhibitor treatment in hTDP-43-ΔNLS mice, we conducted motor behavior assays on rotarod and forelimb grip strength tests, recorded CMAPs of the TA muscle, and noted general health measures for body mass and survival. For the rotarod assay, forelimb grip strength test, and neurophysiology CMAP recordings, there was no significant difference throughout disease progression over the course of 47 days between treated and untreated groups (Figure 4.7A-C). Body mass data suggested that while there was no difference between groups, the symptoms of the treated mice were not exacerbated compared to untreated mice which indicated a safe metabolic profile for the inhibitor (Figure 4.7D).

The Kaplan-Meier curve showed that treated mice reached median survival and end stage before untreated mice did (Figure 4.7E). We were unable to collect samples from mice found at end stage due to long and undetermined postmortem interval (PMI) that would have compromised sample quality. During our dose-finding and PK/PD studies, we identified the maximal tolerated dose (MTD) for CK1δ/ε-specific PF-05236216 inhibitor was 80 mg/kg, which resulted in fatal neurological side effects within 24 hours of a single IP injection. This indicated that there may also be long-term side effects of CK1δ/ε-specific PF-05236216 inhibitor treatment even when used at a dose below the MTD. We suspected there may have been other kinases or altered genes that contributed to the survival outcomes of treated mice. To investigate this, we pursued global transcriptomic studies with bulk-RNA sequencing of samples from the 14-day and 22-day treated and untreated mice groups, noting that expression levels of kinases do not

necessarily equate with kinase activity (Figure 4.8A). Comparing highly differentiated genes between the two timepoints revealed *MAP3K6* as significantly upregulated in the treated groups compared to untreated groups (Figure 4.8B). *MAP3K6* is a serine/threonine kinase that regulates vascular endothelial growth factor (VEGF) expression and angiogenesis for the formation of new blood vessels, and also activates the JNK signaling pathway which regulates programmed cell death and apoptosis. The significant upregulation of *MAP3K6* expression likely contributed to the premature death of treated mice and would be considered an unintended adverse event with long-term CK1δ/ε-specific PF-05236216 inhibitor treatment. To ascertain whether the inhibitor treatment was significantly detrimental to the health of the mice, we performed gene set enrichment analysis (GSEA) between the 22-day treated, 22-day untreated, and non-Tg WT mice and did not identify any notable differences between the gene ontology (GO) groups and enrichment scores (Figure 4.8C-D).

We had concerns that our IP daily dosing delivery strategy may not have allowed for sustained inhibition of CK1δ/ε-mediated phosphorylation for TDP-43 throughout the day, so we conducted an additional efficacy study using special diet chow formulated with CK1δ/ε-specific PF-05236216 inhibitor for continuous delivery of inhibitor. We tested a lower dose of 20 mg/kg due to the potential long-term side-effects uncovered from our transcriptomic profiling data. Ultimately, whether mice were treated with IP injection or continuous chow infusion, the results were comparable on pTDP-43 levels in immunoblots and there was no significant improvement for motor deficits or other health measures (data not shown).

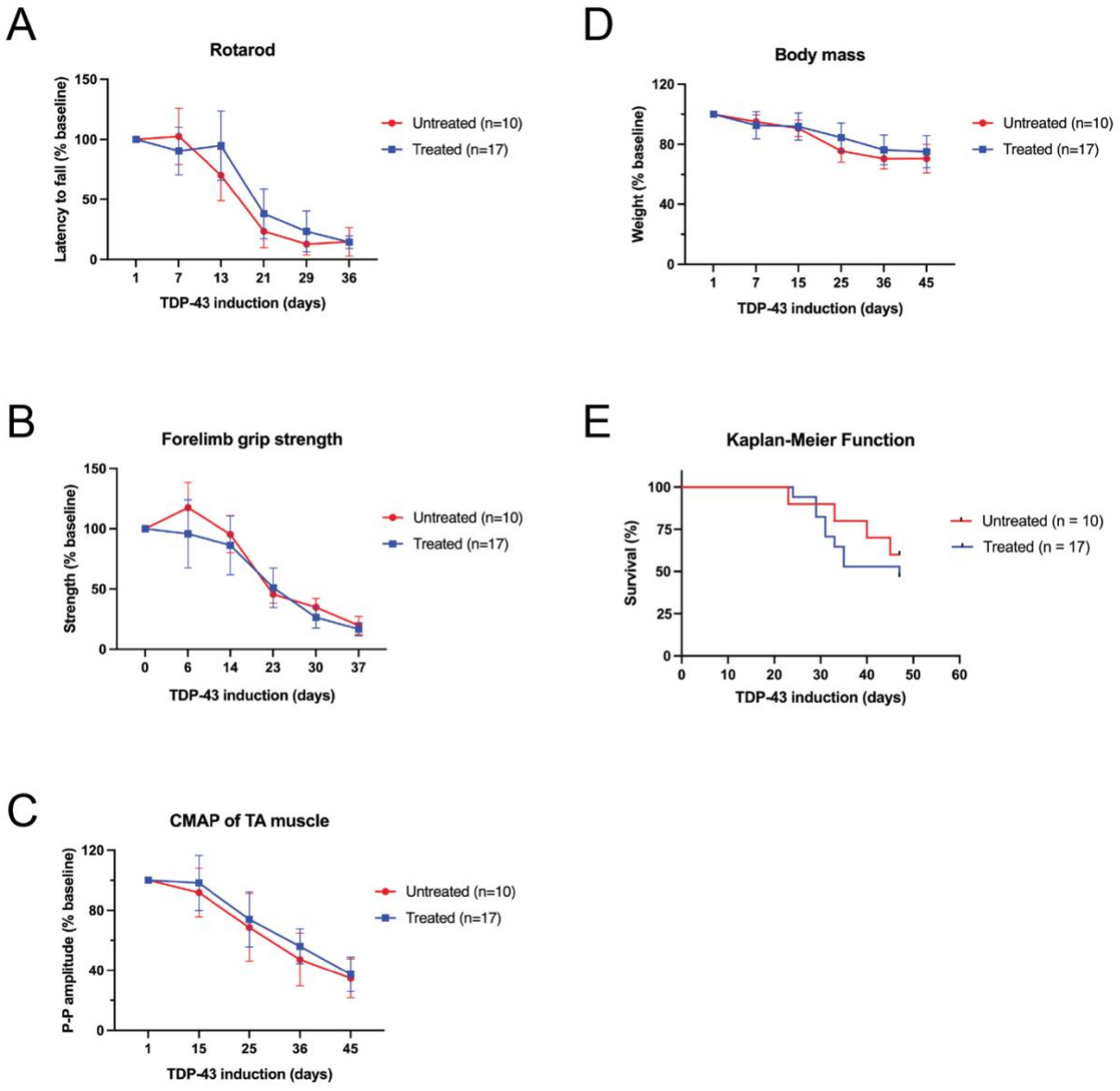


Figure 4.7 Treated mice did not show a difference in motor behavior assays or health measures.

(A) Rotarod performance for treated mice did not improve as compared to untreated control mice. (B) Forelimb grip strength test also did not display improvements. (C) Treated mice did not display changes in CMAP recordings of the TA muscles. (D) The overall health of mice treated with inhibitor was not exacerbated since the body mass declined similarly as untreated mice. (E) Treated mice reached median survival and end stage faster than untreated mice. Two-way ANOVA, *$p < 0.03$, **$p < 0.002$, ***$p < 0.0002$, ****$p < 0.0001$. Error bars represent SEM.

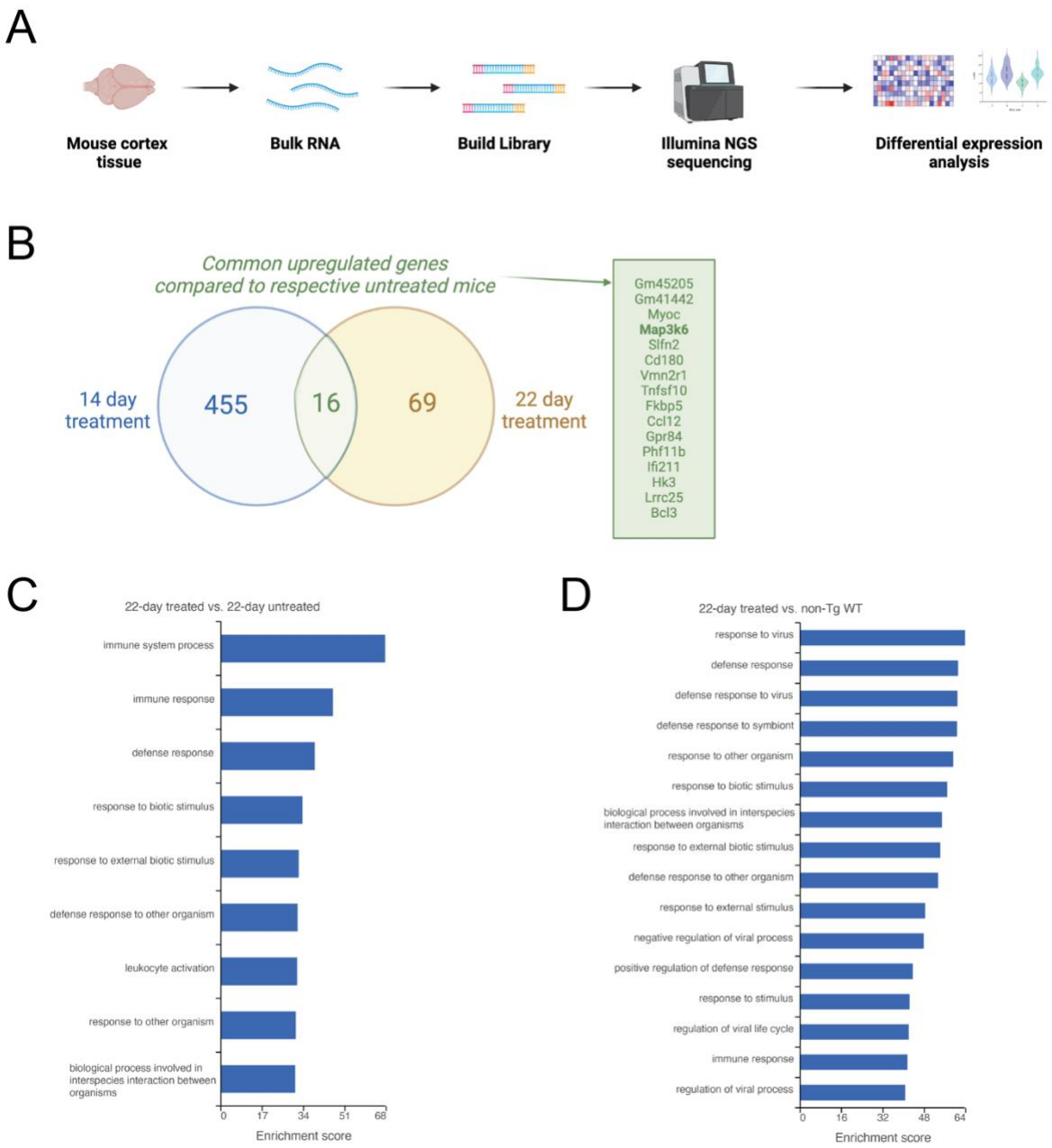


Figure 4.8 Transcriptomic study reveals potential side effects of long-term inhibitor treatment.

(A) Schematic of experimental design to perform bulk-RNA sequencing of samples from the 14-day and 22-day treated and untreated mice groups. (B) Venn diagram comparing highly differentiated genes between treated and untreated mice for 14 and 22 days. *MAP3K6* was identified to be significantly upregulated in the treated groups compared to untreated groups at both timepoints. (C-D) Gene set enrichment analysis of 22-day treated, 22-day untreated, and non-Tg WT mice did not identify notable differences between the gene ontology groups and enrichment scores.

Discussion

In this present study, we tested the preclinical efficacy of targeting CK1δ and CK1ε kinases by way of small molecule chemical inhibitors in the hTDP-43-ΔNLS mouse model. Knowledge from our *Csnk1e* genetic deletion mouse studies (discussed in Chapter 3) and additional characterization from our dose-finding PK profile and PD target engagement of mechanism studies informed our selection to advance the CK1δ/ε-selective PF-05236216 inhibitor into long-term efficacy study. From our biochemical analysis of protein fractions at multiple timepoints before and after onset of motor deficits, we determined that selective CK1δ/ε inhibition effectively lowered pTDP-43 levels and delayed the formation of pTDP-43, but the reduction was not sustained. The pTDP-43 reduction was more pronounced in the soluble fraction compared to insoluble fraction, indicating that the soluble TDP-43 may have been more amenable to the inhibitor treatment. In addition, cryo-EM studies of TDP-43 structure revealed that S410 is exposed on the surface while S409 is buried in the interior of the structure, indicating that there may be variable effectiveness at targeting S409/410 sites, especially as TDP-43 self-aggregates into an insoluble state (Q. Li et al., 2021).

We demonstrated that we were able to reduce TDP-43 phosphorylation and lower Nf-L levels. However, inhibiting CK1δ/ε was not sufficient enough to rescue neurodegeneration to a level that would have ameliorated the disease phenotypes for functional benefit in hTDP-43-ΔNLS mice. While we did not observe beneficial effects on clinical outcome measures of body mass, motor behavior, or survival, the inhibitor treatment was able to reduce Nf-L levels in line with reduced pTDP-43 levels, which supports the disease-promoting role of TDP-43 phosphorylation in ALS. We established

that manipulation of the S409/410 site on TDP-43 by selective CK1δ/ε inhibition may not be a suitable candidate target on its own for ALS therapy. Selective CK1δ/ε inhibition showed moderate beneficial effects *in vivo*, but perhaps reducing another kinase, or multiple kinases, would have produced a more significant effect. Despite the uncertain value of TDP-43 phosphorylation as a mechanism to target for therapy, pTDP-43 could still be a valuable marker for efficacy of therapeutics that aim to modify TDP-43 aggregation.

Throughout our studies, we made sure to examine the effect CK1δ/ε inhibitor treatment had on pTDP-43 formation in both soluble and insoluble protein fractions at multiple timepoints. Not all studies of TDP-43 phosphorylation in ALS *in vitro* cellular and *in vivo* mouse models have examined multiple timepoints, which we have demonstrated is a critical component for insight into the chronological dynamics of neurodegenerative disease mechanisms and progression. Our studies of *Csnk1e* gene deletion knockout and CK1δ/ε inhibitor treatment in this specific hTDP-43-ΔNLS mouse model suggest there may have been a critical period early in disease progression, prior to any motor deficit symptom onset, where CK1-mediated phosphorylation actively affected TDP-43 solubility, but then had a decreased and more limited role at later stages of disease as the hTDP-43-ΔNLS overexpression dominated in these mice. Our results add evidence for the important role of S409/410 phosphorylation in mediating TDP-43 phase separation and aggregation.

There are a variety of ALS mouse models available for research purposes, each with their own set of strengths and weaknesses depending on the mechanism of interest. They allow for many efforts to be made but can also easily cripple results within a study.

Some of the most popularly used mouse genetic models include expressions of SOD1-G38A, C9orf72, FUS, ATXN2, TDP-43, TDP-43-Q331K, TDP-43-A315T, and STMN2. Despite their use for ALS research, each mouse model displays variable disease phenotypes, none of which comprehensively perfectly capture all the observations in ALS human patients (Lutz, 2018; Philips & Rothstein, 2015). We selected the inducible hTDP-43-ΔNLS model for our studies due to its robust phenotypes of cytoplasmic TDP-43 accumulation with detectable phosphorylation and motor behavior deficits. The other ALS mouse models did not possess the features we were interested in analyzing, particularly the cytoplasmic accumulation of pTDP-43. Nevertheless, a limitation of our study stems from the mouse model itself. The hTDP-43-ΔNLS transgene remained highly expressed by 10-fold throughout the disease progression and resulted in widespread diffuse cytoplasmic pTDP-43 accumulation with some inclusion formation (Walker et al., 2015), but these phenotypes do not reflect neuropathological observations in patient postmortem samples. The mouse model also fails to reflect the focal onset and spread of TDP-43 proteinopathy across different regions over time, as seen in ALS patients. The transgene overexpression may have been too aggressive and fast-progressing for our investigation, where the CK1-dependent phosphorylation mechanistically was unable to keep pace with the levels of TDP-43 being produced in this artificial experimental system. TDP-43 is known to self-aggregate, so it is plausible for TDP-43 overexpression beyond a saturation point to become a consequence of the model itself. This limits the translatability of our results to human ALS disease. Perhaps titrating the dox dose and maintaining the mice on a low dose of dox chow throughout the study would have helped to temper the

transgene expression levels so mice would mildly decline while still generating the TDP-43 proteinopathy phenotypes of interest.

The hTDP-43-ΔNLS transgene being overexpressed was a mutated TDP-43 that contained a defective nuclear localization signal (NLS), so TDP-43 could not translocate back into the nucleus and was retained and accumulated in the cytoplasm of cells. Thus, we were unable to study the effect of CK1-phosphorylation on the nucleo-cytoplasmic shuttling of TDP-43 since it has been suggested that CK1δ inhibition ensured the physiological nuclear compartmentalization of TDP-43 and regulated the nucleo-cytosol translocation of TDP-43 (Alquezar et al., 2016b). A study performed in AD lymphoblasts found that a CK1δ/ε inhibitor restored TDP-43 homeostasis and prevented cell-to-cell propagation of TDP-43 pathology (Martinez-Gonzalez et al., 2023). Such a study could have been informative for the field and provided insight on the relative contributions of TDP-43 nuclear loss-of-function and cytoplasmic gain-of-toxicity in driving ALS pathogenesis as well as the role of CK1-mediated phosphorylation in potentially regulating these disease mechanisms. It could have also provided insight as to whether there may be two independent roles for TDP-43 phosphorylation during disease depending on its cellular localization in the nucleus versus the cytoplasm.

Interestingly, a study on the FUS mutation-associated ALS (where *FUS* mutation-associated ALS patients do not develop TDP-43 proteinopathy) found that CK1δ/ε-mediated phosphorylation of FUS protein increased the solubility of FUS *in vitro* and overexpression of CK1δ significantly rescued degeneration in a transgenic fly model (Kishino et al., 2022). However, for ALS cases with TDP-43 proteinopathy, phosphorylation may have an alternative effect since we demonstrated that CK1δ/ε-

selective inhibition could reduce Nf-L levels and moderately rescue neurodegeneration in mice. Given that CK1δ/ε-selective inhibition alone was not sufficient to ameliorate disease progression for functional benefit, a strategy targeting an alternative kinase, or multiple kinases may yield a more significant rescue effect. Altogether, these results suggest that CK1 inhibitors likely will have limited potential on their own for the therapeutic treatment in ALS and related TDP-43 proteinopathies.

Methods

Mouse breeding and maintenance of hTDP-43-ΔNLS mice

Bigenic transgenic mice for the hTDP-43-ΔNLS model (JAX Stock No. 028412) were generated by crossing monogenic NEFH-tTA mice (JAX Stock No. 025397) with monogenic tetO-hTDP-43-ΔNLS mice (JAX Stock No. 014650) obtained from the Jackson Laboratory (Bar Harbour, Maine, USA). Parent lines were maintained on a B6C3F1/J (JAX Stock No. 100010) background. Mice were fed with 200 mg/kg doxycycline (dox) supplemented chow (Envigo TD.08541) throughout breeding and weaning to suppress the hTDP-43-ΔNLS transgene. To induce hTDP-43-ΔNLS transgene expression, mice were switched to and fed standard chow without dox (PicoLab Rodent Diet 20 #5053). Genotyping was performed using tail DNA and sent to the commercial vendor Transnetyx for automated test results. All procedures were formed in accordance with NIH Guide for the Care and Use of Experimental Animals and Studies were approved by the Institutional Animal Care and Use Committee (IACUC) of the University of California, San Diego. Littermates were randomly grouped into designated treatment cohorts in a gender-

balanced way. Experimenters were blinded to the treatment cohort assignment throughout the study.

Rotarod behavior

To assay motor coordination and balance, the rotarod (Ugo Basile) rotated at a speed of 4 rpm and accelerated to 40 rpm over 300 seconds. The time to fall was recorded with a maximum score of 300 seconds if the mouse was still running on the rod at the end of the session. There was one training session and three test sessions for each mouse with at least 30 minutes of rest in between sessions. The final score for each mouse was the average time of the three test sessions.

Grip test behavior

Mice were lowered onto a triangular bar of the grip meter (Columbus Instruments) until they gripped the bar with their hindlimbs. Then, mice were pulled backwards by their tail until they released their grip and the maximum force in kilograms was recorded. One training session and five testing sessions were performed, with at least 5 minutes of rest in between sessions. The final score for each mouse was an average of the five test sessions.

Compound muscle action potential (CMAP) recordings

Mice were anesthetized by inhalation of 2.5% isoflurane. Once completely anesthetized (checked by pinching toes for reflexes), mice were immobilized on a heated operating table. Animals were placed prone on the table, and the backs and legs were

shaved with professional hair clippers and cleaned with ethanol and Betadine. Each leg was positioned at a 45-degree angle from the body and the feet were taped down using surgical tape to prevent any excess motion that could have affected the recordings. Disposable monopolar needle electrodes (28-gauge TECA model 902-DMF25-TP) were used for stimulation and recording. All five electrodes used were connected to the appropriate port of the Natus XLTEK XCalibur LT machine. The sciatic nerve was stimulated using an electrode pair and current was delivered using a stimulating cathode placed subdermally at the sciatic notch, roughly 8 mm lateral from the midline and 2 cm anterior to the base of the tail. The anode was placed subdermally roughly 4 mm lateral from the midline. The reference electrode was placed 3-4 mm subdermally above the ankle near the tendons. The recording electrode was subdermally placed on the surface of the middle of the tibialis anterior (TA) muscle of either the right or left leg (both legs were recorded for each subject). The ground electrode was placed near the midline subdermally.

Each animal was stimulated with incremental pulse intensity for 0.1 ms beginning at 1.0 mA and increasing in 0.5 mA steps until the CMAP amplitude stopped increasing (maximum current 5 mA). Once the maximum amplitude was identified, 5 recordings were taken at this supra-maximal stimulus intensity. Responses were recorded separately for both the left and right TA muscles of each mouse with the left hind limb recorded before the right hind limb and analysis for each mouse was an average of the right and left hind limb measurements.

Neurofilament-Light (Nf-L) measures

Mice were anesthetized by isoflurane vapors in a glass chamber box and toe pinch was used to test depth of anesthesia. Once anesthetized, scissors were used to decapitate the mouse and the trunk blood was poured into K2 EDTA tubes (BD #365974). To separate plasma from blood, samples were spun at 11,000 rpm for 5 minutes at 4°C and the supernatant was saved in a fresh Eppendorf tube and stored at -80°C until use.

Plasma samples were sent to collaborators at Biogen Inc. for Nf-L measurements. Nf-L was measured in plasma samples using the ProteinSimple Nf-L cartridge V5 kit according to the manufacturer's guidelines. In brief, plasma samples were brought to room temperature and diluted 1:6 in Sample Diluent buffer. Samples were mixed and 50 μL volumes were transferred to wells within the Ella cartridge. One milliliter of Wash Buffer A was added to each designated well of the Ella cartridge and the cartridge was run on the Ella machine using the Simple Plex Runner software.

Pharmacokinetic characterization

The compound exposure concentration-time profile of CK1δ/ε-specific PF-05236216 inhibitor and CK1ε-specific PF-4800567 inhibitor in whole brain and plasma were analyzed in B6C3F1/J (JAX Stock No. 100010) mice after a single intraperitoneal (IP) injection. The compound was injected at either a dose of 40 mg/kg (for CK1δ/ε-specific PF-05236216 inhibitor) or 100 mg/kg (for CK1ε-specific PF-4800567 inhibitor) in vehicle solution of 10% DMSO with 90% of 20% hydroxypropyl β-cyclodextrin in 0.9% saline. The dosing volume for the compound was 2 mg/mL. Mice were weighed prior to injection to ensure appropriate volume was administered.

Samples were collected at 1, 2, 4, 8, and 24 hours after dosing (n = 6, with 3 females and 3 males for each time point). Mice were anesthetized by isoflurane vapors in a glass chamber box and toe pinch was used to test depth of anesthesia. Once anesthetized, scissors were used to decapitate the mouse and the trunk blood was poured into K2 EDTA tubes (BD #365974) and brain was quickly extracted into 4.5 mL TallPrep Lysing matrix tubes (MP Biomedical #116973100). Brain tissues were snap frozen and stored at -80°C until use. To separate plasma from blood, samples were spun at 11,000 rpm for 5 minutes at 4°C and the supernatant was saved in a 96-well plate and stored at -80°C until use.

LC-MS/MS for compound detection

Brain tissue and plasma samples were sent to collaborators at Biogen Inc. for pharmacokinetic compound exposure measurements. Generally, for protein extraction via precipitation method, a 1 mg/mL (1000 ng/mL) stock solution was first prepared in DMSO for each compound, either CK1δ/ε-specific PF-05236216 inhibitor or CK1ε-specific PF-4800567 inhibitor. A calibration curve was constructed using a 12-point serial dilution scheme with final concentrations 1000 ng/mL down to 0.100 ng/mL. Brains were homogenized at 5x, with 1:4 tissue:1x PBS (w/v). Aliquots of 10 μL of each sample, standard, and matrix blanks were added to designated wells in a 96-well extraction plate. Matrix matching was done to normalize all samples 1:1, plasma: brain homogenate, with a total extraction volume of 20 μL. Double blanks were precipitated with 6x volume of acetonitrile. All other wells were precipitated with 6x volume of internal standard (25 ng/mL glyburide, 50 ng/mL chrysin and carbutamide in acetonitrile). Samples were

vortexed for 30 seconds then centrifuged at 3500 rpm for 5 minutes. Next, 50 μL of supernatant was transferred to an empty 96-well injection plate and diluted with 50 μL of water. Samples were vortexed gently, then plate was capped and placed into the autosampler for injection into the mass spectrometer (Triple Quad 5500, AB Sciex Instruments). The LC-MS/MS analytical conditions used were Ace 3 C18-PFP (2.1 x 50 mm) for the column, 0.1% formic acid in water for mobile phase A, 0.1% formic acid in acetonitrile for mobile phase B, 0.1% formic acid in (80:10:10 H2O:ACN:MeOH) for needle rinse 1 port, 0.1% formic acid in (50:50 ACN:MeOH) for needle rinse 2 pump, and 50 μL loop volume.

Tissue collection for biochemistry assays

Mice were anesthetized by isoflurane vapors in a glass chamber box. Toe pinch was used to test depth of anesthesia. Once anesthetized, scissors were used to decapitate the mouse and the brain and spinal cord tissues were extracted and partitioned into 1.5 mL Eppendorf tubes. Once tissues were collected, tubes were flash frozen onto dry ice and stored in -80°C until use.

RNA-sequencing and gene expression analysis

RNA was extracted using the Direct-zol RNA miniprep kit (Bio-Rad) according to the manufacturer's protocol and samples were measured for RNA quantity (OD260/280) and purity (OD230/260) using a NanoDrop spectrophotometer (Thermo Fisher). The RNA was sent to UCSD Institute for Genomic Medicine (IGM) Genomics Center for sample QC, library prep, and sequencing. RNA-seq library was constructed using the Illumina

Stranded Total RNA Prep with Ribo-Zero Plus kit (Illumina) according to manufacturer's protocol. The sequencing was completed using the Illumina NovaSeq X Plus system.

For analysis of the transcriptomic data, reads were aligned to UCSC genome browser *mus musculus* (mouse) genome mm39 using STAR alignment tool with standard parameters. The aligned reads were quantified to the ensemble transcripts release 110 annotation model using standard parameters. Genes with more than 20 counts were filtered for and then normalized. DESeq2 was used to analyze for differentially expressed genes and filtered for a fold change (FC) <-2 or >2 and a false discovery rate (FDR) < 0.05. Gene set enrichment analysis (GSEA) was performed according to standard protocols.

Protein extraction

To characterize pTDP-43 expression in samples, cells were homogenized in ice-cold N-PER buffer (Thermo Fisher) with protease and phosphatase inhibitors (Thermo Fisher) and then incubated on ice for 10 minutes. Samples were then centrifuged at 13,500 rpm for 20 minutes at 4°C and the supernatant was saved in a new tube as the soluble fraction. The pellet was washed twice with N-PER buffer to remove residual soluble protein. The pellet was resuspended in lysis buffer + 8 M urea + 3% SDS and then sonicated, followed by incubation on ice for 15 minutes, then centrifuged at 14,000 rpm for 10 minutes at 10°C. The supernatant was then saved as the insoluble protein fraction.

Immunoblotting

To determine protein sample concentrations, Pierce BCA Protein Assay (Thermo Fisher) was used. Samples were loaded in equal volumes and normalized to 10 μg with PBS and then boiled with 4X Protein Loading Buffer (LI-COR) + β-mercaptoethanol for 5 minutes at 90°C. Samples were then loaded onto a 4-15% SDS–PAGE gel to run (80 V for 10 minutes, then 100 V for 50 minutes), then transferred to PVDF membranes (85 V for 60 minutes on ice) using a Bio-Rad Mini-Protean Tetra Cell Electrophoresis System. Membranes were blocked using TBS Intercept blocking buffer (LI-COR) and then incubated with primary antibodies diluted in Intercept T20 Antibody Diluent (LI-COR) overnight at 4°C. The primary antibodies used were pTDP-43 (S409/410) (1:1000, Proteintech #22309-1-AP), TDP-43 (1:500, Proteintech #12892-1-AP), β-actin (1:20,000, Proteintech #66009-1-Ig), and GAPDH (1:20,000, Proteintech #60004-1-Ig). The following day, the membranes were washed with TBST (0.1% Tween-20 in TBS) three times for 10 minutes each at room temperature and then incubated with secondary antibodies (1:20,000 IRDye 800CW and 1:20,000 IRDye 680RD, LI-COR) diluted in Intercept T20 Antibody Diluent (LI-COR) for 1 hour at room temperature. Membranes were then washed 3 times with TBST for 10 minutes each and then 2 times with TBS for 10 minutes each before imaging on the Odyssey® Fc Imaging System (LI-COR). ImageStudioLite was used to analyze signal intensity. Quantification of band intensity was based upon immunoblot densitometry values. The pTDP-43 band signal was first normalized to β-Actin, as was the total TDP-43 band signal. These two normalized values were then computed as a ratio with pTDP-43 relative to total TDP-43. This analysis incorporated normalization not only to an internal protein control within each sample using

the housekeeping gene β-Actin, but also considered the expression of the total TDP-43 (hTDP-43-ΔNLS transgene) since there may have been inherent genetic regulatory variability between samples.

Statistical analyses

Data were analyzed using GraphPad Prism10 and are expressed as the mean ± standard error of the mean (SEM). Immunoblotting analysis was performed by normalizing bands of interest to the signal intensity for the internal sample control β-actin, and then a ratio for pTDP-43 (S409/410) over total TDP-43 levels was calculated and reported as a relative intensity measure. Statistics were performed with either two-way ANOVA or Mann-Whitney t-test using GraphPad Prism 10 with p-values less than 0.05 considered significant.

Acknowledgements

We thank Melissa McAlonis from the Cleveland lab for sharing her expert knowledge on *in vivo* experimental design and assistance with the mouse husbandry and IACUC approvals. We also thank the late Professor Steve Wagner for his encouragement and insight of our preclinical study design. In addition, we thank members of the Neuromuscular and Muscle Research Unit at Biogen Inc. and Sophie Parmentier-Batteur for their suggestions and support throughout our efficacy study, and for providing the compound inhibitors for testing. Some figures, like schematics for experimental setups, were created with BioRender.com.

This research was supported by grants from FightMND (Drug Development Grant); ALS Association (ALSA); Target ALS; UC Academic Senate; and UCSD Microscopy Core (NINDS-P30NS047101). This publication includes data generated at the UC San Diego IGM Genomics Center utilizing an Illumina NovaSeq X Plus that was purchased with funding from a National Institutes of Health SIG grant (#S10 OD026929).

Chapter 4, in part, is being prepared for submission for publication of the material as “Manipulation of the S409/410 site on TDP-43 by selective CK1δ/ε inhibition as a candidate therapeutic target”. Other co-authors will be Kailee Ong, Deborah Y. Kwon, Xueying Li, Alicia Pietrasiewicz, James Harvey, Mukesh Lulla, Guruharsha Bhat, Don W. Cleveland, and senior author John M. Ravits. The dissertation author will be the primary investigator and author of this paper.

Chapter 5 : Conclusion

This dissertation has explored the role of CK1δ/ε in mediating TDP-43 phosphorylation and neuronal toxicity in cellular and mammalian models of ALS. Chapter 1 provided an introduction into the current state of knowledge of ALS clinical observations, disease pathogenesis and progression, molecular and cellular mechanisms, along with current efforts in therapeutic development. Overall, there is no consensus, and little is known about the mechanism responsible for TDP-43 phosphorylation and its influence on the formation of cytoplasmic, aggregated, and pathological TDP-43. With the weight of the current evidence, we proposed that dysregulated CK1δ and CK1ε protein kinases hyperphosphorylate TDP-43 which then contribute to neurotoxicity in ALS.

In Chapter 2, we explored the binding interaction between CK1δ/ε protein kinases and TDP-43 and validated them as upstream regulators of TDP-43 phosphorylation. Our *in vitro* studies utilizing genetic interference and CNS-penetrant small molecule inhibitors established CK1δ and CK1ε as the primary kinases involved in the phosphorylation of TDP-43 at ALS disease-relevant serine sites. These kinases could be targeted via small molecule chemical inhibitors to reduce disease-relevant TDP-43 hyperphosphorylation in both soluble and insoluble protein fractions. Further, we provided proof-of-principle to test the *in vivo* efficacy of CK1δ and CK1ε inhibitors and determine whether CK1 inhibitors should be translated for therapeutic use in the treatment of ALS and other TDP-43 proteinopathies.

Of note, all of our readouts of TDP-43 phosphorylation depended upon the S409/410 site on TDP-43, as antibody detection methods were limited. We attempted to characterize the phosphorylation of other serine sites, like S403/404, with limited success

as the commercial antibodies for this detection were lot dependent for detection, and some products were no longer manufactured. Alternative approaches like with mass spectrometry also presented challenges, with the C-terminal glycine-rich domain of TDP-43 being resistant to cleavage into peptides with appropriate resolution for mass spectrometry. Thus, it is not known whether other phosphorylation sites were impacted with CK1δ/ε genetic reduction or CK1δ/ε inhibitor treatment, and whether analyzing S409/410 phosphorylation status and levels of TDP-43 was the appropriate surrogate marker for all TDP-43 phosphorylation sites. Perhaps other serine or threonine sites, or even other PTMs like acetylation or ubiquitination, would be better indicators of abnormal TDP-43 toxicity.

A couple types of phosphorylation cascades have been proposed in kinase biology. One type is a phospho-priming initiating event, which depends on a proximal residue to be phosphorylated first to trigger subsequent phosphorylation of nearby residues. CK1s have been found to require phospho-priming to initiate its activity in some signaling cascades, but not in all of its biological regulatory roles, which was discussed in Chapter 2. An alternative cascade could be initiated by Ser/Thr sites much more distal to S409/410 on TDP-43, indicating a long-range interdependent relationship between these distant residues. A systematic study of Ser/Thr sites proximal and distal to S409/410, within the C-terminal or N-terminal and RRM1/2 regions, would help reveal whether a particular PTM cascade or initiator site would be a master regulator to modify cytoplasmic TDP-43 and drive aggregate formation. It is possible that a modification towards the N-terminus might change the 3D conformation of TDP-43 and allow access for kinases to target residues within the C-terminus. Another component to add to the complexity of

kinase biology are the role of phosphatases, as the complementary force to dephosphorylate residues. The dynamic nature and balance between CK1δ/ε kinases and potential partner phosphatases would be valuable to study and improve our understanding of the role of CK1δ/ε in phosphorylating TDP-43 and resulting effects on contributing to toxicity.

In chapters 3 and 4, we tested two CK1 intervention strategies in the hTDP-43-ΔNLS ALS disease mouse model. We selected the hTDP-43-ΔNLS ALS disease mouse model for our *in vivo* studies due to its striking TDP-43 phosphorylation and clinical phenotypes, as there were no other ALS mouse models that would have been sufficient for our needs. A significant limitation of the translatability of *in vivo* ALS research is the lack of appropriate and relevant mouse disease models. A number of landmark findings completed in mice has spurred human clinical trials, only to fail in these trials because the models were not an accurate reflection of human ALS disease, and the applicability of the research results should have been interpreted with more caution. No mouse model depicts the motor neuron vulnerability in disease either, which should be included as a caveat in research discussions. A major barrier to producing accurate ALS research models is an in-depth understanding of the clinical etiology and disease progression in humans, which can be studied using postmortem donor samples. An increase in molecular and cellular neuropathology studies will advance the disease modeling field, which will then allow for more accurate and relevant models of ALS disease for detailed mechanistic pathway studies.

Despite the limitations in the mouse model we selected, testing two intervention strategies, deletion of *Csnk1e* and CK1δ/ε inhibition, revealed that both approaches were

sufficient to delay pTDP-43 formation. The pTDP-43 reduction was more pronounced in the soluble fraction, indicating that the soluble TDP-43 was more amenable to the inhibitor treatment. While we did not observe beneficial effects on body mass, motor behavior deficits, or survival, the inhibitor treatment was able to reduce Nf-L levels in line with reduced pTDP-43 levels, which supports the disease-promoting role of TDP-43 phosphorylation in ALS. Our results from genetic deletion of *Csnk1e* also suggested that phosphorylation may be a mechanism that facilitates TDP-43 liquid-liquid phase separation and promotes protein solubility to drive TDP-43 into a soluble state. An open question that remains is how TDP-43 degradation may occur in ALS disease, and whether phosphorylation affects the degradation rate of TDP-43. Taken together, these results suggest two paradoxical effects of CK1δ/ε-mediated TDP-43 phosphorylation. On one hand, it appears to enhance toxicity since inhibiting it delayed disease attributes, if only temporarily. On the other hand, phosphorylation also appears to modify insoluble TDP-43, possibly after aggregate formation, in an attempt to restore protein solubility and functional protein phase of TDP-43, suggesting a protective role. These two contrasting roles of TDP-43 phosphorylation may be best explained by Occam's razor, which is a problem-solving principle in which the simplest explanation is usually the best one. In this case, both may be true, where phosphorylation serves a hodgepodge of roles in disease states, some mechanisms which may increase toxicity and others as a response to rescue disease progression (Figure 5.1A).

CK1δ/ε inhibitor treatment effectively lowered Nf-L levels but was not sufficient to rescue neurodegeneration to a level that would have ameliorated the disease phenotypes for functional benefit in this mouse model. The CK1δ and CK1ε kinases are low

expressing in mice and these genes are expressed in all neurons without strong specificity to particular motor neuron subtypes. Selective CK1δ/ε inhibition showed moderate beneficial effects *in vivo*, but perhaps reducing another kinase, or multiple kinases, would have produced a more significant effect. Importantly, it is the kinase activity that drive mechanisms, and not necessarily the kinase expression level. The pleiotropic roles of kinases make it a challenging target in ALS where there seems to be a cell-specific motor neuron vulnerability to disease. Despite the uncertain feasibility and value of TDP-43 phosphorylation as a mechanism to target for therapy, pTDP-43 could still be a valuable marker for efficacy of therapeutics that aim to modify TDP-43 aggregation. Overall, we determined that selective CK1δ/ε inhibitors likely will have limited potential on their own for the therapeutic treatment in ALS and related TDP-43 proteinopathies.

A

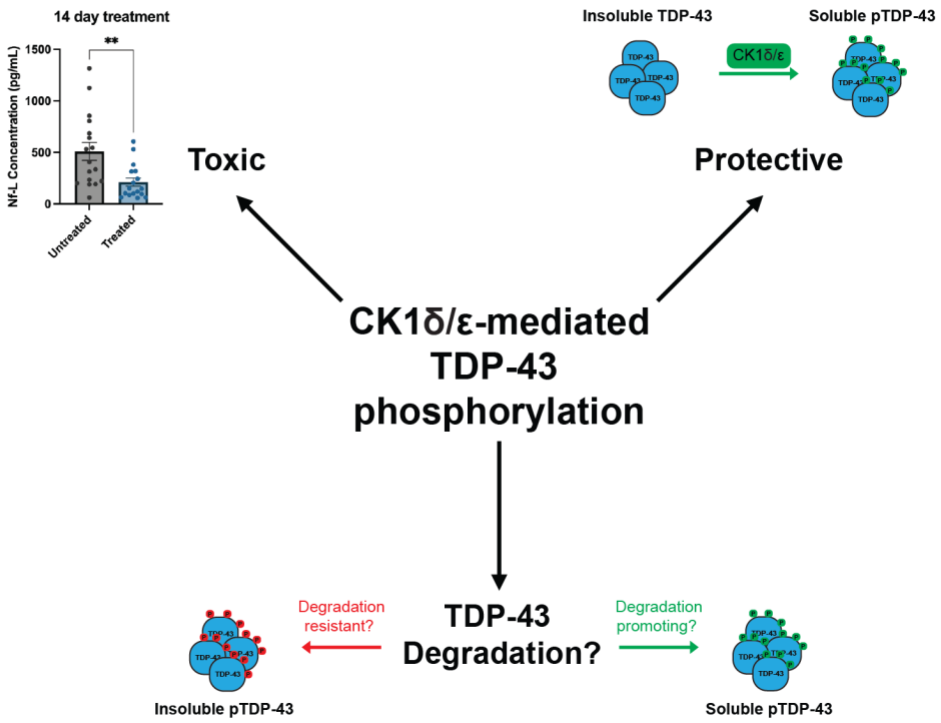


Figure 5.1 Various roles of TDP-43 phosphorylation in ALS disease.

(A) Phosphorylation likely serves a hodgepodge of roles in ALS disease, with some mechanisms increasing toxicity and other pathways as a response to rescue disease progression.

References

Ababneh, N. A., Scaber, J., Flynn, R., Douglas, A., Barbagallo, P., Candalija, A., Turner, M. R., Sims, D., Dafinca, R., Cowley, S. A., & Talbot, K. (2020). Correction of amyotrophic lateral sclerosis related phenotypes in induced pluripotent stem cell-derived motor neurons carrying a hexanucleotide expansion mutation in C9orf72 by CRISPR/Cas9 genome editing using homology-directed repair. *Human Molecular Genetics*, *29*(13), 2200–2217. https://doi.org/10.1093/hmg/ddaa106

Abulimiti, A., Lai, M. S.-L., & Chang, R. C.-C. (2021). Applications of adeno-associated virus vector-mediated gene delivery for neurodegenerative diseases and psychiatric diseases: Progress, advances, and challenges. *Mechanisms of Ageing and Development*, *199*, 111549. https://doi.org/10.1016/j.mad.2021.111549

Adler, P., Mayne, J., Walker, K., Ning, Z., & Figeys, D. (2019). Therapeutic Targeting of Casein Kinase 1δ/ε in an Alzheimer's Disease Mouse Model. *Journal of Proteome Research*, *18*(9), 3383–3393. https://doi.org/10.1021/acs.jproteome.9b00312

Afroz, T., Chevalier, E., Audrain, M., Dumayne, C., Ziehm, T., Moser, R., Egesipe, A.-L., Mottier, L., Ratnam, M., Neumann, M., Havas, D., Ollier, R., Piorkowska, K., Chauhan, M., Silva, A. B., Thapa, S., Stöhr, J., Bavdek, A., Eligert, V., … Seredenina, T. (2023). Immunotherapy targeting the C-terminal domain of TDP-43 decreases neuropathology and confers neuroprotection in mouse models of ALS/FTD. *Neurobiology of Disease*, *179*, 106050. https://doi.org/10.1016/j.nbd.2023.106050

Aikio, M., Wobst, H. J., Odeh, H. M., Lee, B. L., Class, B., Ollerhead, T. A., Mack, K. L., Ford, A. F., Barbieri, E. M., Cupo, R. R., Drake, L. E., Castello, N., Baral, A., Dunlop, J., Gitler, A. D., Javaherian, A., Finkbeiner, S., Brown, D. G., Moss, S. J., … Shorter, J. (2021). *Opposing roles of p38α-mediated phosphorylation and arginine methylation in driving TDP-43 proteinopathy*. https://doi.org/10.1101/2021.08.04.455154

Alarcón-Arís, D., Pavia-Collado, R., Miquel-Rio, L., Coppola-Segovia, V., Ferrés-Coy, A., Ruiz-Bronchal, E., Galofré, M., Paz, V., Campa, L., Revilla, R., Montefeltro, A., Kordower, J. H., Vila, M., Artigas, F., & Bortolozzi, A. (2020). Anti-α-synuclein ASO delivered to monoamine neurons prevents α-synuclein accumulation in a Parkinson's disease-like mouse model and in monkeys. *eBioMedicine*, *59*, 102944. https://doi.org/10.1016/j.ebiom.2020.102944

Alfieri, J. A., Pino, N. S., & Igaz, L. M. (2014). Reversible Behavioral Phenotypes in a Conditional Mouse Model of TDP-43 Proteinopathies. *The Journal of Neuroscience*, *34*(46), 15244–15259. https://doi.org/10.1523/JNEUROSCI.1918-14.2014

Alquezar, C., Salado, I. G., De La Encarnación, A., Pérez, D. I., Moreno, F., Gil, C., De Munain, A. L., Martínez, A., & Martín-Requero, Á. (2016). Targeting TDP-43 phosphorylation by Casein Kinase-1δ inhibitors: A novel strategy for the treatment of frontotemporal dementia. *Molecular Neurodegeneration*, *11*(1), 36. https://doi.org/10.1186/s13024-016-0102-7

Amado, D. A., & Davidson, B. L. (2021). Gene therapy for ALS: A review. *Molecular Therapy*, *29*(12), 3345–3358. https://doi.org/10.1016/j.ymthe.2021.04.008

Arai, T., Hasegawa, M., Akiyama, H., Ikeda, K., Nonaka, T., Mori, H., Mann, D., Tsuchiya, K., Yoshida, M., Hashizume, Y., & Oda, T. (2006). TDP-43 is a component of ubiquitin-positive tau-negative inclusions in frontotemporal lobar degeneration and amyotrophic lateral sclerosis. *Biochemical and Biophysical Research Communications*, *351*(3), 602–611. https://doi.org/10.1016/j.bbrc.2006.10.093

Arai, T., Hasegawa, M., Nonoka, T., Kametani, F., Yamashita, M., Hosokawa, M., Niizato, K., Tsuchiya, K., Kobayashi, Z., Ikeda, K., Yoshida, M., Onaya, M., Fujishiro, H., & Akiyama, H. (2010). Phosphorylated and cleaved TDP-43 in ALS, FTLD and other neurodegenerative disorders and in cellular models of TDP-43 proteinopathy. *Neuropathology*, *30*(2), 170–181. https://doi.org/10.1111/j.1440-1789.2009.01089.x

Arnold, E. S., Ling, S.-C., Huelga, S. C., Lagier-Tourenne, C., Polymenidou, M., Ditsworth, D., Kordasiewicz, H. B., McAlonis-Downes, M., Platoshyn, O., Parone, P. A., Da Cruz, S., Clutario, K. M., Swing, D., Tessarollo, L., Marsala, M., Shaw, C. E., Yeo, G. W., & Cleveland, D. W. (2013). ALS-linked TDP-43 mutations produce aberrant RNA splicing and adult-onset motor neuron disease without aggregation or loss of nuclear TDP-43. *Proceedings of the National Academy of Sciences*, *110*(8). https://doi.org/10.1073/pnas.1222809110

Arnold, F. J., Cui, Y., Michels, S., Colwin, M. R., Stockford, C., Ye, W., Tam, O. H., Menon, S., Situ, W. G., Ehsani, K. C. K., Howard, S., Hammell, M. G., Li, W., & La Spada, A. R. (2024). *TDP-43 dysregulation of polyadenylation site selection is a defining feature of RNA misprocessing in ALS/FTD and related disorders*. https://doi.org/10.1101/2024.01.22.576709

Ayala, Y. M., Zago, P., D'Ambrogio, A., Xu, Y.-F., Petrucelli, L., Buratti, E., & Baralle, F. E. (2008). Structural determinants of the cellular localization and shuttling of TDP-43. *Journal of Cell Science*, *121*(22), 3778–3785. https://doi.org/10.1242/jcs.038950

Badura, L., Swanson, T., Adamowicz, W., Adams, J., Cianfrogna, J., Fisher, K., Holland, J., Kleiman, R., Nelson, F., Reynolds, L., St. Germain, K., Schaeffer, E., Tate, B., & Sprouse, J. (2007). An Inhibitor of Casein Kinase Iε Induces Phase Delays in Circadian Rhythms under Free-Running and Entrained Conditions. *Journal of*

Pharmacology and Experimental Therapeutics, *322*(2), 730–738. https://doi.org/10.1124/jpet.107.122846

Barmada, S. J., Skibinski, G., Korb, E., Rao, E. J., Wu, J. Y., & Finkbeiner, S. (2010). Cytoplasmic Mislocalization of TDP-43 Is Toxic to Neurons and Enhanced by a Mutation Associated with Familial Amyotrophic Lateral Sclerosis. *The Journal of Neuroscience*, *30*(2), 639–649. https://doi.org/10.1523/JNEUROSCI.4988-09.2010

Baughn, M. W., Melamed, Z., López-Erauskin, J., Beccari, M. S., Ling, K., Zuberi, A., Presa, M., Gonzalo-Gil, E., Maimon, R., Vazquez-Sanchez, S., Chaturvedi, S., Bravo-Hernández, M., Taupin, V., Moore, S., Artates, J. W., Acks, E., Ndayambaje, I. S., Agra De Almeida Quadros, A. R., Jafar-nejad, P., … Cleveland, D. W. (2023). Mechanism of *STMN2* cryptic splice-polyadenylation and its correction for TDP-43 proteinopathies. *Science*, *379*(6637), 1140–1149. https://doi.org/10.1126/science.abq5622

Becker, L. A., Huang, B., Bieri, G., Ma, R., Knowles, D. A., Jafar-Nejad, P., Messing, J., Kim, H. J., Soriano, A., Auburger, G., Pulst, S. M., Taylor, J. P., Rigo, F., & Gitler, A. D. (2017). Therapeutic reduction of ataxin-2 extends lifespan and reduces pathology in TDP-43 mice. *Nature*, *544*(7650), 367–371. https://doi.org/10.1038/nature22038

Benatar, M., Boylan, K., Jeromin, A., Rutkove, S. B., Berry, J., Atassi, N., & Bruijn, L. (2016). ALS biomarkers for therapy development: State of the field and future directions: ALS Biomarkers. *Muscle & Nerve*, *53*(2), 169–182. https://doi.org/10.1002/mus.24979

Benatar, M., Zhang, L., Wang, L., Granit, V., Statland, J., Barohn, R., Swenson, A., Ravits, J., Jackson, C., Burns, T. M., Trivedi, J., Pioro, E. P., Caress, J., Katz, J., McCauley, J. L., Rademakers, R., Malaspina, A., Ostrow, L. W., Wuu, J., … Blitterswijk, M. V. (2020). Validation of serum neurofilaments as prognostic and potential pharmacodynamic biomarkers for ALS. *Neurology*, *95*(1). https://doi.org/10.1212/WNL.0000000000009559

Bennett, C. F. (2019). Therapeutic Antisense Oligonucleotides Are Coming of Age. *Annual Review of Medicine*, *70*(1), 307–321. https://doi.org/10.1146/annurev-med-041217-010829

Bensimon, G., Lacomblez, L., & Meininger, V. (1994). A Controlled Trial of Riluzole in Amyotrophic Lateral Sclerosis. *New England Journal of Medicine*, *330*(9), 585–591. https://doi.org/10.1056/NEJM199403033300901

Berning, B. A., & Walker, A. K. (2019). The Pathobiology of TDP-43 C-Terminal Fragments in ALS and FTLD. *Frontiers in Neuroscience*, *13*, 335. https://doi.org/10.3389/fnins.2019.00335

Biferi, M. G., Cohen-Tannoudji, M., Cappelletto, A., Giroux, B., Roda, M., Astord, S., Marais, T., Bos, C., Voit, T., Ferry, A., & Barkats, M. (2017). A New AAV10-U7-Mediated Gene Therapy Prolongs Survival and Restores Function in an ALS Mouse Model. *Molecular Therapy*, *25*(9), 2038–2052. https://doi.org/10.1016/j.ymthe.2017.05.017

Birsa, N., Bentham, M. P., & Fratta, P. (2020). Cytoplasmic functions of TDP-43 and FUS and their role in ALS. *Seminars in Cell & Developmental Biology*, *99*, 193–201. https://doi.org/10.1016/j.semcdb.2019.05.023

Bissaro, M., Federico, S., Salmaso, V., Sturlese, M., Spalluto, G., & Moro, S. (2018). Targeting Protein Kinase CK1δ with Riluzole: Could It Be One of the Possible Missing Bricks to Interpret Its Effect in the Treatment of ALS from a Molecular Point of View? *ChemMedChem*, *13*(24), 2601–2605. https://doi.org/10.1002/cmdc.201800632

Borel, F., Gernoux, G., Cardozo, B., Metterville, J. P., T. Cabrera, G., Song, L., Su, Q., Gao, G. P., Elmallah, M. K., Brown, R. H., & Mueller, C. (2016). Therapeutic rAAVrh10 Mediated *SOD1* Silencing in Adult *SOD1* ^{G93A} Mice and Nonhuman Primates. *Human Gene Therapy*, *27*(1), 19–31. https://doi.org/10.1089/hum.2015.122

Borel, F., Gernoux, G., Sun, H., Stock, R., Blackwood, M., Brown, R. H., & Mueller, C. (2018). Safe and effective superoxide dismutase 1 silencing using artificial microRNA in macaques. *Science Translational Medicine*, *10*(465), eaau6414. https://doi.org/10.1126/scitranslmed.aau6414

Bose, J. K., Huang, C.-C., & Shen, C.-K. J. (2011). Regulation of Autophagy by Neuropathological Protein TDP-43. *Journal of Biological Chemistry*, *286*(52), 44441–44448. https://doi.org/10.1074/jbc.M111.237115

Boulis, N. M., & Donsante, A. (2023). A novel antibody to treat SOD1-related amyotrophic lateral sclerosis. *Molecular Therapy - Methods & Clinical Development*, *29*, 236–237. https://doi.org/10.1016/j.omtm.2023.03.011

Brady, O. A., Meng, P., Zheng, Y., Mao, Y., & Hu, F. (2011). Regulation of TDP-43 aggregation by phosphorylation andp62/SQSTM1: Regulation of TDP-43 aggregation by phosphorylation and p62. *Journal of Neurochemistry*, *116*(2), 248–259. https://doi.org/10.1111/j.1471-4159.2010.07098.x

Bravo-Hernandez, M., Tadokoro, T., Navarro, M. R., Platoshyn, O., Kobayashi, Y., Marsala, S., Miyanohara, A., Juhas, S., Juhasova, J., Skalnikova, H., Tomori, Z., Vanicky, I., Studenovska, H., Proks, V., Chen, P., Govea-Perez, N., Ditsworth, D., Ciacci, J. D., Gao, S., … Marsala, M. (2020). Spinal subpial delivery of AAV9 enables widespread gene silencing and blocks motoneuron degeneration in ALS. *Nature Medicine*, *26*(1), 118–130. https://doi.org/10.1038/s41591-019-0674-1

Brettschneider, J., Del Tredici, K., Toledo, J. B., Robinson, J. L., Irwin, D. J., Grossman, M., Suh, E., Van Deerlin, V. M., Wood, E. M., Baek, Y., Kwong, L., Lee, E. B., Elman, L., McCluskey, L., Fang, L., Feldengut, S., Ludolph, A. C., Lee, V. M. -Y., Braak, H., & Trojanowski, J. Q. (2013). Stages of pTDP-43 pathology in amyotrophic lateral sclerosis. *Annals of Neurology*, *74*(1), 20–38. https://doi.org/10.1002/ana.23937

Briese, M., Saal-Bauernschubert, L., Lüningschrör, P., Moradi, M., Dombert, B., Surrey, V., Appenzeller, S., Deng, C., Jablonka, S., & Sendtner, M. (2020). Loss of Tdp-43 disrupts the axonal transcriptome of motoneurons accompanied by impaired axonal translation and mitochondria function. *Acta Neuropathologica Communications*, *8*(1), 116. https://doi.org/10.1186/s40478-020-00987-6

Brooks, B. R., Thisted, R. A., Appel, S. H., Bradley, W. G., Olney, R. K., Berg, J. E., Pope, L. E., & Smith, R. A. (2004). Treatment of pseudobulbar affect in ALS with dextromethorphan/quinidine: A randomized trial. *Neurology*, *63*(8), 1364–1370. https://doi.org/10.1212/01.WNL.0000142042.50528.2F

Brown, A.-L., Wilkins, O. G., Keuss, M. J., Hill, S. E., Zanovello, M., Lee, W. C., Bampton, A., Lee, F. C. Y., Masino, L., Qi, Y. A., Bryce-Smith, S., Gatt, A., Hallegger, M., Fagegaltier, D., Phatnani, H., NYGC ALS Consortium, Phatnani, H., Kwan, J., Sareen, D., … Fratta, P. (2022). TDP-43 loss and ALS-risk SNPs drive mis-splicing and depletion of UNC13A. *Nature*, *603*(7899), 131–137. https://doi.org/10.1038/s41586-022-04436-3

Brown, D. G., Shorter, J., & Wobst, H. J. (2020). Emerging small-molecule therapeutic approaches for amyotrophic lateral sclerosis and frontotemporal dementia. *Bioorganic & Medicinal Chemistry Letters*, *30*(4), 126942. https://doi.org/10.1016/j.bmcl.2019.126942

Brown, R. H., & Al-Chalabi, A. (2017). Amyotrophic Lateral Sclerosis. *New England Journal of Medicine*, *377*(2), 162–172. https://doi.org/10.1056/NEJMra1603471

Bryce-Smith, S., Brown, A.-L., Mehta, P. R., Mattedi, F., Mikheenko, A., Barattucci, S., Zanovello, M., Dattilo, D., Yome, M., Hill, S. E., Qi, Y. A., Wilkins, O. G., Sun, K., Ryadnov, E., Wan, Y., NYGC ALS Consortium, Vargas, J. N. S., Birsa, N., Raj, T., … Fratta, P. (2024). *TDP-43 loss induces extensive cryptic polyadenylation in ALS/FTD*. https://doi.org/10.1101/2024.01.22.576625

Budini, M., Buratti, E., Morselli, E., & Criollo, A. (2017). Autophagy and Its Impact on Neurodegenerative Diseases: New Roles for TDP-43 and C9orf72. *Frontiers in Molecular Neuroscience*, *10*, 170. https://doi.org/10.3389/fnmol.2017.00170

Buratti, E. (2018). TDP-43 post-translational modifications in health and disease. *Expert Opinion on Therapeutic Targets*, *22*(3), 279–293. https://doi.org/10.1080/14728222.2018.1439923

Buratti, E., & Baralle, F. E. (2010). The multiple roles of TDP-43 in pre-mRNA processing and gene expression regulation. *RNA Biology*, *7*(4), 420–429. https://doi.org/10.4161/rna.7.4.12205

Bustos, V. H., Marin, O., Meggio, F., Cesaro, L., Allende, C. C., Allende, J. E., & Pinna, L. A. (2005). Generation of protein kinase Ck1α mutants which discriminate between canonical and non-canonical substrates. *Biochemical Journal*, *391*(2), 417–424. https://doi.org/10.1042/BJ20050717

Cao, M. C., Ryan, B., Wu, J., Curtis, M. A., Faull, R. L. M., Dragunow, M., & Scotter, E. L. (2023). A panel of TDP-43-regulated splicing events verifies loss of TDP-43 function in amyotrophic lateral sclerosis brain tissue. *Neurobiology of Disease*, *185*, 106245. https://doi.org/10.1016/j.nbd.2023.106245

Carlomagno, Y., Zhang, Y., Davis, M., Lin, W.-L., Cook, C., Dunmore, J., Tay, W., Menkosky, K., Cao, X., Petrucelli, L., & DeTure, M. (2014). Casein Kinase II Induced Polymerization of Soluble TDP-43 into Filaments Is Inhibited by Heat Shock Proteins. *PLoS ONE*, *9*(3), e90452. https://doi.org/10.1371/journal.pone.0090452

Cassel, J. A., & Reitz, A. B. (2013). Ubiquilin-2 (UBQLN2) binds with high affinity to the C-terminal region of TDP-43 and modulates TDP-43 levels in H4 cells: Characterization of inhibition by nucleic acids and 4-aminoquinolines. *Biochimica et Biophysica Acta (BBA) - Proteins and Proteomics*, *1834*(6), 964–971. https://doi.org/10.1016/j.bbapap.2013.03.020

Castanotto, D., & Rossi, J. J. (2009). The promises and pitfalls of RNA-interference-based therapeutics. *Nature*, *457*(7228), 426–433. https://doi.org/10.1038/nature07758

Chen, C., Gu, J., Basurto-Islas, G., Jin, N., Wu, F., Gong, C.-X., Iqbal, K., & Liu, F. (2017). Up-regulation of casein kinase 1ε is involved in tau pathogenesis in Alzheimer's disease. *Scientific Reports*, *7*(1), 13478. https://doi.org/10.1038/s41598-017-13791-5

Cheong, J. K., & Virshup, D. M. (2011). Casein kinase 1: Complexity in the family. *The International Journal of Biochemistry & Cell Biology*, *43*(4), 465–469. https://doi.org/10.1016/j.biocel.2010.12.004

Chhangani, D., Martín-Peña, A., & Rincon-Limas, D. E. (2021). Molecular, functional, and pathological aspects of TDP-43 fragmentation. *iScience*, *24*(5), 102459. https://doi.org/10.1016/j.isci.2021.102459

Chiang, W.-C., Fang, Y.-S., Lye, Y. S., Weng, T.-Y., Ganesan, K., Huang, S.-H., Chang, L.-Y., Chou, S.-C., & Chen, Y.-R. (2022). Hyperphosphorylation-Mimetic TDP-43 Drives Amyloid Formation and Possesses Neuronal Toxicity at the Oligomeric

Stage. *ACS Chemical Neuroscience*, *13*(17), 2599–2612. https://doi.org/10.1021/acschemneuro.1c00873

Chiriboga, C. A. (2017). Nusinersen for the treatment of spinal muscular atrophy. *Expert Review of Neurotherapeutics*, *17*(10), 955–962. https://doi.org/10.1080/14737175.2017.1364159

Choksi, D. K., Roy, B., Chatterjee, S., Yusuff, T., Bakhoum, M. F., Sengupta, U., Ambegaokar, S., Kayed, R., & Jackson, G. R. (2014). TDP-43 Phosphorylation by casein kinase Iε promotes oligomerization and enhances toxicity in vivo. *Human Molecular Genetics*, *23*(4), 1025–1035. https://doi.org/10.1093/hmg/ddt498

Choudhary, C., Weinert, B. T., Nishida, Y., Verdin, E., & Mann, M. (2014). The growing landscape of lysine acetylation links metabolism and cell signalling. *Nature Reviews Molecular Cell Biology*, *15*(8), 536–550. https://doi.org/10.1038/nrm3841

Cohen, P., Cross, D., & Jänne, P. A. (2021). Kinase drug discovery 20 years after imatinib: Progress and future directions. *Nature Reviews Drug Discovery*, *20*(7), 551–569. https://doi.org/10.1038/s41573-021-00195-4

Cohen, T. J., Hwang, A. W., Restrepo, C. R., Yuan, C.-X., Trojanowski, J. Q., & Lee, V. M. Y. (2015). An acetylation switch controls TDP-43 function and aggregation propensity. *Nature Communications*, *6*(1), 5845. https://doi.org/10.1038/ncomms6845

Cohen, T. J., Hwang, A. W., Unger, T., Trojanowski, J. Q., & Lee, V. M. Y. (2012). Redox signalling directly regulates TDP-43 via cysteine oxidation and disulphide cross-linking: Oxidative stress regulates TDP-43. *The EMBO Journal*, *31*(5), 1241–1252. https://doi.org/10.1038/emboj.2011.471

Cole, T. A., Zhao, H., Collier, T. J., Sandoval, I., Sortwell, C. E., Steece-Collier, K., Daley, B. F., Booms, A., Lipton, J., Welch, M., Berman, M., Jandreski, L., Graham, D., Weihofen, A., Celano, S., Schulz, E., Cole-Strauss, A., Luna, E., Quach, D., … Paumier, K. L. (2021). α-Synuclein antisense oligonucleotides as a disease-modifying therapy for Parkinson's disease. *JCI Insight*, *6*(5), e135633. https://doi.org/10.1172/jci.insight.135633

Colombrita, C., Zennaro, E., Fallini, C., Weber, M., Sommacal, A., Buratti, E., Silani, V., & Ratti, A. (2009). TDP-43 is recruited to stress granules in conditions of oxidative insult. *Journal of Neurochemistry*, *111*(4), 1051–1061. https://doi.org/10.1111/j.1471-4159.2009.06383.x

Cozza, G., & Pinna, L. A. (2016). Casein kinases as potential therapeutic targets. *Expert Opinion on Therapeutic Targets*, *20*(3), 319–340. https://doi.org/10.1517/14728222.2016.1091883

Cuevas, E. P., Martinez-Gonzalez, L., Gordillo, C., Tosat-Bitrián, C., Pérez De La Lastra, C., Sáenz, A., Gil, C., Palomo, V., Martin-Requero, Á., & Martinez, A. (2024). Casein kinase 1 inhibitor avoids TDP-43 pathology propagation in a patient-derived cellular model of amyotrophic lateral sclerosis. *Neurobiology of Disease*, *192*, 106430. https://doi.org/10.1016/j.nbd.2024.106430

Cullati, S. N., Chaikuad, A., Chen, J.-S., Gebel, J., Tesmer, L., Zhubi, R., Navarrete-Perea, J., Guillen, R. X., Gygi, S. P., Hummer, G., Dötsch, V., Knapp, S., & Gould, K. L. (2022). Kinase domain autophosphorylation rewires the activity and substrate specificity of CK1 enzymes. *Molecular Cell*, *82*(11), 2006-2020.e8. https://doi.org/10.1016/j.molcel.2022.03.005

Curtis, H. J., Seow, Y., Wood, M. J. A., & Varela, M. A. (2017). Knockdown and replacement therapy mediated by artificial mirtrons in spinocerebellar ataxia 7. *Nucleic Acids Research*, *45*(13), 7870–7885. https://doi.org/10.1093/nar/gkx483

Da Cruz, S., Bui, A., Saberi, S., Lee, S. K., Stauffer, J., McAlonis-Downes, M., Schulte, D., Pizzo, D. P., Parone, P. A., Cleveland, D. W., & Ravits, J. (2017). Misfolded SOD1 is not a primary component of sporadic ALS. *Acta Neuropathologica*, *134*(1), 97–111. https://doi.org/10.1007/s00401-017-1688-8

Day, J. W., Chiriboga, C. A., Crawford, T. O., Darras, B. T., Finkel, R. S., Connolly, A. M., Iannaccone, S. T., Kuntz, N. L., Peña, L. D. M., Shieh, P. B., Smith, E. C., Schultz, M., Feltner, D. E., Tauscher-Wisniewski, S., Ogrinc, F. G., Shah, A., Ouyang, H., Macek, T., Kernbauer, E., … Mendell, J. R. (2020). Onasemnogene Abeparvovec-xioi Gene-Replacement Therapy for Spinal Muscular Atrophy Type 1 (SMA1): Phase 3 US Study (STR1VE) Update (1828). *Neurology*, *94*(15_supplement), 1828. https://doi.org/10.1212/WNL.94.15_supplement.1828

Deng, H.-X., Chen, W., Hong, S.-T., Boycott, K. M., Gorrie, G. H., Siddique, N., Yang, Y., Fecto, F., Shi, Y., Zhai, H., Jiang, H., Hirano, M., Rampersaud, E., Jansen, G. H., Donkervoort, S., Bigio, E. H., Brooks, B. R., Ajroud, K., Sufit, R. L., … Siddique, T. (2011). Mutations in UBQLN2 cause dominant X-linked juvenile and adult-onset ALS and ALS/dementia. *Nature*, *477*(7363), 211–215. https://doi.org/10.1038/nature10353

Deng, H.-X., Zhai, H., Shi, Y., Liu, G., Lowry, J., Liu, B., Ryan, É. B., Yan, J., Yang, Y., Zhang, N., Yang, Z., Liu, E., Ma, Y. C., & Siddique, T. (2021). Efficacy and long-term safety of CRISPR/Cas9 genome editing in the SOD1-linked mouse models of ALS. *Communications Biology*, *4*(1), 396. https://doi.org/10.1038/s42003-021-01942-4

Dewil, M., Dela Cruz, V. F., Van Den Bosch, L., & Robberecht, W. (2007). Inhibition of p38 mitogen activated protein kinase activation and mutant SOD1G93A-induced motor neuron death. *Neurobiology of Disease*, *26*(2), 332–341. https://doi.org/10.1016/j.nbd.2006.12.023

Donnelly, C. J., Zhang, P.-W., Pham, J. T., Haeusler, A. R., Mistry, N. A., Vidensky, S., Daley, E. L., Poth, E. M., Hoover, B., Fines, D. M., Maragakis, N., Tienari, P. J., Petrucelli, L., Traynor, B. J., Wang, J., Rigo, F., Bennett, C. F., Blackshaw, S., Sattler, R., & Rothstein, J. D. (2013). RNA Toxicity from the ALS/FTD C9ORF72 Expansion Is Mitigated by Antisense Intervention. *Neuron*, *80*(2), 415–428. https://doi.org/10.1016/j.neuron.2013.10.015

Dormann, D., Capell, A., Carlson, A. M., Shankaran, S. S., Rodde, R., Neumann, M., Kremmer, E., Matsuwaki, T., Yamanouchi, K., Nishihara, M., & Haass, C. (2009). Proteolytic processing of TAR DNA binding protein-43 by caspases produces C-terminal fragments with disease defining properties independent of progranulin. *Journal of Neurochemistry*, *110*(3), 1082–1094. https://doi.org/10.1111/j.1471-4159.2009.06211.x

Duan, W., Guo, M., Yi, L., Liu, Y., Li, Z., Ma, Y., Zhang, G., Liu, Y., Bu, H., Song, X., & Li, C. (2020). The deletion of mutant SOD1 via CRISPR/Cas9/sgRNA prolongs survival in an amyotrophic lateral sclerosis mouse model. *Gene Therapy*, *27*(3–4), 157–169. https://doi.org/10.1038/s41434-019-0116-1

Eck, R. J., Kraemer, B. C., & Liachko, N. F. (2021). Regulation of TDP-43 phosphorylation in aging and disease. *GeroScience*, *43*(4), 1605–1614. https://doi.org/10.1007/s11357-021-00383-5

Eide, E. J., & Virshup, D. M. (2001). CASEIN KINASE I: ANOTHER COG IN THE CIRCADIAN CLOCKWORKS. *Chronobiology International*, *18*(3), 389–398. https://doi.org/10.1081/CBI-100103963

Eide, E. J., Woolf, M. F., Kang, H., Woolf, P., Hurst, W., Camacho, F., Vielhaber, E. L., Giovanni, A., & Virshup, D. M. (2005). Control of Mammalian Circadian Rhythm by CKIε-Regulated Proteasome-Mediated PER2 Degradation. *Molecular and Cellular Biology*, *25*(7), 2795–2807. https://doi.org/10.1128/MCB.25.7.2795-2807.2005

Etchegaray, J.-P., Machida, K. K., Noton, E., Constance, C. M., Dallmann, R., Di Napoli, M. N., DeBruyne, J. P., Lambert, C. M., Yu, E. A., Reppert, S. M., & Weaver, D. R. (2009). Casein Kinase 1 Delta Regulates the Pace of the Mammalian Circadian Clock. *Molecular and Cellular Biology*, *29*(14), 3853–3866. https://doi.org/10.1128/MCB.00338-09

Etchegaray, J.-P., Yu, E. A., Indic, P., Dallmann, R., & Weaver, D. R. (2010). Casein Kinase 1 Delta (CK1δ) Regulates Period Length of the Mouse Suprachiasmatic Circadian Clock In Vitro. *PLoS ONE*, *5*(4), e10303. https://doi.org/10.1371/journal.pone.0010303

Fabian, M. A., Biggs, W. H., Treiber, D. K., Atteridge, C. E., Azimioara, M. D., Benedetti, M. G., Carter, T. A., Ciceri, P., Edeen, P. T., Floyd, M., Ford, J. M., Galvin, M., Gerlach, J. L., Grotzfeld, R. M., Herrgard, S., Insko, D. E., Insko, M. A., Lai, A. G.,

Lélias, J.-M., … Lockhart, D. J. (2005). A small molecule–kinase interaction map for clinical kinase inhibitors. *Nature Biotechnology*, *23*(3), 329–336. https://doi.org/10.1038/nbt1068

Fallini, C., Bassell, G. J., & Rossoll, W. (2012). The ALS disease protein TDP-43 is actively transported in motor neuron axons and regulates axon outgrowth. *Human Molecular Genetics*, *21*(16), 3703–3718. https://doi.org/10.1093/hmg/dds205

Fang, F., Ingre, C., Roos, P., Kamel, F., & Piehl, F. (2015). Risk factors for amyotrophic lateral sclerosis. *Clinical Epidemiology*, 181. https://doi.org/10.2147/CLEP.S37505

Feneberg, E., Gray, E., Ansorge, O., Talbot, K., & Turner, M. R. (2018). Towards a TDP-43-Based Biomarker for ALS and FTLD. *Molecular Neurobiology*, *55*(10), 7789–7801. https://doi.org/10.1007/s12035-018-0947-6

Ferguson, F. M., & Gray, N. S. (2018). Kinase inhibitors: The road ahead. *Nature Reviews Drug Discovery*, *17*(5), 353–377. https://doi.org/10.1038/nrd.2018.21

Finkel, R. S., Mercuri, E., Darras, B. T., Connolly, A. M., Kuntz, N. L., Kirschner, J., Chiriboga, C. A., Saito, K., Servais, L., Tizzano, E., Topaloglu, H., Tulinius, M., Montes, J., Glanzman, A. M., Bishop, K., Zhong, Z. J., Gheuens, S., Bennett, C. F., Schneider, E., … De Vivo, D. C. (2017). Nusinersen versus Sham Control in Infantile-Onset Spinal Muscular Atrophy. *New England Journal of Medicine*, *377*(18), 1723–1732. https://doi.org/10.1056/NEJMoa1702752

Fish, K. J., Cegielska, A., Getman, M. E., Landes, G. M., & Virshup, D. M. (1995). Isolation and Characterization of Human Casein Kinase Iϵ (CKI), a Novel Member of the CKI Gene Family. *Journal of Biological Chemistry*, *270*(25), 14875–14883. https://doi.org/10.1074/jbc.270.25.14875

Flotow, H., Graves, P. R., Wang, A. Q., Fiol, C. J., Roeske, R. W., & Roach, P. J. (1990). Phosphate groups as substrate determinants for casein kinase I action. *Journal of Biological Chemistry*, *265*(24), 14264–14269. https://doi.org/10.1016/S0021-9258(18)77295-5

Flotow, H., & Roach, P. J. (1991). Role of acidic residues as substrate determinants for casein kinase I. *Journal of Biological Chemistry*, *266*(6), 3724–3727. https://doi.org/10.1016/S0021-9258(19)67854-3

Foust, K. D., Salazar, D. L., Likhite, S., Ferraiuolo, L., Ditsworth, D., Ilieva, H., Meyer, K., Schmelzer, L., Braun, L., Cleveland, D. W., & Kaspar, B. K. (2013). Therapeutic AAV9-mediated Suppression of Mutant SOD1 Slows Disease Progression and Extends Survival in Models of Inherited ALS. *Molecular Therapy*, *21*(12), 2148–2159. https://doi.org/10.1038/mt.2013.211

Franich, N. R., Fitzsimons, H. L., Fong, D. M., Klugmann, M., During, M. J., & Young, D. (2008). AAV Vector–mediated RNAi of Mutant Huntingtin Expression Is Neuroprotective in a Novel Genetic Rat Model of Huntington's Disease. *Molecular Therapy*, *16*(5), 947–956. https://doi.org/10.1038/mt.2008.50

Fulcher, L. J., & Sapkota, G. P. (2020). Functions and regulation of the serine/threonine protein kinase CK1 family: Moving beyond promiscuity. *Biochemical Journal*, *477*(23), 4603–4621. https://doi.org/10.1042/BCJ20200506

Gaj, T., Ojala, D. S., Ekman, F. K., Byrne, L. C., Limsirichai, P., & Schaffer, D. V. (2017). In vivo genome editing improves motor function and extends survival in a mouse model of ALS. *Science Advances*, *3*(12), eaar3952. https://doi.org/10.1126/sciadv.aar3952

Garcia Morato, J., Hans, F., Von Zweydorf, F., Feederle, R., Elsässer, S. J., Skodras, A. A., Gloeckner, C. J., Buratti, E., Neumann, M., & Kahle, P. J. (2022). Sirtuin-1 sensitive lysine-136 acetylation drives phase separation and pathological aggregation of TDP-43. *Nature Communications*, *13*(1), 1223. https://doi.org/10.1038/s41467-022-28822-7

Gasset-Rosa, F., Lu, S., Yu, H., Chen, C., Melamed, Z., Guo, L., Shorter, J., Da Cruz, S., & Cleveland, D. W. (2019). Cytoplasmic TDP-43 De-mixing Independent of Stress Granules Drives Inhibition of Nuclear Import, Loss of Nuclear TDP-43, and Cell Death. *Neuron*, *102*(2), 339-357.e7. https://doi.org/10.1016/j.neuron.2019.02.038

Gendron, T. F., Rademakers, R., & Petrucelli, L. (2012). TARDBP Mutation Analysis in TDP-43 Proteinopathies and Deciphering the Toxicity of Mutant TDP-43. *Journal of Alzheimer's Disease*, *33*(s1), S35–S45. https://doi.org/10.3233/JAD-2012-129036

Giacomelli, E., Vahsen, B. F., Calder, E. L., Xu, Y., Scaber, J., Gray, E., Dafinca, R., Talbot, K., & Studer, L. (2022). Human stem cell models of neurodegeneration: From basic science of amyotrophic lateral sclerosis to clinical translation. *Cell Stem Cell*, *29*(1), 11–35. https://doi.org/10.1016/j.stem.2021.12.008

Gibbs, K. L., Kalmar, B., Rhymes, E. R., Fellows, A. D., Ahmed, M., Whiting, P., Davies, C. H., Greensmith, L., & Schiavo, G. (2018). Inhibiting p38 MAPK alpha rescues axonal retrograde transport defects in a mouse model of ALS. *Cell Death & Disease*, *9*(6), 596. https://doi.org/10.1038/s41419-018-0624-8

Gonzalez-Gonzalez, S., Caumes, B., & Cazevieille, C. (2021). The Silencing of Casein Kinase I Attenuated Neuromuscular Impairment in a Preclinical Mouse Model of Amyotrophic Lateral Sclerosis. *Journal of Experimental Pathology*, *2*(2). https://doi.org/10.33696/pathology.2.016

Goossens, J., Vanmechelen, E., Trojanowski, J. Q., Lee, V. M., Van Broeckhoven, C., Van Der Zee, J., & Engelborghs, S. (2015). TDP-43 as a possible biomarker for frontotemporal lobar degeneration: A systematic review of existing antibodies. *Acta Neuropathologica Communications*, *3*(1), 15. https://doi.org/10.1186/s40478-015-0195-1

Grabowska-Pyrzewicz, W., Want, A., Leszek, J., & Wojda, U. (2021). Antisense oligonucleotides for Alzheimer's disease therapy: From the mRNA to miRNA paradigm. *eBioMedicine*, *74*, 103691. https://doi.org/10.1016/j.ebiom.2021.103691

Gros-Louis, F., Soucy, G., Larivière, R., & Julien, J. (2010). Intracerebroventricular infusion of monoclonal antibody or its derived Fab fragment against misfolded forms of SOD1 mutant delays mortality in a mouse model of ALS. *Journal of Neurochemistry*, *113*(5), 1188–1199. https://doi.org/10.1111/j.1471-4159.2010.06683.x

Gruijs Da Silva, L. A., Simonetti, F., Hutten, S., Riemenschneider, H., Sternburg, E. L., Pietrek, L. M., Gebel, J., Dötsch, V., Edbauer, D., Hummer, G., Stelzl, L. S., & Dormann, D. (2022). Disease-linked TDP-43 hyperphosphorylation suppresses TDP-43 condensation and aggregation. *The EMBO Journal*, *41*(8), e108443. https://doi.org/10.15252/embj.2021108443

Gu, J., Hu, W., Tan, X., Qu, S., Chu, D., Gong, C., Iqbal, K., & Liu, F. (2020). Elevation of casein kinase 1ε associated with TDP-43 and tau pathologies in Alzheimer's disease. *Brain Pathology*, *30*(2), 283–297. https://doi.org/10.1111/bpa.12775

Guenther, E. L., Cao, Q., Trinh, H., Lu, J., Sawaya, M. R., Cascio, D., Boyer, D. R., Rodriguez, J. A., Hughes, M. P., & Eisenberg, D. S. (2018). Atomic structures of TDP-43 LCD segments and insights into reversible or pathogenic aggregation. *Nature Structural & Molecular Biology*, *25*(6), 463–471. https://doi.org/10.1038/s41594-018-0064-2

Guo, L., Fare, C. M., & Shorter, J. (2019). Therapeutic Dissolution of Aberrant Phases by Nuclear-Import Receptors. *Trends in Cell Biology*, *29*(4), 308–322. https://doi.org/10.1016/j.tcb.2018.12.004

Guo, W., Fumagalli, L., Prior, R., & Van Den Bosch, L. (2017). Current Advances and Limitations in Modeling ALS/FTD in a Dish Using Induced Pluripotent Stem Cells. *Frontiers in Neuroscience*, *11*, 671. https://doi.org/10.3389/fnins.2017.00671

Guo, W., Vandoorne, T., Steyaert, J., Staats, K. A., & Van Den Bosch, L. (2020). The multifaceted role of kinases in amyotrophic lateral sclerosis: Genetic, pathological and therapeutic implications. *Brain*, *143*(6), 1651–1673. https://doi.org/10.1093/brain/awaa022

Han, J.-H., Yu, T.-H., Ryu, H.-H., Jun, M.-H., Ban, B.-K., Jang, D.-J., & Lee, J.-A. (2013). ALS/FTLD-linked TDP-43 regulates neurite morphology and cell survival in differentiated neurons. *Experimental Cell Research*, *319*(13), 1998–2005. https://doi.org/10.1016/j.yexcr.2013.05.025

Hasegawa, M., Arai, T., Nonaka, T., Kametani, F., Yoshida, M., Hashizume, Y., Beach, T. G., Buratti, E., Baralle, F., Morita, M., Nakano, I., Oda, T., Tsuchiya, K., & Akiyama, H. (2008). Phosphorylated TDP-43 in frontotemporal lobar degeneration and amyotrophic lateral sclerosis. *Annals of Neurology*, *64*(1), 60–70. https://doi.org/10.1002/ana.21425

Hasegawa, M., Nonaka, T., Tsuji, H., Tamaoka, A., Yamashita, M., Kametani, F., Yoshida, M., Arai, T., & Akiyama, H. (2011). Molecular Dissection of TDP-43 Proteinopathies. *Journal of Molecular Neuroscience*, *45*(3), 480–485. https://doi.org/10.1007/s12031-011-9571-x

Hergesheimer, R. C., Chami, A. A., De Assis, D. R., Vourc'h, P., Andres, C. R., Corcia, P., Lanznaster, D., & Blasco, H. (2019). The debated toxic role of aggregated TDP-43 in amyotrophic lateral sclerosis: A resolution in sight? *Brain*, *142*(5), 1176–1194. https://doi.org/10.1093/brain/awz078

Herzog, J. J., Deshpande, M., Shapiro, L., Rodal, A. A., & Paradis, S. (2017). TDP-43 misexpression causes defects in dendritic growth. *Scientific Reports*, *7*(1), 15656. https://doi.org/10.1038/s41598-017-15914-4

Hicks, D. A., Cross, L. L., Williamson, R., & Rattray, M. (2020). Endoplasmic Reticulum Stress Signalling Induces Casein Kinase 1-Dependent Formation of Cytosolic TDP-43 Inclusions in Motor Neuron-Like Cells. *Neurochemical Research*, *45*(6), 1354–1364. https://doi.org/10.1007/s11064-019-02832-2

Hoy, S. M. (2019). Onasemnogene Abeparvovec: First Global Approval. *Drugs*, *79*(11), 1255–1262. https://doi.org/10.1007/s40265-019-01162-5

Iannitti, T., Scarrott, J. M., Likhite, S., Coldicott, I. R. P., Lewis, K. E., Heath, P. R., Higginbottom, A., Myszczynska, M. A., Milo, M., Hautbergue, G. M., Meyer, K., Kaspar, B. K., Ferraiuolo, L., Shaw, P. J., & Azzouz, M. (2018). Translating SOD1 Gene Silencing toward the Clinic: A Highly Efficacious, Off-Target-free, and Biomarker-Supported Strategy for fALS. *Molecular Therapy - Nucleic Acids*, *12*, 75–88. https://doi.org/10.1016/j.omtn.2018.04.015

Igaz, L. M., Kwong, L. K., Chen-Plotkin, A., Winton, M. J., Unger, T. L., Xu, Y., Neumann, M., Trojanowski, J. Q., & Lee, V. M.-Y. (2009). Expression of TDP-43 C-terminal Fragments in Vitro Recapitulates Pathological Features of TDP-43 Proteinopathies. *Journal of Biological Chemistry*, *284*(13), 8516–8524. https://doi.org/10.1074/jbc.M809462200

Igaz, L. M., Kwong, L. K., Lee, E. B., Chen-Plotkin, A., Swanson, E., Unger, T., Malunda, J., Xu, Y., Winton, M. J., Trojanowski, J. Q., & Lee, V. M.-Y. (2011). Dysregulation of the ALS-associated gene TDP-43 leads to neuronal death and degeneration in mice. *Journal of Clinical Investigation*, *121*(2), 726–738. https://doi.org/10.1172/JCI44867

Igaz, L. M., Kwong, L. K., Xu, Y., Truax, A. C., Uryu, K., Neumann, M., Clark, C. M., Elman, L. B., Miller, B. L., Grossman, M., McCluskey, L. F., Trojanowski, J. Q., & Lee, V. M.-Y. (2008). Enrichment of C-Terminal Fragments in TAR DNA-Binding Protein-43 Cytoplasmic Inclusions in Brain but not in Spinal Cord of Frontotemporal Lobar Degeneration and Amyotrophic Lateral Sclerosis. *The American Journal of Pathology*, *173*(1), 182–194. https://doi.org/10.2353/ajpath.2008.080003

Iguchi, Y., Katsuno, M., Niwa, J., Takagi, S., Ishigaki, S., Ikenaka, K., Kawai, K., Watanabe, H., Yamanaka, K., Takahashi, R., Misawa, H., Sasaki, S., Tanaka, F., & Sobue, G. (2013). Loss of TDP-43 causes age-dependent progressive motor neuron degeneration. *Brain*, *136*(5), 1371–1382. https://doi.org/10.1093/brain/awt029

Iguchi, Y., Katsuno, M., Takagi, S., Ishigaki, S., Niwa, J., Hasegawa, M., Tanaka, F., & Sobue, G. (2012). Oxidative stress induced by glutathione depletion reproduces pathological modifications of TDP-43 linked to TDP-43 proteinopathies. *Neurobiology of Disease*, *45*(3), 862–870. https://doi.org/10.1016/j.nbd.2011.12.002

Ikeda, K., & Tsuchiya, K. (2004). Motor neuron disease group accompanied by inclusions of unidentified protein signaled by ubiquitin. *Neuropathology*, *24*(2), 117–124. https://doi.org/10.1111/j.1440-1789.2003.00537.x

Inukai, Y., Nonaka, T., Arai, T., Yoshida, M., Hashizume, Y., Beach, T. G., Buratti, E., Baralle, F. E., Akiyama, H., Hisanaga, S., & Hasegawa, M. (2008). Abnormal phosphorylation of Ser409/410 of TDP-43 in FTLD-U and ALS. *FEBS Letters*, *582*(19), 2899–2904. https://doi.org/10.1016/j.febslet.2008.07.027

Jankovska, N., & Matej, R. (2021). Molecular Pathology of ALS: What We Currently Know and What Important Information Is Still Missing. *Diagnostics*, *11*(8), 1365. https://doi.org/10.3390/diagnostics11081365

Jeong, Y. H., Ling, J. P., Lin, S. Z., Donde, A. N., Braunstein, K. E., Majounie, E., Traynor, B. J., LaClair, K. D., Lloyd, T. E., & Wong, P. C. (2017). Tdp-43 cryptic exons are highly variable between cell types. *Molecular Neurodegeneration*, *12*(1), 13. https://doi.org/10.1186/s13024-016-0144-x

Johnson, J. L., Yaron, T. M., Huntsman, E. M., Kerelsky, A., Song, J., Regev, A., Lin, T.-Y., Liberatore, K., Cizin, D. M., Cohen, B. M., Vasan, N., Ma, Y., Krismer, K.,

Robles, J. T., Van De Kooij, B., Van Vlimmeren, A. E., Andrée-Busch, N., Käufer, N. F., Dorovkov, M. V., … Cantley, L. C. (2023). An atlas of substrate specificities for the human serine/threonine kinome. *Nature*, *613*(7945), 759–766. https://doi.org/10.1038/s41586-022-05575-3

Kametani, F., Nonaka, T., Suzuki, T., Arai, T., Dohmae, N., Akiyama, H., & Hasegawa, M. (2009). Identification of casein kinase-1 phosphorylation sites on TDP-43. *Biochemical and Biophysical Research Communications*, *382*(2), 405–409. https://doi.org/10.1016/j.bbrc.2009.03.038

Kametani, F., Obi, T., Shishido, T., Akatsu, H., Murayama, S., Saito, Y., Yoshida, M., & Hasegawa, M. (2016). Mass spectrometric analysis of accumulated TDP-43 in amyotrophic lateral sclerosis brains. *Scientific Reports*, *6*(1), 23281. https://doi.org/10.1038/srep23281

Kang, L., Jin, S., Wang, J., Lv, Z., Xin, C., Tan, C., Zhao, M., Wang, L., & Liu, J. (2023). AAV vectors applied to the treatment of CNS disorders: Clinical status and challenges. *Journal of Controlled Release*, *355*, 458–473. https://doi.org/10.1016/j.jconrel.2023.01.067

Kantor, B., Tagliafierro, L., Gu, J., Zamora, M. E., Ilich, E., Grenier, C., Huang, Z. Y., Murphy, S., & Chiba-Falek, O. (2018). Downregulation of SNCA Expression by Targeted Editing of DNA Methylation: A Potential Strategy for Precision Therapy in PD. *Molecular Therapy*, *26*(11), 2638–2649. https://doi.org/10.1016/j.ymthe.2018.08.019

Karaman, M. W., Herrgard, S., Treiber, D. K., Gallant, P., Atteridge, C. E., Campbell, B. T., Chan, K. W., Ciceri, P., Davis, M. I., Edeen, P. T., Faraoni, R., Floyd, M., Hunt, J. P., Lockhart, D. J., Milanov, Z. V., Morrison, M. J., Pallares, G., Patel, H. K., Pritchard, S., … Zarrinkar, P. P. (2008). A quantitative analysis of kinase inhibitor selectivity. *Nature Biotechnology*, *26*(1), 127–132. https://doi.org/10.1038/nbt1358

Kawahara, Y., & Mieda-Sato, A. (2012). TDP-43 promotes microRNA biogenesis as a component of the Drosha and Dicer complexes. *Proceedings of the National Academy of Sciences*, *109*(9), 3347–3352. https://doi.org/10.1073/pnas.1112427109

Keam, S. J. (2021). Elivaldogene Autotemcel: First Approval. *Molecular Diagnosis & Therapy*, *25*(6), 803–809. https://doi.org/10.1007/s40291-021-00555-1

Kim, K. Y., Lee, H.-W., Shim, Y., Mook-Jung, I., Jeon, G. S., & Sung, J.-J. (2015). A phosphomimetic mutant TDP-43 (S409/410E) induces Drosha instability and cytotoxicity in Neuro 2A cells. *Biochemical and Biophysical Research Communications*, *464*(1), 236–243. https://doi.org/10.1016/j.bbrc.2015.06.125

Kishino, Y., Matsukawa, K., Matsumoto, T., Miyazaki, R., Wakabayashi, T., Nonaka, T., Kametani, F., Hasegawa, M., Hashimoto, T., & Iwatsubo, T. (2022). Casein kinase 1δ/ε phosphorylates fused in sarcoma (FUS) and ameliorates FUS-mediated neurodegeneration. *Journal of Biological Chemistry*, *298*(8), 102191. https://doi.org/10.1016/j.jbc.2022.102191

Kiyota, T., Zhang, G., Morrison, C. M., Bosch, M. E., Weir, R. A., Lu, Y., Dong, W., & Gendelman, H. E. (2015). AAV2/1 CD74 Gene Transfer Reduces β-amyloidosis and Improves Learning and Memory in a Mouse Model of Alzheimer's Disease. *Molecular Therapy*, *23*(11), 1712–1721. https://doi.org/10.1038/mt.2015.142

Klim, J. R., Pintacuda, G., Nash, L. A., Guerra San Juan, I., & Eggan, K. (2021). Connecting TDP-43 Pathology with Neuropathy. *Trends in Neurosciences*, *44*(6), 424–440. https://doi.org/10.1016/j.tins.2021.02.008

Klim, J. R., Williams, L. A., Limone, F., Guerra San Juan, I., Davis-Dusenbery, B. N., Mordes, D. A., Burberry, A., Steinbaugh, M. J., Gamage, K. K., Kirchner, R., Moccia, R., Cassel, S. H., Chen, K., Wainger, B. J., Woolf, C. J., & Eggan, K. (2019). ALS-implicated protein TDP-43 sustains levels of STMN2, a mediator of motor neuron growth and repair. *Nature Neuroscience*, *22*(2), 167–179. https://doi.org/10.1038/s41593-018-0300-4

Ko, V. I., Ong, K., Cleveland, D. W., Yu, H., & Ravits, J. M. (2024). CK1δ/ε kinases regulate TDP-43 phosphorylation and are therapeutic targets for ALS-related TDP-43 hyperphosphorylation. *Neurobiology of Disease*, *196*, 106516. https://doi.org/10.1016/j.nbd.2024.106516

Konstantinidis, E., Molisak, A., Perrin, F., Streubel-Gallasch, L., Fayad, S., Kim, D. Y., Petri, K., Aryee, M. J., Aguilar, X., György, B., Giedraitis, V., Joung, J. K., Pattanayak, V., Essand, M., Erlandsson, A., Berezovska, O., & Ingelsson, M. (2022). CRISPR-Cas9 treatment partially restores amyloid-β 42/40 in human fibroblasts with the Alzheimer's disease PSEN1 M146L mutation. *Molecular Therapy - Nucleic Acids*, *28*, 450–461. https://doi.org/10.1016/j.omtn.2022.03.022

Korobeynikov, V. A., Lyashchenko, A. K., Blanco-Redondo, B., Jafar-Nejad, P., & Shneider, N. A. (2022). Antisense oligonucleotide silencing of FUS expression as a therapeutic approach in amyotrophic lateral sclerosis. *Nature Medicine*, *28*(1), 104–116. https://doi.org/10.1038/s41591-021-01615-z

Krach, F., Batra, R., Wheeler, E. C., Vu, A. Q., Wang, R., Hutt, K., Rabin, S. J., Baughn, M. W., Libby, R. T., Diaz-Garcia, S., Stauffer, J., Pirie, E., Saberi, S., Rodriguez, M., Madrigal, A. A., Kohl, Z., Winner, B., Yeo, G. W., & Ravits, J. (2018). Transcriptome–pathology correlation identifies interplay between TDP-43 and the expression of its kinase CK1E in sporadic ALS. *Acta Neuropathologica*, *136*(3), 405–423. https://doi.org/10.1007/s00401-018-1870-7

Krishnan, G., Zhang, Y., Gu, Y., Kankel, M. W., Gao, F.-B., & Almeida, S. (2020). CRISPR deletion of the C9ORF72 promoter in ALS/FTD patient motor neurons abolishes production of dipeptide repeat proteins and rescues neurodegeneration. *Acta Neuropathologica*, *140*(1), 81–84. https://doi.org/10.1007/s00401-020-02154-6

Kwong, L. K., Neumann, M., Sampathu, D. M., Lee, V. M.-Y., & Trojanowski, J. Q. (2007). TDP-43 proteinopathy: The neuropathology underlying major forms of sporadic and familial frontotemporal lobar degeneration and motor neuron disease. *Acta Neuropathologica*, *114*(1), 63–70. https://doi.org/10.1007/s00401-007-0226-5

Lagier-Tourenne, C., & Cleveland, D. W. (2009). Rethinking ALS: The FUS about TDP-43. *Cell*, *136*(6), 1001–1004. https://doi.org/10.1016/j.cell.2009.03.006

Larkin, H. D. (2022). Autologous Gene Therapy Approved for Childhood CALD. *JAMA*, *328*(17), 1679. https://doi.org/10.1001/jama.2022.19800

Lattante, S., Ciura, S., Rouleau, G. A., & Kabashi, E. (2015). Defining the genetic connection linking amyotrophic lateral sclerosis (ALS) with frontotemporal dementia (FTD). *Trends in Genetics*, *31*(5), 263–273. https://doi.org/10.1016/j.tig.2015.03.005

Lee, C., Etchegaray, J.-P., Cagampang, F. R. A., Loudon, A. S. I., & Reppert, S. M. (2001). Posttranslational Mechanisms Regulate the Mammalian Circadian Clock. *Cell*, *107*(7), 855–867. https://doi.org/10.1016/S0092-8674(01)00610-9

Li, H.-Y., Yeh, P.-A., Chiu, H.-C., Tang, C.-Y., & Tu, B. P. (2011). Hyperphosphorylation as a Defense Mechanism to Reduce TDP-43 Aggregation. *PLoS ONE*, *6*(8), e23075. https://doi.org/10.1371/journal.pone.0023075

Li, Q., Babinchak, W. M., & Surewicz, W. K. (2021). Cryo-EM structure of amyloid fibrils formed by the entire low complexity domain of TDP-43. *Nature Communications*, *12*(1), 1620. https://doi.org/10.1038/s41467-021-21912-y

Li, S.-S., Dong, Y.-H., & Liu, Z.-P. (2021). Recent Advances in the Development of Casein Kinase 1 Inhibitors. *Current Medicinal Chemistry*, *28*(8), 1585–1604. https://doi.org/10.2174/0929867327666200713185413

Li, W., Reeb, A. N., Lin, B., Subramanian, P., Fey, E. E., Knoverek, C. R., French, R. L., Bigio, E. H., & Ayala, Y. M. (2017). Heat Shock-induced Phosphorylation of TAR DNA-binding Protein 43 (TDP-43) by MAPK/ERK Kinase Regulates TDP-43 Function. *Journal of Biological Chemistry*, *292*(12), 5089–5100. https://doi.org/10.1074/jbc.M116.753913

Liachko, N. F., Guthrie, C. R., & Kraemer, B. C. (2010). Phosphorylation Promotes Neurotoxicity in a *Caenorhabditis elegans* Model of TDP-43 Proteinopathy. *The*

Journal of Neuroscience, *30*(48), 16208–16219. https://doi.org/10.1523/JNEUROSCI.2911-10.2010

Liachko, N. F., McMillan, P. J., Guthrie, C. R., Bird, T. D., Leverenz, J. B., & Kraemer, B. C. (2013). CDC7 inhibition blocks pathological TDP-43 phosphorylation and neurodegeneration. *Annals of Neurology*, *74*(1), 39–52. https://doi.org/10.1002/ana.23870

Liachko, N. F., McMillan, P. J., Strovas, T. J., Loomis, E., Greenup, L., Murrell, J. R., Ghetti, B., Raskind, M. A., Montine, T. J., Bird, T. D., Leverenz, J. B., & Kraemer, B. C. (2014). The Tau Tubulin Kinases TTBK1/2 Promote Accumulation of Pathological TDP-43. *PLoS Genetics*, *10*(12), e1004803. https://doi.org/10.1371/journal.pgen.1004803

Lim, C. K. W., Gapinske, M., Brooks, A. K., Woods, W. S., Powell, J. E., Zeballos C., M. A., Winter, J., Perez-Pinera, P., & Gaj, T. (2020). Treatment of a Mouse Model of ALS by In Vivo Base Editing. *Molecular Therapy*, *28*(4), 1177–1189. https://doi.org/10.1016/j.ymthe.2020.01.005

Ling, J. P., Pletnikova, O., Troncoso, J. C., & Wong, P. C. (2015). TDP-43 repression of nonconserved cryptic exons is compromised in ALS-FTD. *Science*, *349*(6248), 650–655. https://doi.org/10.1126/science.aab0983

Ling, Q., Herstine, J. A., Bradbury, A., & Gray, S. J. (2023). AAV-based in vivo gene therapy for neurological disorders. *Nature Reviews Drug Discovery*, *22*(10), 789–806. https://doi.org/10.1038/s41573-023-00766-7

Ling, S.-C., Polymenidou, M., & Cleveland, D. W. (2013). Converging Mechanisms in ALS and FTD: Disrupted RNA and Protein Homeostasis. *Neuron*, *79*(3), 416–438. https://doi.org/10.1016/j.neuron.2013.07.033

Liu, R., Yang, G., Nonaka, T., Arai, T., Jia, W., & Cynader, M. S. (2013). Reducing TDP-43 aggregation does not prevent its cytotoxicity. *Acta Neuropathologica Communications*, *1*(1), 49. https://doi.org/10.1186/2051-5960-1-49

Long, A. M., Zhao, H., & Huang, X. (2012). Structural Basis for the Potent and Selective Inhibition of Casein Kinase 1 Epsilon. *Journal of Medicinal Chemistry*, *55*(22), 10307–10311. https://doi.org/10.1021/jm301336n

Lubroth, P., Colasante, G., & Lignani, G. (2021). In vivo Genome Editing Therapeutic Approaches for Neurological Disorders: Where Are We in the Translational Pipeline? *Frontiers in Neuroscience*, *15*, 632522. https://doi.org/10.3389/fnins.2021.632522

Luo, L., Song, Z., Li, X., Huiwang, Zeng, Y., Qinwang, Meiqi, & He, J. (2019). Efficacy and safety of edaravone in treatment of amyotrophic lateral sclerosis—A

systematic review and meta-analysis. *Neurological Sciences*, *40*(2), 235–241. https://doi.org/10.1007/s10072-018-3653-2

Lutz, C. (2018). Mouse models of ALS: Past, present and future. *Brain Research*, *1693*, 1–10. https://doi.org/10.1016/j.brainres.2018.03.024

Ma, X. R., Prudencio, M., Koike, Y., Vatsavayai, S. C., Kim, G., Harbinski, F., Briner, A., Rodriguez, C. M., Guo, C., Akiyama, T., Schmidt, H. B., Cummings, B. B., Wyatt, D. W., Kurylo, K., Miller, G., Mekhoubad, S., Sallee, N., Mekonnen, G., Ganser, L., … Gitler, A. D. (2022). TDP-43 represses cryptic exon inclusion in the FTD–ALS gene UNC13A. *Nature*, *603*(7899), 124–130. https://doi.org/10.1038/s41586-022-04424-7

Mackenzie, I. R. A., Bigio, E. H., Ince, P. G., Geser, F., Neumann, M., Cairns, N. J., Kwong, L. K., Forman, M. S., Ravits, J., Stewart, H., Eisen, A., McClusky, L., Kretzschmar, H. A., Monoranu, C. M., Highley, J. R., Kirby, J., Siddique, T., Shaw, P. J., Lee, V. M., & Trojanowski, J. Q. (2007). Pathological TDP-43 distinguishes sporadic amyotrophic lateral sclerosis from amyotrophic lateral sclerosis with *SOD1* mutations. *Annals of Neurology*, *61*(5), 427–434. https://doi.org/10.1002/ana.21147

Maier, M., Welt, T., Wirth, F., Montrasio, F., Preisig, D., McAfoose, J., Vieira, F. G., Kulic, L., Späni, C., Stehle, T., Perrin, S., Weber, M., Hock, C., Nitsch, R. M., & Grimm, J. (2018). A human-derived antibody targets misfolded SOD1 and ameliorates motor symptoms in mouse models of amyotrophic lateral sclerosis. *Science Translational Medicine*, *10*(470), eaah3924. https://doi.org/10.1126/scitranslmed.aah3924

Majumder, P., Chen, Y.-T., Bose, J. K., Wu, C.-C., Cheng, W.-C., Cheng, S.-J., Fang, Y.-H., Chen, Y.-L., Tsai, K.-J., Lien, C.-C., & Shen, C.-K. J. (2012). TDP-43 regulates the mammalian spinogenesis through translational repression of Rac1. *Acta Neuropathologica*, *124*(2), 231–245. https://doi.org/10.1007/s00401-012-1006-4

Markmiller, S., Soltanieh, S., Server, K. L., Mak, R., Jin, W., Fang, M. Y., Luo, E.-C., Krach, F., Yang, D., Sen, A., Fulzele, A., Wozniak, J. M., Gonzalez, D. J., Kankel, M. W., Gao, F.-B., Bennett, E. J., Lécuyer, E., & Yeo, G. W. (2018). Context-Dependent and Disease-Specific Diversity in Protein Interactions within Stress Granules. *Cell*, *172*(3), 590-604.e13. https://doi.org/10.1016/j.cell.2017.12.032

Martier, R., & Konstantinova, P. (2020). Gene Therapy for Neurodegenerative Diseases: Slowing Down the Ticking Clock. *Frontiers in Neuroscience*, *14*, 580179. https://doi.org/10.3389/fnins.2020.580179

Martier, R., Liefhebber, J. M., García-Osta, A., Miniarikova, J., Cuadrado-Tejedor, M., Espelosin, M., Ursua, S., Petry, H., Van Deventer, S. J., Evers, M. M., & Konstantinova, P. (2019). Targeting RNA-Mediated Toxicity in C9orf72 ALS and/or

FTD by RNAi-Based Gene Therapy. *Molecular Therapy - Nucleic Acids*, *16*, 26–37. https://doi.org/10.1016/j.omtn.2019.02.001

Martier, R., Liefhebber, J. M., Miniarikova, J., Van Der Zon, T., Snapper, J., Kolder, I., Petry, H., Van Deventer, S. J., Evers, M. M., & Konstantinova, P. (2019). Artificial MicroRNAs Targeting C9orf72 Can Reduce Accumulation of Intra-nuclear Transcripts in ALS and FTD Patients. *Molecular Therapy - Nucleic Acids*, *14*, 593–608. https://doi.org/10.1016/j.omtn.2019.01.010

Martinez-Gonzalez, L., Cuevas, E. P., Tosat-Bitrián, C., Nozal, V., Gil, C., Palomo, V., Martín-Requero, Á., & Martinez, A. (2023). TTBK1 and CK1 inhibitors restore TDP-43 pathology and avoid disease propagation in lymphoblast from Alzheimer's disease patients. *Frontiers in Molecular Neuroscience*, *16*, 1243277. https://doi.org/10.3389/fnmol.2023.1243277

Martínez-González, L., Rodríguez-Cueto, C., Cabezudo, D., Bartolomé, F., Andrés-Benito, P., Ferrer, I., Gil, C., Martín-Requero, Á., Fernández-Ruiz, J., Martínez, A., & De Lago, E. (2020). Motor neuron preservation and decrease of in vivo TDP-43 phosphorylation by protein CK-1δ kinase inhibitor treatment. *Scientific Reports*, *10*(1), 4449. https://doi.org/10.1038/s41598-020-61265-y

McCampbell, A., Cole, T., Wegener, A. J., Tomassy, G. S., Setnicka, A., Farley, B. J., Schoch, K. M., Hoye, M. L., Shabsovich, M., Sun, L., Luo, Y., Zhang, M., Thankamony, S., Salzman, D. W., Cudkowicz, M., Graham, D. L., Bennett, C. F., Kordasiewicz, H. B., Swayze, E. E., & Miller, T. M. (2018). Antisense oligonucleotides extend survival and reverse decrement in muscle response in ALS models. *Journal of Clinical Investigation*, *128*(8), 3558–3567. https://doi.org/10.1172/JCI99081

McGurk, L., Gomes, E., Guo, L., Mojsilovic-Petrovic, J., Tran, V., Kalb, R. G., Shorter, J., & Bonini, N. M. (2018). Poly(ADP-Ribose) Prevents Pathological Phase Separation of TDP-43 by Promoting Liquid Demixing and Stress Granule Localization. *Molecular Cell*, *71*(5), 703-717.e9. https://doi.org/10.1016/j.molcel.2018.07.002

Meijboom, K. E., Abdallah, A., Fordham, N. P., Nagase, H., Rodriguez, T., Kraus, C., Gendron, T. F., Krishnan, G., Esanov, R., Andrade, N. S., Rybin, M. J., Ramic, M., Stephens, Z. D., Edraki, A., Blackwood, M. T., Kahriman, A., Henninger, N., Kocher, J.-P. A., Benatar, M., … Mueller, C. (2022). CRISPR/Cas9-mediated excision of ALS/FTD-causing hexanucleotide repeat expansion in C9ORF72 rescues major disease mechanisms in vivo and in vitro. *Nature Communications*, *13*(1), 6286. https://doi.org/10.1038/s41467-022-33332-7

Melamed, Z., López-Erauskin, J., Baughn, M. W., Zhang, O., Drenner, K., Sun, Y., Freyermuth, F., McMahon, M. A., Beccari, M. S., Artates, J. W., Ohkubo, T., Rodriguez, M., Lin, N., Wu, D., Bennett, C. F., Rigo, F., Da Cruz, S., Ravits, J.,

Lagier-Tourenne, C., & Cleveland, D. W. (2019). Premature polyadenylation-mediated loss of stathmin-2 is a hallmark of TDP-43-dependent neurodegeneration. *Nature Neuroscience*, *22*(2), 180–190. https://doi.org/10.1038/s41593-018-0293-z

Mendell, J. R., Sahenk, Z., Lehman, K. J., Lowes, L. P., Reash, N. F., Iammarino, M. A., Alfano, L. N., Lewis, S., Church, K., Shell, R., Potter, R. A., Griffin, D. A., Hogan, M., Wang, S., Mason, S., Darton, E., & Rodino-Klapac, L. R. (2024). Long-term safety and functional outcomes of delandistrogene moxeparvovec gene therapy in patients with Duchenne muscular dystrophy: A phase 1/2a nonrandomized trial. *Muscle & Nerve*, *69*(1), 93–98. https://doi.org/10.1002/mus.27955

Mendell, J. R., Shell, R., Lehman, K. J., McColly, M., Lowes, L. P., Alfano, L. N., Miller, N. F., Iammarino, M. A., Church, K., Ogrinc, F. G., Ouyang, H., Kernbauer, E., Joshi, S., Sproule, D. M., Meriggioli, M., Feltner, D. E., & Al-Zaidy, S. (2020). Gene-Replacement Therapy in Spinal Muscular Atrophy Type 1: Long-Term Follow-Up From the Onasemnogene Abeparvovec-xioi Phase 1/2a Clinical Trial (1808). *Neurology*, *94*(15_supplement), 1808. https://doi.org/10.1212/WNL.94.15_supplement.1808

Meng, Q.-J., Maywood, E. S., Bechtold, D. A., Lu, W.-Q., Li, J., Gibbs, J. E., Dupré, S. M., Chesham, J. E., Rajamohan, F., Knafels, J., Sneed, B., Zawadzke, L. E., Ohren, J. F., Walton, K. M., Wager, T. T., Hastings, M. H., & Loudon, A. S. I. (2010). Entrainment of disrupted circadian behavior through inhibition of casein kinase 1 (CK1) enzymes. *Proceedings of the National Academy of Sciences*, *107*(34), 15240–15245. https://doi.org/10.1073/pnas.1005101107

Miller, R., Mitchell, J., Lyon, M., & Moore, D. (2002). Riluzole for amyotrophic lateral sclerosis (ALS)/motor neuron disease (MND). In The Cochrane Collaboration (Ed.), *Cochrane Database of Systematic Reviews* (p. CD001447). John Wiley & Sons, Ltd. https://doi.org/10.1002/14651858.CD001447

Miller, T., Cudkowicz, M., Shaw, P. J., Andersen, P. M., Atassi, N., Bucelli, R. C., Genge, A., Glass, J., Ladha, S., Ludolph, A. L., Maragakis, N. J., McDermott, C. J., Pestronk, A., Ravits, J., Salachas, F., Trudell, R., Van Damme, P., Zinman, L., Bennett, C. F., … Ferguson, T. A. (2020). Phase 1–2 Trial of Antisense Oligonucleotide Tofersen for *SOD1* ALS. *New England Journal of Medicine*, *383*(2), 109–119. https://doi.org/10.1056/NEJMoa2003715

Miller, T. M., Pestronk, A., David, W., Rothstein, J., Simpson, E., Appel, S. H., Andres, P. L., Mahoney, K., Allred, P., Alexander, K., Ostrow, L. W., Schoenfeld, D., Macklin, E. A., Norris, D. A., Manousakis, G., Crisp, M., Smith, R., Bennett, C. F., Bishop, K. M., & Cudkowicz, M. E. (2013). An antisense oligonucleotide against SOD1 delivered intrathecally for patients with SOD1 familial amyotrophic lateral sclerosis: A phase 1, randomised, first-in-man study. *The Lancet Neurology*, *12*(5), 435–442. https://doi.org/10.1016/S1474-4422(13)70061-9

Miniarikova, J., Zimmer, V., Martier, R., Brouwers, C. C., Pythoud, C., Richetin, K., Rey, M., Lubelski, J., Evers, M. M., Van Deventer, S. J., Petry, H., Déglon, N., & Konstantinova, P. (2017). AAV5-miHTT gene therapy demonstrates suppression of mutant huntingtin aggregation and neuronal dysfunction in a rat model of Huntington's disease. *Gene Therapy*, *24*(10), 630–639. https://doi.org/10.1038/gt.2017.71

Mittermeyer, G., Christine, C. W., Rosenbluth, K. H., Baker, S. L., Starr, P., Larson, P., Kaplan, P. L., Forsayeth, J., Aminoff, M. J., & Bankiewicz, K. S. (2012). Long-Term Evaluation of a Phase 1 Study of AADC Gene Therapy for Parkinson's Disease. *Human Gene Therapy*, *23*(4), 377–381. https://doi.org/10.1089/hum.2011.220

Montalbano, M., McAllen, S., Cascio, F. L., Sengupta, U., Garcia, S., Bhatt, N., Ellsworth, A., Heidelman, E. A., Johnson, O. D., Doskocil, S., & Kayed, R. (2020). TDP-43 and Tau Oligomers in Alzheimer's Disease, Amyotrophic Lateral Sclerosis, and Frontotemporal Dementia. *Neurobiology of Disease*, *146*, 105130. https://doi.org/10.1016/j.nbd.2020.105130

Mueller, C., Berry, J. D., McKenna-Yasek, D. M., Gernoux, G., Owegi, M. A., Pothier, L. M., Douthwright, C. L., Gelevski, D., Luppino, S. D., Blackwood, M., Wightman, N. S., Oakley, D. H., Frosch, M. P., Flotte, T. R., Cudkowicz, M. E., & Brown, R. H. (2020). *SOD1* Suppression with Adeno-Associated Virus and MicroRNA in Familial ALS. *New England Journal of Medicine*, *383*(2), 151–158. https://doi.org/10.1056/NEJMoa2005056

Mullard, A. (2021). ALS antisense drug falters in phase III. *Nature Reviews Drug Discovery*, *20*(12), 883–885. https://doi.org/10.1038/d41573-021-00181-w

Mummery, C. J., Börjesson-Hanson, A., Blackburn, D. J., Vijverberg, E. G. B., De Deyn, P. P., Ducharme, S., Jonsson, M., Schneider, A., Rinne, J. O., Ludolph, A. C., Bodenschatz, R., Kordasiewicz, H., Swayze, E. E., Fitzsimmons, B., Mignon, L., Moore, K. M., Yun, C., Baumann, T., Li, D., … Lane, R. M. (2023). Tau-targeting antisense oligonucleotide MAPTRx in mild Alzheimer's disease: A phase 1b, randomized, placebo-controlled trial. *Nature Medicine*, *29*(6), 1437–1447. https://doi.org/10.1038/s41591-023-02326-3

Muntoni, F., Mercuri, E., Schmidt, U. S., Komaki, H., Richardson, J., Singh, T., Guridi, M., Mason, S., Murphy, A., Yu, L., Reid, C., Darton, E., Wandel, C., & Mendell, J. (2023). EMBARK, a Phase 3 Trial Evaluating Safety and Efficacy of Delandistrogene Moxeparvovec (SRP- 9001) in Duchenne Muscular Dystrophy (DMD): Study Design and Baseline Characteristics (P5-8.012). *Neurology*, *100*(17_supplement_2), 3691. https://doi.org/10.1212/WNL.0000000000203455

Nagata, T., Dwyer, C. A., Yoshida-Tanaka, K., Ihara, K., Ohyagi, M., Kaburagi, H., Miyata, H., Ebihara, S., Yoshioka, K., Ishii, T., Miyata, K., Miyata, K., Powers, B., Igari, T., Yamamoto, S., Arimura, N., Hirabayashi, H., Uchihara, T., Hara, R. I., … Yokota,

T. (2021). Cholesterol-functionalized DNA/RNA heteroduplexes cross the blood–brain barrier and knock down genes in the rodent CNS. *Nature Biotechnology*, *39*(12), 1529–1536. https://doi.org/10.1038/s41587-021-00972-x

Neumann, M. (2009). Molecular Neuropathology of TDP-43 Proteinopathies. *International Journal of Molecular Sciences*, *10*(1), 232–246. https://doi.org/10.3390/ijms10010232

Neumann, M., Frick, P., Paron, F., Kosten, J., Buratti, E., & Mackenzie, I. R. (2020). Antibody against TDP-43 phosphorylated at serine 375 suggests conformational differences of TDP-43 aggregates among FTLD–TDP subtypes. *Acta Neuropathologica*, *140*(5), 645–658. https://doi.org/10.1007/s00401-020-02207-w

Neumann, M., Frick, P., Paron, F., Kosten, J., Buratti, E., & Mackenzie, I. R. (2021). Correction to: Antibody against TDP-43 phosphorylated at serine 369 suggests conformational differences of TDP-43 aggregates among FTLD-TDP subtypes. *Acta Neuropathologica*, *141*(1), 137–137. https://doi.org/10.1007/s00401-020-02242-7

Neumann, M., Kwong, L. K., Lee, E. B., Kremmer, E., Flatley, A., Xu, Y., Forman, M. S., Troost, D., Kretzschmar, H. A., Trojanowski, J. Q., & Lee, V. M.-Y. (2009). Phosphorylation of S409/410 of TDP-43 is a consistent feature in all sporadic and familial forms of TDP-43 proteinopathies. *Acta Neuropathologica*, *117*(2), 137–149. https://doi.org/10.1007/s00401-008-0477-9

Neumann, M., Sampathu, D. M., Kwong, L. K., Truax, A. C., Micsenyi, M. C., Chou, T. T., Bruce, J., Schuck, T., Grossman, M., Clark, C. M., McCluskey, L. F., Miller, B. L., Masliah, E., Mackenzie, I. R., Feldman, H., Feiden, W., Kretzschmar, H. A., Trojanowski, J. Q., & Lee, V. M.-Y. (2006). Ubiquitinated TDP-43 in Frontotemporal Lobar Degeneration and Amyotrophic Lateral Sclerosis. *Science*, *314*(5796), 130–133. https://doi.org/10.1126/science.1134108

Newell, K., Paron, F., Mompean, M., Murrell, J., Salis, E., Stuani, C., Pattee, G., Romano, M., Laurents, D., Ghetti, B., & Buratti, E. (2019). Dysregulation of TDP-43 intracellular localization and early onset ALS are associated with a *TARDBP* S375G variant. *Brain Pathology*, *29*(3), 397–413. https://doi.org/10.1111/bpa.12680

Nguyen, L., Montrasio, F., Pattamatta, A., Tusi, S. K., Bardhi, O., Meyer, K. D., Hayes, L., Nakamura, K., Banez-Coronel, M., Coyne, A., Guo, S., Laboissonniere, L. A., Gu, Y., Narayanan, S., Smith, B., Nitsch, R. M., Kankel, M. W., Rushe, M., Rothstein, J., … Ranum, L. P. W. (2020). Antibody Therapy Targeting RAN Proteins Rescues C9 ALS/FTD Phenotypes in C9orf72 Mouse Model. *Neuron*, *105*(4), 645-662.e11. https://doi.org/10.1016/j.neuron.2019.11.007

Niethammer, M., Tang, C. C., LeWitt, P. A., Rezai, A. R., Leehey, M. A., Ojemann, S. G., Flaherty, A. W., Eskandar, E. N., Kostyk, S. K., Sarkar, A., Siddiqui, M. S., Tatter, S. B., Schwalb, J. M., Poston, K. L., Henderson, J. M., Kurlan, R. M., Richard, I. H., Sapan, C. V., Eidelberg, D., … Feigin, A. (2017). Long-term follow-up of a randomized AAV2-GAD gene therapy trial for Parkinson's disease. *JCI Insight*, *2*(7), e90133. https://doi.org/10.1172/jci.insight.90133

Nolan, M., Scott, C., Gamarallage, M. P., Lunn, D., Carpenter, K., McDonough, E., Meyer, D., Kaanumalle, S., Santamaria-Pang, A., Turner, M. R., Talbot, K., & Ansorge, O. (2020). Quantitative patterns of motor cortex proteinopathy across ALS genotypes. *Acta Neuropathologica Communications*, *8*(1), 98. https://doi.org/10.1186/s40478-020-00961-2

Nonaka, T., Masuda-Suzukake, M., Arai, T., Hasegawa, Y., Akatsu, H., Obi, T., Yoshida, M., Murayama, S., Mann, D. M. A., Akiyama, H., & Hasegawa, M. (2013). Prion-like Properties of Pathological TDP-43 Aggregates from Diseased Brains. *Cell Reports*, *4*(1), 124–134. https://doi.org/10.1016/j.celrep.2013.06.007

Nonaka, T., Suzuki, G., Tanaka, Y., Kametani, F., Hirai, S., Okado, H., Miyashita, T., Saitoe, M., Akiyama, H., Masai, H., & Hasegawa, M. (2016). Phosphorylation of TAR DNA-binding Protein of 43 kDa (TDP-43) by Truncated Casein Kinase 1δ Triggers Mislocalization and Accumulation of TDP-43. *Journal of Biological Chemistry*, *291*(11), 5473–5483. https://doi.org/10.1074/jbc.M115.695379

Nozal, V., Martínez-González, L., Gomez-Almeria, M., Gonzalo-Consuegra, C., Santana, P., Chaikuad, A., Pérez-Cuevas, E., Knapp, S., Lietha, D., Ramírez, D., Petralla, S., Monti, B., Gil, C., Martín-Requero, A., Palomo, V., De Lago, E., & Martinez, A. (2022). TDP-43 Modulation by Tau-Tubulin Kinase 1 Inhibitors: A New Avenue for Future Amyotrophic Lateral Sclerosis Therapy. *Journal of Medicinal Chemistry*, *65*(2), 1585–1607. https://doi.org/10.1021/acs.jmedchem.1c01942

Ortiz-Virumbrales, M., Moreno, C. L., Kruglikov, I., Marazuela, P., Sproul, A., Jacob, S., Zimmer, M., Paull, D., Zhang, B., Schadt, E. E., Ehrlich, M. E., Tanzi, R. E., Arancio, O., Noggle, S., & Gandy, S. (2017). CRISPR/Cas9-Correctable mutation-related molecular and physiological phenotypes in iPSC-derived Alzheimer's PSEN2 N141I neurons. *Acta Neuropathologica Communications*, *5*(1), 77. https://doi.org/10.1186/s40478-017-0475-z

Osaka, M., Ito, D., & Suzuki, N. (2016). Disturbance of proteasomal and autophagic protein degradation pathways by amyotrophic lateral sclerosis-linked mutations in ubiquilin 2. *Biochemical and Biophysical Research Communications*, *472*(2), 324–331. https://doi.org/10.1016/j.bbrc.2016.02.107

Oskarsson, B., Gendron, T. F., & Staff, N. P. (2018). Amyotrophic Lateral Sclerosis: An Update for 2018. *Mayo Clinic Proceedings*, *93*(11), 1617–1628. https://doi.org/10.1016/j.mayocp.2018.04.007

Palomo, V., Nozal, V., Rojas-Prats, E., Gil, C., & Martinez, A. (2021). Protein kinase inhibitors for amyotrophic lateral sclerosis therapy. *British Journal of Pharmacology*, *178*(6), 1316–1335. https://doi.org/10.1111/bph.15221

Perez, D. I., Gil, C., & Martinez, A. (2011). Protein kinases CK1 and CK2 as new targets for neurodegenerative diseases. *Medicinal Research Reviews*, *31*(6), 924–954. https://doi.org/10.1002/med.20207

Philips, T., & Rothstein, J. D. (2015). Rodent Models of Amyotrophic Lateral Sclerosis. *Current Protocols in Pharmacology*, *69*(1). https://doi.org/10.1002/0471141755.ph0567s69

Piao, X., Meng, D., Zhang, X., Song, Q., Lv, H., & Jia, Y. (2022). Dual-gRNA approach with limited off-target effect corrects C9ORF72 repeat expansion in vivo. *Scientific Reports*, *12*(1), 5672. https://doi.org/10.1038/s41598-022-07746-8

Picher-Martel, V., Dutta, K., Phaneuf, D., Sobue, G., & Julien, J.-P. (2015). Ubiquilin-2 drives NF-κB activity and cytosolic TDP-43 aggregation in neuronal cells. *Molecular Brain*, *8*(1), 71. https://doi.org/10.1186/s13041-015-0162-6

Polymenidou, M., Lagier-Tourenne, C., Hutt, K. R., Bennett, C. F., Cleveland, D. W., & Yeo, G. W. (2012). Misregulated RNA processing in amyotrophic lateral sclerosis. *Brain Research*, *1462*, 3–15. https://doi.org/10.1016/j.brainres.2012.02.059

Polymenidou, M., Lagier-Tourenne, C., Hutt, K. R., Huelga, S. C., Moran, J., Liang, T. Y., Ling, S.-C., Sun, E., Wancewicz, E., Mazur, C., Kordasiewicz, H., Sedaghat, Y., Donohue, J. P., Shiue, L., Bennett, C. F., Yeo, G. W., & Cleveland, D. W. (2011). Long pre-mRNA depletion and RNA missplicing contribute to neuronal vulnerability from loss of TDP-43. *Nature Neuroscience*, *14*(4), 459–468. https://doi.org/10.1038/nn.2779

Poulin-Brière, A., Rezaei, E., & Pozzi, S. (2021). Antibody-Based Therapeutic Interventions for Amyotrophic Lateral Sclerosis: A Systematic Literature Review. *Frontiers in Neuroscience*, *15*, 790114. https://doi.org/10.3389/fnins.2021.790114

Prasad, A., Bharathi, V., Sivalingam, V., Girdhar, A., & Patel, B. K. (2019). Molecular Mechanisms of TDP-43 Misfolding and Pathology in Amyotrophic Lateral Sclerosis. *Frontiers in Molecular Neuroscience*, *12*, 25. https://doi.org/10.3389/fnmol.2019.00025

Pulgar, V., Marin, O., Meggio, F., Allende, C. C., Allende, J. E., & Pinna, L. A. (1999). Optimal sequences for non-phosphate-directed phoshorylation by protein kinase CK1 (casein kinase-1) – a re-evaluation. *European Journal of Biochemistry*, *260*(2), 520–526. https://doi.org/10.1046/j.1432-1327.1999.00195.x

Ragagnin, A. M. G., Shadfar, S., Vidal, M., Jamali, M. S., & Atkin, J. D. (2019). Motor Neuron Susceptibility in ALS/FTD. *Frontiers in Neuroscience*, *13*, 532. https://doi.org/10.3389/fnins.2019.00532

Ramos, D. M., d'Ydewalle, C., Gabbeta, V., Dakka, A., Klein, S. K., Norris, D. A., Matson, J., Taylor, S. J., Zaworski, P. G., Prior, T. W., Snyder, P. J., Valdivia, D., Hatem, C. L., Waters, I., Gupte, N., Swoboda, K. J., Rigo, F., Bennett, C. F., Naryshkin, N., … Sumner, C. J. (2019). Age-dependent SMN expression in disease-relevant tissue and implications for SMA treatment. *Journal of Clinical Investigation*, *129*(11), 4817–4831. https://doi.org/10.1172/JCI124120

Ravits, J. M., & La Spada, A. R. (2009). ALS motor phenotype heterogeneity, focality, and spread: Deconstructing motor neuron degeneration. *Neurology*, *73*(10), 805–811. https://doi.org/10.1212/WNL.0b013e3181b6bbbd

Ren, Y., Li, S., Chen, S., Sun, X., Yang, F., Wang, H., Li, M., Cui, F., & Huang, X. (2021). TDP-43 and Phosphorylated TDP-43 Levels in Paired Plasma and CSF Samples in Amyotrophic Lateral Sclerosis. *Frontiers in Neurology*, *12*, 663637. https://doi.org/10.3389/fneur.2021.663637

Richard, J.-P., & Maragakis, N. J. (2015). Induced pluripotent stem cells from ALS patients for disease modeling. *Brain Research*, *1607*, 15–25. https://doi.org/10.1016/j.brainres.2014.09.017

Riemenschneider, H., Simonetti, F., Sheth, U., Katona, E., Roth, S., Hutten, S., Farny, D., Michaelsen, M., Nuscher, B., Schmidt, M. K., Flatley, A., Schepers, A., Gruijs Da Silva, L. A., Zhou, Q., Klopstock, T., Liesz, A., Arzberger, T., Herms, J., Feederle, R., … Edbauer, D. (2023). Targeting the glycine-rich domain of TDP-43 with antibodies prevents its aggregation in vitro and reduces neurofilament levels in vivo. *Acta Neuropathologica Communications*, *11*(1), 112. https://doi.org/10.1186/s40478-023-01592-z

Rigo, F., Hua, Y., Krainer, A. R., & Bennett, C. F. (2012). Antisense-based therapy for the treatment of spinal muscular atrophy. *Journal of Cell Biology*, *199*(1), 21–25. https://doi.org/10.1083/jcb.201207087

Rodriguez-Calienes, A., Chavez-Malpartida, S., Alvarado-Gamarra, G., Pacheco-Barrios, N., Martinez-Esteban, P., & Alva-Diaz, C. (2021). Efficacy and security of onasemnogene abeparvovec-XIOI in spinal muscular atrophy: A systematic review and meta-analysis. *Journal of the Neurological Sciences*, *429*, 118887. https://doi.org/10.1016/j.jns.2021.118887

Rojas-Prats, E., Martinez-Gonzalez, L., Gonzalo-Consuegra, C., Liachko, N. F., Perez, C., Ramírez, D., Kraemer, B. C., Martin-Requero, Á., Perez, D. I., Gil, C., De Lago, E., & Martinez, A. (2021). Targeting nuclear protein TDP-43 by cell division cycle kinase 7 inhibitors: A new therapeutic approach for amyotrophic lateral sclerosis.

European Journal of Medicinal Chemistry, *210*, 112968. https://doi.org/10.1016/j.ejmech.2020.112968

Romano, N., Catalani, A., Lattante, S., Belardo, A., Proietti, S., Bertini, L., Silvestri, F., Catalani, E., Cervia, D., Zolla, L., Sabatelli, M., Welshhans, K., & Ceci, M. (2020). ALS skin fibroblasts reveal oxidative stress and ERK1/2-mediated cytoplasmic localization of TDP-43. *Cellular Signalling*, *70*, 109591. https://doi.org/10.1016/j.cellsig.2020.109591

Rot, G., Wang, Z., Huppertz, I., Modic, M., Lenče, T., Hallegger, M., Haberman, N., Curk, T., Von Mering, C., & Ule, J. (2017). High-Resolution RNA Maps Suggest Common Principles of Splicing and Polyadenylation Regulation by TDP-43. *Cell Reports*, *19*(5), 1056–1067. https://doi.org/10.1016/j.celrep.2017.04.028

Roth, A., Sander, A., Oswald, M. S., Gärtner, F., Knippschild, U., & Bischof, J. (2022). Comprehensive Characterization of CK1δ-Mediated Tau Phosphorylation in Alzheimer's Disease. *Frontiers in Molecular Biosciences*, *9*, 872171. https://doi.org/10.3389/fmolb.2022.872171

Rothstein, J. D. (2017). Edaravone: A new drug approved for ALS. *Cell*, *171*(4), 725. https://doi.org/10.1016/j.cell.2017.10.011

Rowland, L. P. (2001). How Amyotrophic Lateral Sclerosis Got Its Name: The Clinical-Pathologic Genius of Jean-Martin Charcot. *Archives of Neurology*, *58*(3). https://doi.org/10.1001/archneur.58.3.512

Saberi, S., Stauffer, J. E., Schulte, D. J., & Ravits, J. (2015). Neuropathology of Amyotrophic Lateral Sclerosis and Its Variants. *Neurologic Clinics*, *33*(4), 855–876. https://doi.org/10.1016/j.ncl.2015.07.012

Sahu, R., Upadhayay, S., & Mehan, S. (2021). Inhibition of extracellular regulated kinase (ERK)-1/2 signaling pathway in the prevention of ALS: Target inhibitors and influences on neurological dysfunctions. *European Journal of Cell Biology*, *100*(7–8), 151179. https://doi.org/10.1016/j.ejcb.2021.151179

Salado, I. G., Redondo, M., Bello, M. L., Perez, C., Liachko, N. F., Kraemer, B. C., Miguel, L., Lecourtois, M., Gil, C., Martinez, A., & Perez, D. I. (2014). Protein Kinase CK-1 Inhibitors As New Potential Drugs for Amyotrophic Lateral Sclerosis. *Journal of Medicinal Chemistry*, *57*(6), 2755–2772. https://doi.org/10.1021/jm500065f

Sambandan, S., Akbalik, G., Kochen, L., Rinne, J., Kahlstatt, J., Glock, C., Tushev, G., Alvarez-Castelao, B., Heckel, A., & Schuman, E. M. (2017). Activity-dependent spatially localized miRNA maturation in neuronal dendrites. *Science*, *355*(6325), 634–637. https://doi.org/10.1126/science.aaf8995

Sasaguri, H., Chew, J., Xu, Y.-F., Gendron, T. F., Garrett, A., Lee, C. W., Jansen-West, K., Bauer, P. O., Perkerson, E. A., Tong, J., Stetler, C., & Zhang, Y.-J. (2016). The extreme N-terminus of TDP-43 mediates the cytoplasmic aggregation of TDP-43 and associated toxicity in vivo. *Brain Research*, *1647*, 57–64. https://doi.org/10.1016/j.brainres.2016.04.069

Sattler, R., Traynor, B. J., Robertson, J., Van Den Bosch, L., Barmada, S. J., Svendsen, C. N., Disney, M. D., Gendron, T. F., Wong, P. C., Turner, M. R., Boxer, A., Babu, S., Benatar, M., Kurnellas, M., Rohrer, J. D., Donnelly, C. J., Bustos, L. M., Van Keuren-Jensen, K., Dacks, P. A., … Vieira, F. G. (2023). Roadmap for C9ORF72 in Frontotemporal Dementia and Amyotrophic Lateral Sclerosis: Report on the C9ORF72 FTD/ALS Summit. *Neurology and Therapy*, *12*(6), 1821–1843. https://doi.org/10.1007/s40120-023-00548-8

Schmidt, M. F., Gan, Z. Y., Komander, D., & Dewson, G. (2021). Ubiquitin signalling in neurodegeneration: Mechanisms and therapeutic opportunities. *Cell Death & Differentiation*, *28*(2), 570–590. https://doi.org/10.1038/s41418-020-00706-7

Scoles, D. R., Meera, P., Schneider, M. D., Paul, S., Dansithong, W., Figueroa, K. P., Hung, G., Rigo, F., Bennett, C. F., Otis, T. S., & Pulst, S. M. (2017). Antisense oligonucleotide therapy for spinocerebellar ataxia type 2. *Nature*, *544*(7650), 362–366. https://doi.org/10.1038/nature22044

Scotter, E. L., Chen, H.-J., & Shaw, C. E. (2015). TDP-43 Proteinopathy and ALS: Insights into Disease Mechanisms and Therapeutic Targets. *Neurotherapeutics*, *12*(2), 352–363. https://doi.org/10.1007/s13311-015-0338-x

Segref, A., & Hoppe, T. (2009). Think locally: Control of ubiquitin-dependent protein degradation in neurons. *EMBO Reports*, *10*(1), 44–50. https://doi.org/10.1038/embor.2008.229

Shin, J. W., Kim, K.-H., Chao, M. J., Atwal, R. S., Gillis, T., MacDonald, M. E., Gusella, J. F., & Lee, J.-M. (2016). Permanent inactivation of Huntington's disease mutation by personalized allele-specific CRISPR/Cas9. *Human Molecular Genetics*, ddw286. https://doi.org/10.1093/hmg/ddw286

Sternburg, E. L., Gruijs Da Silva, L. A., & Dormann, D. (2022). Post-translational modifications on RNA-binding proteins: Accelerators, brakes, or passengers in neurodegeneration? *Trends in Biochemical Sciences*, *47*(1), 6–22. https://doi.org/10.1016/j.tibs.2021.07.004

Stevens, D., Claborn, M. K., Gildon, B. L., Kessler, T. L., & Walker, C. (2020). Onasemnogene Abeparvovec-xioi: Gene Therapy for Spinal Muscular Atrophy. *Annals of Pharmacotherapy*, *54*(10), 1001–1009. https://doi.org/10.1177/1060028020914274

Stoica, L., Todeasa, S. H., Cabrera, G. T., Salameh, J. S., ElMallah, M. K., Mueller, C., Brown, R. H., & Sena-Esteves, M. (2016). Adeno-associated virus–delivered artificial microRNA extends survival and delays paralysis in an amyotrophic lateral sclerosis mouse model. *Annals of Neurology*, *79*(4), 687–700. https://doi.org/10.1002/ana.24618

Suk, T. R., & Rousseaux, M. W. C. (2020). The role of TDP-43 mislocalization in amyotrophic lateral sclerosis. *Molecular Neurodegeneration*, *15*(1), 45. https://doi.org/10.1186/s13024-020-00397-1

Suvarna, V., Deshmukh, K., & Murahari, M. (2022). miRNA and antisense oligonucleotide-based α-synuclein targeting as disease-modifying therapeutics in Parkinson's disease. *Frontiers in Pharmacology*, *13*, 1034072. https://doi.org/10.3389/fphar.2022.1034072

Swinnen, B., & Robberecht, W. (2014). The phenotypic variability of amyotrophic lateral sclerosis. *Nature Reviews Neurology*, *10*(11), 661–670. https://doi.org/10.1038/nrneurol.2014.184

Tabrizi, S. J., Leavitt, B. R., Landwehrmeyer, G. B., Wild, E. J., Saft, C., Barker, R. A., Blair, N. F., Craufurd, D., Priller, J., Rickards, H., Rosser, A., Kordasiewicz, H. B., Czech, C., Swayze, E. E., Norris, D. A., Baumann, T., Gerlach, I., Schobel, S. A., Paz, E., … Lane, R. M. (2019). Targeting Huntingtin Expression in Patients with Huntington's Disease. *New England Journal of Medicine*, *380*(24), 2307–2316. https://doi.org/10.1056/NEJMoa1900907

Talbott, E. O., Malek, A. M., & Lacomis, D. (2016). The epidemiology of amyotrophic lateral sclerosis. In *Handbook of Clinical Neurology* (Vol. 138, pp. 225–238). Elsevier. https://doi.org/10.1016/B978-0-12-802973-2.00013-6

Taylor, J. P., Brown, R. H., & Cleveland, D. W. (2016). Decoding ALS: From genes to mechanism. *Nature*, *539*(7628), 197–206. https://doi.org/10.1038/nature20413

Taylor, L. M., McMillan, P. J., Liachko, N. F., Strovas, T. J., Ghetti, B., Bird, T. D., Keene, C. D., & Kraemer, B. C. (2018). Pathological phosphorylation of tau and TDP-43 by TTBK1 and TTBK2 drives neurodegeneration. *Molecular Neurodegeneration*, *13*(1), 7. https://doi.org/10.1186/s13024-018-0237-9

Tian, Y., Wang, Y., Jablonski, A. M., Hu, Y., Sugam, J. A., Koglin, M., Stachel, S. J., Zhou, H., Uslaner, J. M., & Parmentier-Batteur, S. (2021). Tau-tubulin kinase 1 phosphorylates TDP-43 at disease-relevant sites and exacerbates TDP-43 pathology. *Neurobiology of Disease*, *161*, 105548. https://doi.org/10.1016/j.nbd.2021.105548

Tollervey, J. R., Curk, T., Rogelj, B., Briese, M., Cereda, M., Kayikci, M., König, J., Hortobágyi, T., Nishimura, A. L., Župunski, V., Patani, R., Chandran, S., Rot, G.,

Zupan, B., Shaw, C. E., & Ule, J. (2011). Characterizing the RNA targets and position-dependent splicing regulation by TDP-43. *Nature Neuroscience*, *14*(4), 452–458. https://doi.org/10.1038/nn.2778

Tomé, S. O., Vandenberghe, R., Ospitalieri, S., Van Schoor, E., Tousseyn, T., Otto, M., Von Arnim, C. A. F., & Thal, D. R. (2020). Distinct molecular patterns of TDP-43 pathology in Alzheimer's disease: Relationship with clinical phenotypes. *Acta Neuropathologica Communications*, *8*(1), 61. https://doi.org/10.1186/s40478-020-00934-5

Torres, P., Ramírez-Núñez, O., Romero-Guevara, R., Barés, G., Granado-Serrano, A. B., Ayala, V., Boada, J., Fontdevila, L., Povedano, M., Sanchís, D., Pamplona, R., Ferrer, I., & Portero-Otín, M. (2018). Cryptic exon splicing function of TARDBP interacts with autophagy in nervous tissue. *Autophagy*, *14*(8), 1398–1403. https://doi.org/10.1080/15548627.2018.1474311

Tran, H., Moazami, M. P., Yang, H., McKenna-Yasek, D., Douthwright, C. L., Pinto, C., Metterville, J., Shin, M., Sanil, N., Dooley, C., Puri, A., Weiss, A., Wightman, N., Gray-Edwards, H., Marosfoi, M., King, R. M., Kenderdine, T., Fabris, D., Bowser, R., … Brown, R. H. (2022). Suppression of mutant C9orf72 expression by a potent mixed backbone antisense oligonucleotide. *Nature Medicine*, *28*(1), 117–124. https://doi.org/10.1038/s41591-021-01557-6

Turner, M. R., Hardiman, O., Benatar, M., Brooks, B. R., Chio, A., De Carvalho, M., Ince, P. G., Lin, C., Miller, R. G., Mitsumoto, H., Nicholson, G., Ravits, J., Shaw, P. J., Swash, M., Talbot, K., Traynor, B. J., Van Den Berg, L. H., Veldink, J. H., Vucic, S., & Kiernan, M. C. (2013). Controversies and priorities in amyotrophic lateral sclerosis. *The Lancet Neurology*, *12*(3), 310–322. https://doi.org/10.1016/S1474-4422(13)70036-X

Tziortzouda, P., Van Den Bosch, L., & Hirth, F. (2021). Triad of TDP43 control in neurodegeneration: Autoregulation, localization and aggregation. *Nature Reviews Neuroscience*, *22*(4), 197–208. https://doi.org/10.1038/s41583-021-00431-1

Urushitani, M., Sato, T., Bamba, H., Hisa, Y., & Tooyama, I. (2010). Synergistic effect between proteasome and autophagosome in the clearance of polyubiquitinated TDP-43. *Journal of Neuroscience Research*, *88*(4), 784–797. https://doi.org/10.1002/jnr.22243

Van Dyck, C. H., Swanson, C. J., Aisen, P., Bateman, R. J., Chen, C., Gee, M., Kanekiyo, M., Li, D., Reyderman, L., Cohen, S., Froelich, L., Katayama, S., Sabbagh, M., Vellas, B., Watson, D., Dhadda, S., Irizarry, M., Kramer, L. D., & Iwatsubo, T. (2023). Lecanemab in Early Alzheimer's Disease. *New England Journal of Medicine*, *388*(1), 9–21. https://doi.org/10.1056/NEJMoa2212948

Van Eersel, J., Ke, Y. D., Gladbach, A., Bi, M., Götz, J., Kril, J. J., & Ittner, L. M. (2011). Cytoplasmic Accumulation and Aggregation of TDP-43 upon Proteasome Inhibition in Cultured Neurons. *PLoS ONE*, *6*(7), e22850. https://doi.org/10.1371/journal.pone.0022850

Verber, N. S., Shepheard, S. R., Sassani, M., McDonough, H. E., Moore, S. A., Alix, J. J. P., Wilkinson, I. D., Jenkins, T. M., & Shaw, P. J. (2019). Biomarkers in Motor Neuron Disease: A State of the Art Review. *Frontiers in Neurology*, *10*, 291. https://doi.org/10.3389/fneur.2019.00291

Verstraete, E., Kuiperij, H. B., Van Blitterswijk, M. M., Veldink, J. H., Schelhaas, H. J., Van Den Berg, L. H., & Verbeek, M. M. (2012). TDP-43 plasma levels are higher in amyotrophic lateral sclerosis. *Amyotrophic Lateral Sclerosis*, *13*(5), 446–451. https://doi.org/10.3109/17482968.2012.703208

Volpato, V., & Webber, C. (2020). Addressing variability in iPSC-derived models of human disease: Guidelines to promote reproducibility. *Disease Models & Mechanisms*, *13*(1), dmm042317. https://doi.org/10.1242/dmm.042317

Wager, T. T., Galatsis, P., Chandrasekaran, R. Y., Butler, T. W., Li, J., Zhang, L., Mente, S., Subramanyam, C., Liu, S., Doran, A. C., Chang, C., Fisher, K., Grimwood, S., Hedde, J. R., Marconi, M., & Schildknegt, K. (2017). Identification and Profiling of a Selective and Brain Penetrant Radioligand for in Vivo Target Occupancy Measurement of Casein Kinase 1 (CK1) Inhibitors. *ACS Chemical Neuroscience*, *8*(9), 1995–2004. https://doi.org/10.1021/acschemneuro.7b00155

Walker, A. K., Spiller, K. J., Ge, G., Zheng, A., Xu, Y., Zhou, M., Tripathy, K., Kwong, L. K., Trojanowski, J. Q., & Lee, V. M.-Y. (2015). Functional recovery in new mouse models of ALS/FTLD after clearance of pathological cytoplasmic TDP-43. *Acta Neuropathologica*, *130*(5), 643–660. https://doi.org/10.1007/s00401-015-1460-x

Walton, K. M., Fisher, K., Rubitski, D., Marconi, M., Meng, Q.-J., Sládek, M., Adams, J., Bass, M., Chandrasekaran, R., Butler, T., Griffor, M., Rajamohan, F., Serpa, M., Chen, Y., Claffey, M., Hastings, M., Loudon, A., Maywood, E., Ohren, J., … Wager, T. T. (2009). Selective Inhibition of Casein Kinase 1ϵ Minimally Alters Circadian Clock Period. *Journal of Pharmacology and Experimental Therapeutics*, *330*(2), 430–439. https://doi.org/10.1124/jpet.109.151415

Wang, A., Conicella, A. E., Schmidt, H. B., Martin, E. W., Rhoads, S. N., Reeb, A. N., Nourse, A., Ramirez Montero, D., Ryan, V. H., Rohatgi, R., Shewmaker, F., Naik, M. T., Mittag, T., Ayala, Y. M., & Fawzi, N. L. (2018). A single N-terminal phosphomimic disrupts TDP-43 polymerization, phase separation, and RNA splicing. *The EMBO Journal*, *37*(5), e97452. https://doi.org/10.15252/embj.201797452

Wang, H., Yang, B., Qiu, L., Yang, C., Kramer, J., Su, Q., Guo, Y., Brown, R. H., Gao, G., & Xu, Z. (2014). Widespread spinal cord transduction by intrathecal injection of rAAV delivers efficacious RNAi therapy for amyotrophic lateral sclerosis. *Human Molecular Genetics*, *23*(3), 668–681. https://doi.org/10.1093/hmg/ddt454

Wang, P., Wander, C. M., Yuan, C.-X., Bereman, M. S., & Cohen, T. J. (2017). Acetylation-induced TDP-43 pathology is suppressed by an HSF1-dependent chaperone program. *Nature Communications*, *8*(1), 82. https://doi.org/10.1038/s41467-017-00088-4

Wang, X., Zhou, S., Ding, X., Ma, M., Zhang, J., Zhou, Y., Wu, E., & Teng, J. (2015). Activation of ER Stress and Autophagy Induced by TDP-43 A315T as Pathogenic Mechanism and the Corresponding Histological Changes in Skin as Potential Biomarker for ALS with the Mutation. *International Journal of Biological Sciences*, *11*(10), 1140–1149. https://doi.org/10.7150/ijbs.12657

Winton, M. J., Igaz, L. M., Wong, M. M., Kwong, L. K., Trojanowski, J. Q., & Lee, V. M.-Y. (2008). Disturbance of Nuclear and Cytoplasmic TAR DNA-binding Protein (TDP-43) Induces Disease-like Redistribution, Sequestration, and Aggregate Formation. *Journal of Biological Chemistry*, *283*(19), 13302–13309. https://doi.org/10.1074/jbc.M800342200

Wu, L.-S., Cheng, W.-C., Chen, C.-Y., Wu, M.-C., Wang, Y.-C., Tseng, Y.-H., Chuang, T.-J., & Shen, C.-K. J. (2019). Transcriptomopathies of pre- and post-symptomatic frontotemporal dementia-like mice with TDP-43 depletion in forebrain neurons. *Acta Neuropathologica Communications*, *7*(1), 50. https://doi.org/10.1186/s40478-019-0674-x

Wu, L.-S., Cheng, W.-C., & Shen, C.-K. J. (2012). Targeted Depletion of TDP-43 Expression in the Spinal Cord Motor Neurons Leads to the Development of Amyotrophic Lateral Sclerosis-like Phenotypes in Mice. *Journal of Biological Chemistry*, *287*(33), 27335–27344. https://doi.org/10.1074/jbc.M112.359000

Wu, R., Zhou, D., Shen, X., Chen, F., Liu, F., & Gu, J. (2021). Phosphorylation of trans-active response DNA-binding protein-of 43 kDa promotes its cytoplasmic aggregation and modulates its function in tau mRNA stability and exon 10 alternative splicing. *Journal of Neurochemistry*, *158*(3), 766–778. https://doi.org/10.1111/jnc.15450

Xia, Q., Wang, H., Hao, Z., Fu, C., Hu, Q., Gao, F., Ren, H., Chen, D., Han, J., Ying, Z., & Wang, G. (2016). TDP -43 loss of function increases TFEB activity and blocks autophagosome–lysosome fusion. *The EMBO Journal*, *35*(2), 121–142. https://doi.org/10.15252/embj.201591998

Xu, R. M., Carmel, G., Sweet, R. M., Kuret, J., & Cheng, X. (1995). Crystal structure of casein kinase-1, a phosphate-directed protein kinase. *The EMBO Journal*, *14*(5), 1015–1023. https://doi.org/10.1002/j.1460-2075.1995.tb07082.x

Yamashita, T., Teramoto, S., & Kwak, S. (2016). Phosphorylated TDP-43 becomes resistant to cleavage by calpain: A regulatory role for phosphorylation in TDP-43 pathology of ALS/FTLD. *Neuroscience Research*, *107*, 63–69. https://doi.org/10.1016/j.neures.2015.12.006

Yang, M., Qi, R., Liu, Y., Shen, X., Zhao, Y., Jin, N., Wu, R., Liu, F., & Gu, J. (2023). Casein Kinase 1δ Phosphorylates TDP-43 and Suppresses Its Function in Tau mRNA Processing. *Journal of Alzheimer's Disease*, *91*(4), 1527–1539. https://doi.org/10.3233/JAD-220985

Yang, S., Chang, R., Yang, H., Zhao, T., Hong, Y., Kong, H. E., Sun, X., Qin, Z., Jin, P., Li, S., & Li, X.-J. (2017). CRISPR/Cas9-mediated gene editing ameliorates neurotoxicity in mouse model of Huntington's disease. *Journal of Clinical Investigation*, *127*(7), 2719–2724. https://doi.org/10.1172/JCI92087

Yang, Y., Xu, T., Zhang, Y., & Qin, X. (2017). Molecular basis for the regulation of the circadian clock kinases CK1δ and CK1ε. *Cellular Signalling*, *31*, 58–65. https://doi.org/10.1016/j.cellsig.2016.12.010

Yasojima, K., Kuret, J., DeMaggio, A. J., McGeer, E., & McGeer, P. L. (2000). Casein kinase 1 delta mRNA is upregulated in Alzheimer disease brain. *Brain Research*, *865*(1), 116–120. https://doi.org/10.1016/S0006-8993(00)02200-9

Yoshino, H., & Kimura, A. (2006). Investigation of the therapeutic effects of edaravone, a free radical scavenger, on amyotrophic lateral sclerosis (Phase II study). *Amyotrophic Lateral Sclerosis*, *7*(4), 247–251. https://doi.org/10.1080/17482960600881870

Yu, H., Lu, S., Gasior, K., Singh, D., Vazquez-Sanchez, S., Tapia, O., Toprani, D., Beccari, M. S., Yates, J. R., Da Cruz, S., Newby, J. M., Lafarga, M., Gladfelter, A. S., Villa, E., & Cleveland, D. W. (2021). HSP70 chaperones RNA-free TDP-43 into anisotropic intranuclear liquid spherical shells. *Science*, *371*(6529), eabb4309. https://doi.org/10.1126/science.abb4309

Zaidman, C. M., Proud, C. M., McDonald, C. M., Lehman, K. J., Goedeker, N. L., Mason, S., Murphy, A. P., Guridi, M., Wang, S., Reid, C., Darton, E., Wandel, C., Lewis, S., Malhotra, J., Griffin, D. A., Potter, R. A., Rodino-Klapac, L. R., & Mendell, J. R. (2023). Delandistrogene Moxeparvovec Gene Therapy in Ambulatory Patients (Aged ≥4 to <8 Years) with Duchenne Muscular Dystrophy: 1-Year Interim Results from Study SRP -9001-103 (ENDEAVOR). *Annals of Neurology*, *94*(5), 955–968. https://doi.org/10.1002/ana.26755

Zanetta, C., Nizzardo, M., Simone, C., Monguzzi, E., Bresolin, N., Comi, G. P., & Corti, S. (2014). Molecular Therapeutic Strategies for Spinal Muscular Atrophies: Current and Future Clinical Trials. *Clinical Therapeutics*, *36*(1), 128–140. https://doi.org/10.1016/j.clinthera.2013.11.006

Zarei, S., Carr, K., Reiley, L., Diaz, K., Guerra, O., Altamirano, P., Pagani, W., Lodin, D., Orozco, G., & Chinea, A. (2015). A comprehensive review of amyotrophic lateral sclerosis. *Surgical Neurology International*, *6*(1), 171. https://doi.org/10.4103/2152-7806.169561

Zeng, Y., Lovchykova, A., Akiyama, T., Liu, C., Guo, C., Jawahar, V. M., Sianto, O., Calliari, A., Prudencio, M., Dickson, D. W., Petrucelli, L., & Gitler, A. D. (2024). *TDP-43 nuclear loss in FTD/ALS causes widespread alternative polyadenylation changes*. https://doi.org/10.1101/2024.01.22.575730

Zhang, Y.-J., Caulfield, T., Xu, Y.-F., Gendron, T. F., Hubbard, J., Stetler, C., Sasaguri, H., Whitelaw, E. C., Cai, S., Lee, W. C., & Petrucelli, L. (2013). The dual functions of the extreme N-terminus of TDP-43 in regulating its biological activity and inclusion formation. *Human Molecular Genetics*, *22*(15), 3112–3122. https://doi.org/10.1093/hmg/ddt166

Zhang, Y.-J., Gendron, T. F., Xu, Y.-F., Ko, L.-W., Yen, S.-H., & Petrucelli, L. (2010). Phosphorylation regulates proteasomal-mediated degradation and solubility of TAR DNA binding protein-43 C-terminal fragments. *Molecular Neurodegeneration*, *5*(1), 33. https://doi.org/10.1186/1750-1326-5-33

Zhang, Y.-J., Xu, Y.-F., Cook, C., Gendron, T. F., Roettges, P., Link, C. D., Lin, W.-L., Tong, J., Castanedes-Casey, M., Ash, P., Gass, J., Rangachari, V., Buratti, E., Baralle, F., Golde, T. E., Dickson, D. W., & Petrucelli, L. (2009). Aberrant cleavage of TDP-43 enhances aggregation and cellular toxicity. *Proceedings of the National Academy of Sciences*, *106*(18), 7607–7612. https://doi.org/10.1073/pnas.0900688106

Zhao, L., Gottesdiener, A. J., Parmar, M., Li, M., Kaminsky, S. M., Chiuchiolo, M. J., Sondhi, D., Sullivan, P. M., Holtzman, D. M., Crystal, R. G., & Paul, S. M. (2016). Intracerebral adeno-associated virus gene delivery of apolipoprotein E2 markedly reduces brain amyloid pathology in Alzheimer's disease mouse models. *Neurobiology of Aging*, *44*, 159–172. https://doi.org/10.1016/j.neurobiolaging.2016.04.020